DEVELOPMENT AND IMPROVEMENT OF CFRP ADHESIVE JOINTS USING VACUUM-ASSISTED RESIN TRANSFER MOLDING (VARTM)

マハモド, ラマダン, モハメド, アブスリア

https://doi.org/10.15017/1866330

出版情報：九州大学, 2017, 博士（学術）, 課程博士
バージョン：
権利関係：

九州大学
KYUSHU UNIVERSITY

interdisciplinary Graduate School of Engineering Sciences IGSES

DEVELOPMENT AND IMPROVEMENT OF CFRP ADHESIVE JOINTS USING VACUUM-ASSISTED RESIN TRANSFER MOLDING (VARTM)

By

Mahmoud Ramadan Abusrea
マハムド ラマダン　アブスリア

A Thesis Submitted to the
Graduate School of Engineering Sciences at Kyushu University
in Partial Fulfillment of the
Requirements for the Degree of
DOCTOR OF ENGINEERING
in
Molecular and Material Science

KYUSHU UNIVERSITY
Fukuoka, Japan
2017

DEVELOPMENT AND IMPROVEMENT OF CFRP ADHESIVE JOINTS USING VACUUM-ASSISTED RESIN TRANSFER MOLDING (VARTM)

By
Mahmoud Ramadan Abusrea
マハムド ラマダン　アブスリア

A Thesis Submitted to the
Graduate School of Engineering Sciences at Kyushu University
in Partial Fulfillment of the
Requirements for the Degree of
DOCTOR OF ENGINEERING
in
Molecular and Material Science

Under the Supervision of

Prof. Kazuo Arakawa
Research Institute For Applied Mechanics
Kyushu University

KYUSHU UNIVERSITY
Fukuoka, Japan
2017

DEVELOPMENT AND IMPROVEMENT OF CFRP ADHESIVE JOINTS USING VACUUM-ASSISTED RESIN TRANSFER MOLDING (VARTM)

By
Mahmoud Ramadan Abusrea
マハムド ラマダン　アブスリア

A Thesis Submitted to the
Graduate School of Engineering Sciences at Kyushu University
in Partial Fulfillment of the
Requirements for the Degree of
DOCTOR OF ENGINEERING
in
Molecular and Material Science

Approved by the
Examining Committee

_____
Prof.

_____
Prof.

_____
Prof.

KYUSHU UNIVERSITY
Fukuoka, Japan
2017

Name: Mahmoud Ramadan Mohamed Abusrea
Date of Birth: 1984/02/07.
Nationality: Egypt
E-mail: abusrea@riam.kyushu-u.ac.jp
Phone: +81-080-2793-4922
Address: 4-7-8453 Hatta, Higashi-ku, Fukuoka

Registration Date: 2014/10/01
Awarding Date: …./…./……..
Degree: Doctor of Engineering
Department: Molecular and Material Science

Supervisor:

Prof. Kazuo ARAKAWA

Examiners:

Prof. Kazuo ARAKAWA
Prof. Hideharu NAKASHIMA
Prof. Wenxue WANG

Title of Thesis:

Development and Improvement of CFRP adhesive joints Using Vacuum-Assisted Resin Transfer Molding (VARTM)

Key Words:
CFRP joints, vacuum-assisted resin transfer molding, strength of joints

Acknowledgments

بِسْمِ اللَّهِ الرَّحْمَنِ الرَّحِيمِ
In the name of Allah, the Most Gracious and the Most Merciful

Alhamdulillah, all praises to my god, Allah, for the strengths and his blessing in completing this thesis.

First and foremost, I wish to express my sincere gratitude and appreciation to my supervisor, Professor Kazuo Arakawa. Professor Arakawa has fully supported me not only by providing academic guidance, but in all ways. Because he has always given me unlimited freedom and motivation, I was able to indulge my passion for studying various researches without any concern or stress.

I would like to thank our laboratory secretary Ms. Yoshii. She introduced a great help to facilitate all matters belong to our lab and my life as well. I would like to thank all our lab members. I would like to extend my appreciation to prof. Todo for his kindness and generosity.

I would like to acknowledge the scholarship program from Monbukagakusho (the Ministry of Education, Culture, Sports, Science and Technology, Japan), which allowed me to concentrate on my research without financial burden.
I would like to thank prof. Choi and his student Mr. Han for hosting me in their lab in Hanyang University to do a part of the experimental work. I would like to thank Mr. Yoon for his advises. I would like to extend my grateful to prof. Wenxue Wang and Mr. Matsubara for giving permission to cut the samples and do a part of the experimental tests

I would like to Assoc. prof. Kalaitzidou Kyriaki and his lab members, Dr. Amir Asadi and Mr. Mohamed Shafik for hosting me in their lab in Georgia Institute of Technology. They also introduced a great help to me during my stay in Emory hospital in Atlanta.

I would like to express my deepest gratitude to my advisory committee, Prof. Nakashima and Prof. Wenxue Wang for screening this thesis and for their valuable advices.

I'm would like to thank all my Egyptian friends here in Fukuoka. They have supported me and guided me in many situations. I felt I have a big family here in Fukuoka.

Lastly, this thesis would not be possible without the sincere encouragement, support, and patience from my wife Ms. Zeinab Okasha. I am deeply indebted to all my family in Egypt, my mother, my sisters and my brother

Mahmoud Abusrea
マハモド アブスリア
2017/06/13

Dedication

To the soul of my late brother Mohamed Abusrea (1972-2012)
and my late father Ramadan Abusrea (1949-2000)

Table of Contents

List of Tables

List of Figures

Abstract

The use of carbon fiber reinforced plastic CFRP composites in engineering structures brings many advantages because of their high performance and mechanical properties, such as high strength-to-weight and stiffness-to-weight ratios. For this reason, they have been used for heavy duty structures in aviation, space, automotive, shipbuilding, and wind turbine applications. These applications generally involve large scale manufacturing, so the parts are produced from smaller components and are joined together. So, the mechanical performance of these structures is highly dependent on the joining efficiency. Typically, wind-lens turbine structures are fabricated in segments, and then bonded to form the final structure. The main objective of this work is to develop CFRP adhesive joints with high mechanical performance for the wind-lens and other similar structures. This is to be done by either improving the current joints and/or developing new adhesive joints. First, the emphasis is given to develop new joints. Then subsequent improvements on these joints are to be done. All CFRP joints and fabrics is made using vacuum assisted resin transfer molding VARTM manufacturing process. The thesis's chapters are organized as follows:

Chapter 1 introduces a background and general introduction on wind-lens structures, CFRP composites, VARTM, and CFRP adhesive joints

Chapter 2 introduces five new adhesive joints, divided into two types: the first type is constructed between dry carbon and CFRP fabrics, and the second is constructed with two dry carbon fibers. These CFRP joints are made in our laboratory using VARTM manufacturing technique. Specimens are prepared for tensile testing to measure joint performance. The tensile test results show low strength when one half of the joint is CFRP fabrics, which was the case for the first two developed joints,

staircase join-1 and staircase joint-2. On the other hand, second joint type such as laminated joint and multiple-covers joint, showed higher tensile strength. Fracture analysis showed the same fracture pattern, crack initiation at the joint ends followed by crack propagation until fracture.

Chapter 3 describes the effect of using the stitching technique on the tensile strength of both CFRP adhesive joint types. Tensile test results revealed improved strength when stitching was applied to the multiple-covers and staircase joints. The improvement achieved for multi-overlapped joint higher than that for the staircase joint. For the staircase joint, the strength improvement caused by the extra carbon fiber pieces which were put at the joint ends not by applying the stitching technique.

Chapter 4 introduces the improvements that made for the first joint type. For this joint type, three adhesive joints were introduced: the first is the original stepped joint and the other two are improved stepped joints. Specimens were prepared for tensile testing to measure joint performance. The results showed an enhanced tensile load for the modified staircase joints. The percentage increase depended on the number of carbon fiber layers. For example, the total percentage increase in the tensile load recorded was 39% for the five-carbon-fiber- layer CFRP, with a further 14% increase for the seven carbon fiber layers. The final joining efficiencies reached 51% and 59% for five- and seven-carbon-fiber-layer CFRP fabrics.

Chapter 5 introduces the improvements that made for the second joint type. Further improvements were made by overlapping the two halves or adding extra carbon fiber pieces. Four laminated joints were investigated: the original laminated joint (OLJ), two overlapped joints, O20 and O40, with overlap lengths of 20 mm and 40 mm, respectively, and a multiple-covers joint (MLJ). Specimens were prepared for tensile

tests to evaluate joint performance. The overlapped joint O40 achieved the highest ultimate failure load, of 22.3 kN, with a 56% increase over the OLJ. The load-displacement curve showed a linear relationship in the first two stages for the OLJ and a non-linear relationship in the third stage. However, the entire load-displacement curve showed a linear relationship for the other joints. The joining efficiency ranged from 44.5% to 69.5% for all joints. The highest ultimate stress, of 1,250 MPa, was recorded for the O40 overlapped joint. Fracture analysis showed a delamination failure mode for the OLJ and O20 joints, while a mixture of delamination and fiber breakage failure modes was observed for the O40 and MLJ joints.

Chapter 6 continues the improvements that made for the second joint type. For this joint type, some improvements are provided to enhance performance in terms of bending strength. These improvements included stitching of the two halves together by carbon fiber bundles and inserting extra carbon fiber covers in the joint connection. We studied three adhesive joints: a conventional laminated joint and two improved laminated joints. All joints and CFRP fabrics were made in our laboratory using VARTM techniques. Specimens were prepared for bending tests to evaluate the joint performance. Two acoustic emission (AE) sensors were placed on a specimen to monitor fracture progresses during the test. The results, for the six-layer laminates, showed a considerable improvement in bending strength for the modified laminated joints. The percentage increases in the bending strength were 27% and 112% for stitched and multiple-cover laminated joints, respectively.

Chapter 1 : General Introduction

1.1. Introduction

1.1.1. Wind-lens turbines

Due to the limited supply of fossil fuels and environmental problems caused by their use, the development of renewable and clean new energy have become global issues. Particularly in Japan, the application of alternative energy sources is very important. Nuclear energy is one alternative energy source, and it has been developed extensively in Japan. Japan generates 30% of its electrical power from nuclear reactors, and had planned to increase that to 40%. However, the Fukushima Daiichi nuclear disaster caused by the earthquake in March 2011 demonstrated the potentially fatal risks when using nuclear power. Other clean energy sources are expected to replace it.

Wind energy is a promising alternative. It is developing rapidly and will play a major role in the new energy field. However, in comparison with the overall demand for energy, the scale of wind power usage is still small; in fact, the level of development in Japan is extremely small. As an island nation, it is difficult to find suitable areas for wind-power plants. At the same time, the complex terrain and the turbulent nature of the local winds make it difficult to apply current wind-power techniques widely in Japan.

To address these problems, a new efficient wind-power turbine system has been developed by a research group at the Division of Renewable Energy Dynamics of the Research Institute for Applied Mechanics, Kyushu University [1-3]. This system has a

diffuser shroud at the circumference of its rotor to concentrate the wind energy, as shown in Figure 1.1 and Figure 1.2. This diffuser is called a "wind-lens". With this system, even low-speed winds can be used for power. Moreover, a plan for an offshore wind farm is under study. In the future, this wind-power turbine system will likely be used offshore to harness wind power over the sea. Such a wind-power turbine system will be based on a floating structure. Consequently, high-strength and lightweight materials will be required.

Generally, there are three requirements for materials in a turbine system [4]:

1. High material stiffness is needed to maintain optimal aerodynamic performance,
2. Low density is needed to reduce gravity forces, and
3. Long fatigue life is needed to reduce material degradation.

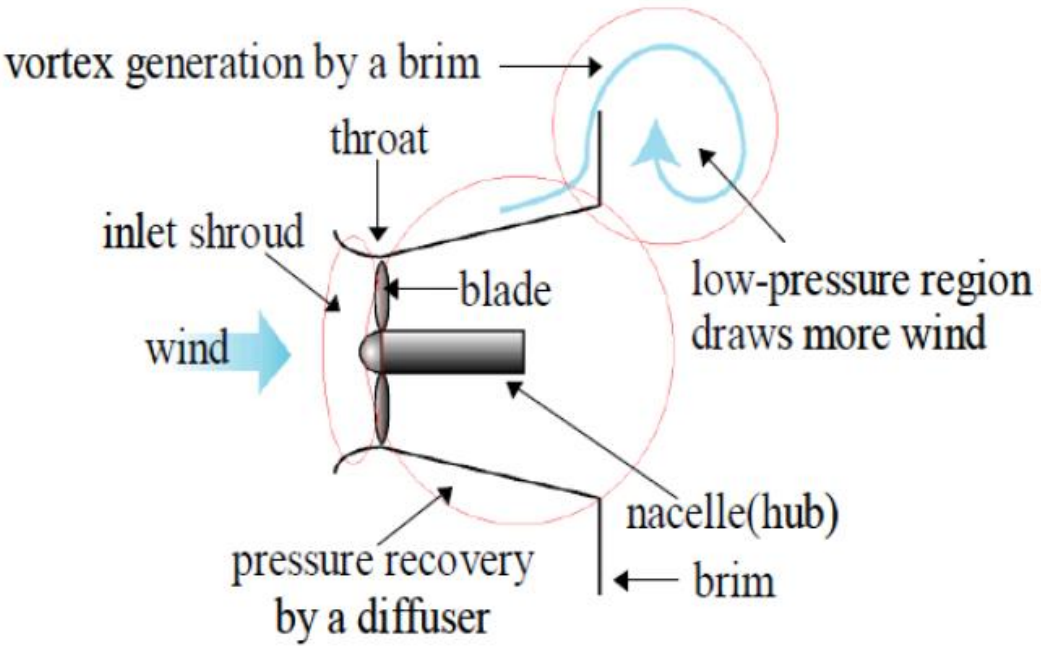

Figure 1.1: Wind power turbine system with a diffuser designed by Kyushu University [3]

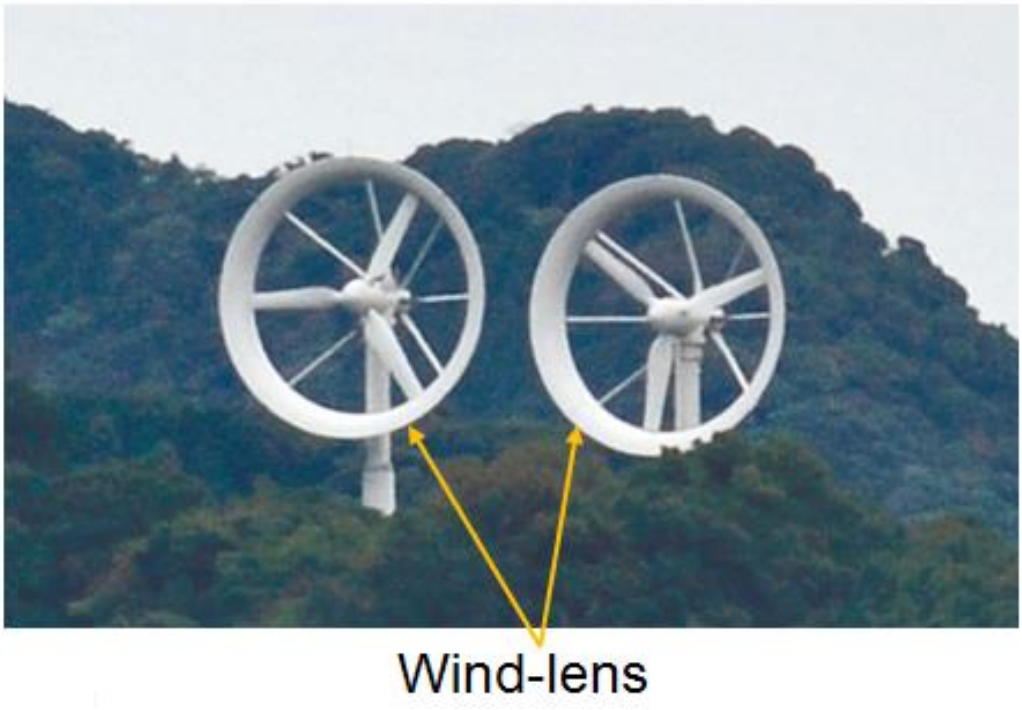

Figure 1. 2: Photograph of the wind-lens power system [3]

1.1.2. Carbon fiber reinforced plastic (CFRP) composite materials

Fiber-reinforced composite materials are promising candidates for many applications such as aviation, space, automotive, shipbuilding as well as wind turbines [5-11]. They have excellent mechanical properties in terms of stiffness-to-weight and strength-to-weight ratios. By far, the most widely used fibers are glass fibers, carbon fibers, aramid, polyethylene, and cellulose [4]. Among these fibers, carbon fibers and their composites have excellent combinations of very high stiffness, high strength, and low density [12]. Therefore, carbon-fiber reinforced composites (CFRPs) would be useful for fabricating a wind-lens for a wind-power generating system at sea.

1.1.3. Vacuum assisted resin transfer molding VARTM process

Composite structures may be fabricated using an autoclave with a pre-preg process (See Figure 1.3). However, it is difficult to fabricate products with complex shapes and large areas using autoclaves, resulting in substantial installation costs [13]. To overcome this limitation, liquid composite molding (LCM) has been utilized as alternative method. The LCM process is one composite manufacturing method in which a low-viscous thermosetting resin is injected into a woven or stitched reinforcement placed inside a mold. Components with complex shapes can be fabricated in a single step. Two common LCM processes are resin transfer molding (RTM, Figure 1.4) and vacuum assisted resin transfer molding (VARTM, Figure 1.5), but there are also other processes such as RTM 'light' and compression resin transfer molding (CRTM) [14]. The features of each method are listed in Table 1.1.

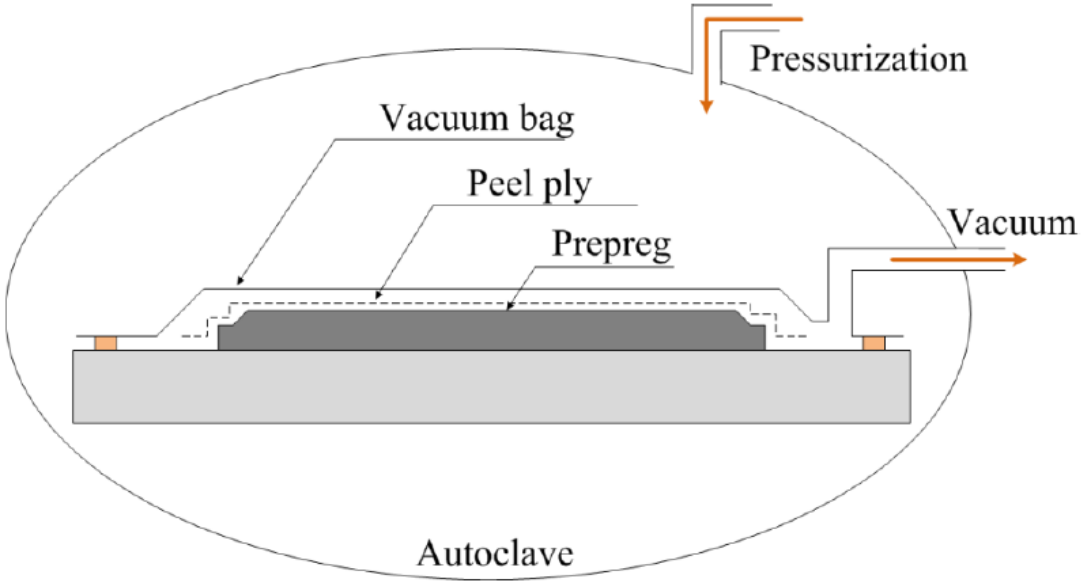

Figure 1.3: Typical illustration of an autoclave process [12]

Table 1. 1: Features of various LCM processes [14]

LCM process	Feature	
RTM	Mold configuration	Two rigid molds are used to compact the product.
	Advantage	The finished product has very good surface quality and excellent dimensional tolerance.
	Limitation	Since the process needs to push the viscous resin through the gap between two compacted molds, the injection process may require a significant amount of time, depending on the flow resistance.
VARTM	Mold configuration	A vacuum bag covers a rigid mold, and a vacuum is drawn. The vacuum plays a role in compacting the mold and drawing the resin in.
	Advantage	Large parts can be fabricated and the equipment cost is reduced.
	Limitation	The bag-side surface quality is relatively low and the dimensional tolerances are also compromised.
RTM-light	Mold configuration	Very similar to VARTM, but a compliant mold is used in the vacuum bag to improve the dimensional tolerances. The distribution medium is usually forms an integral part.
	Advantages	Better surface quality compared to VARTM.
	Limitations	The surface uniformity is worse than VARTM and remains an issue.
CRTM	Mold configuration	The resin is injected into a partially open mold. The resin is quickly distributed in the gap between the mold and the preform, forming a surface with high permeability. Then, the mold is closed and compacted, and the resin is squeezed into the unsaturated regions.
	Advantage	Production rates can be increased.
	Limitation	The mold requires more equipment than other LCM processes.

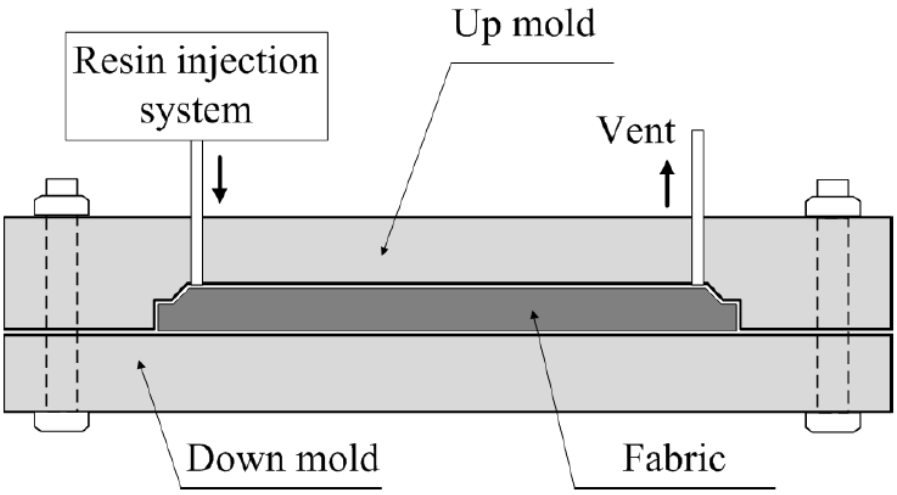

Figure 1.4: Typical illustration of RTM process [12]

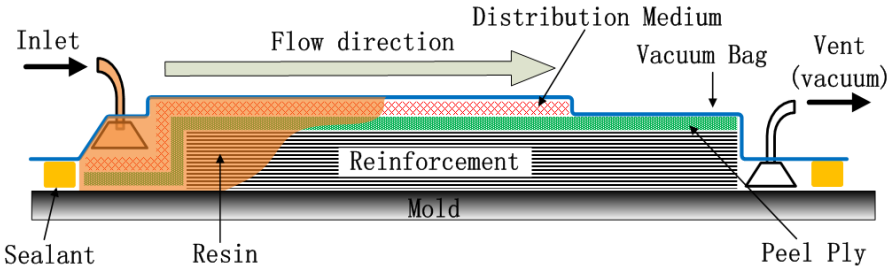

(a)

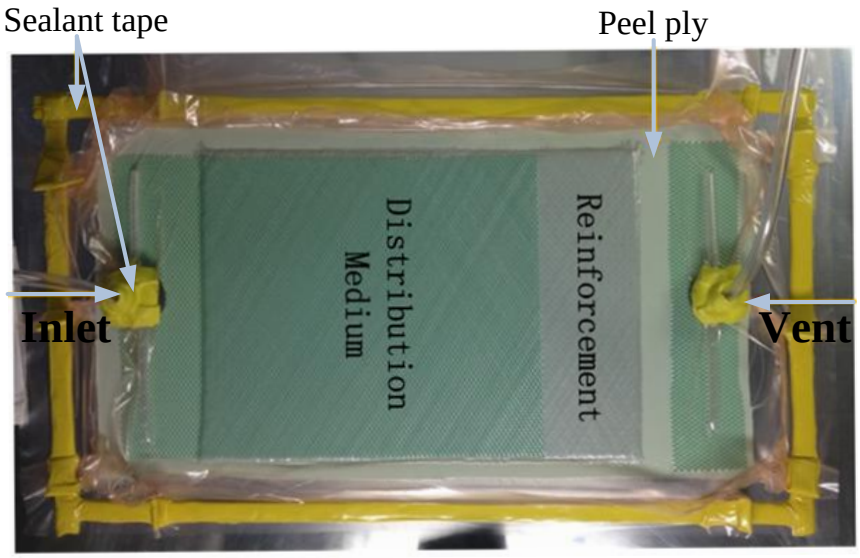

(b)

Figure 1.5: (a) A schematic view of the VARTM process used in this work and (b) Picture of adopted VARTM process

Since this study was aimed at wind-lens turbine components, the costs and accessibility were assigned higher priorities than the products rate. Therefore, the VARTM process was selected for the LCM. Figure 1.5a shows a detailed drawing of the VARTM process.

In a VARTM process, reinforcements are stacked on a solid mold which is prepared with release agent, and covered by a peel ply and a distribution medium. They are enclosed together with an inlet and a vent in a vacuum bag and sealed with tape. Figure 1.5b shows a photograph of a vacuum package in our experiments. After drawing vacuum in the package, the resin can be infused from the inlet by the pressure difference between the inside and the outside of the package. After the reinforcement is completely infused, the inlet is closed. In order to get a higher fiber volume fraction, the vent is usually left open to extrude the extra resin inside the vacuum package until the resin becomes too viscous to flow. After the resin cures, a laminate composite is obtained after demolding process. A release agent painted on a solid mold and peel ply are used to separate the final product from the other layers. Without them, the final composite product will attach to the mold and the distribution medium, making the demolding process very difficult. Because the infusion pressure is only 1 atmosphere, the infusion speed inside the reinforcement is very slow. For large and thick parts, the vacuum level may not be sufficient to complete the infusion. Consequently, a distribution medium is often required, such as a plastic mesh, which has much higher in-plane permeability than a fabric stack, allowing for fast surface resin wet-out. Subsequent resin penetration allows for complete infusion. A spiral tube is often used in the inlet and vent structures to make a point inlet (and vent) become a line inlet (and vent). It is critical to choose the location of the vent

appropriately to completely infuse the reinforcement and avoid creating resin-starved regions near the vent locations after the inlet is closed.

1.1.4. CFRP composite joints

The use of CFRP composite materials in engineering structures brings many advantages because of their high performance and mechanical properties, such as high strength-to-weight and stiffness-to-weight ratios [5]. For this reason, they have been used for heavy duty structures in aviation, space [7-10, 18], automotive [9], shipbuilding [7], and wind turbine applications [19]. These applications generally involve large scale manufacturing, so the parts are produced from smaller components and are joined together. The mechanical performance of these structures is highly dependent on the joining efficiency.

Because composite joints work as structure-critical load-carrying elements, the design and analysis of composite joints have attracted much attention in a series of light, low-cost, and efficient composite integration projects [20]. 'Traditional' mechanical fasteners, such as bolts, pins, and rivets, have been used to join CFRP structures [21-23]. This composite joining technique is generally characterized by simplicity and the fact that such joints can be disassembled [24]. However, drilling holes in composite parts before fastening may cause problems due to stress concentration and weight increases. In contrast, adhesively bonded joints have mechanical advantages over bolted joints because the fibers are not cut, and stresses are transmitted more homogeneously [25]. They offer better structural integrity, lower weight, and higher strength-to-weight ratios [26, 27]. For this reason, the adhesively bonded joints will be focused in the current work.

In the current work, the adhesive joints can be classified into two types: (1) dry carbon fabrics joints and (2) CFRP fabrics joints. In the first joint type, the joint's halves are dry carbon fibers. These two halves are stacked together in different way depending on the joint design and then molded together in one time to the final joint fabric. This kind of joints is featured with high strength and short time fabrication. The second joint constructed using at least one half of CFRP fabric. This type of joint accomplished through two molding times. The first molding is used to fabricate the CFRP fabric and the second to make the joint itself. Compared to the first joint type these joints usually achieve lower joining efficiency. However, it is easier to make CFRP parts first and then join them together rather than making the whole structure in one time which is happening in the first joint type.

1.2. Motivations and objectives of the present work

Today, adhesive composite joints are used widely in many composite structures in aerospace, turbine, and ship designs [6]. These structures are manufactured from several parts, which are joined to form the final structure. Typically, wind-lens turbine structures are fabricated in segments, and then bonded to form the final structure. These structure usually joined conventionally using traditional joints, which include single-lap [25, 28], double-lap [29, 30], and stepped [31, 32] joints. However, the mechanical performance for these joints still limited. It is known that these engineering structures are subjected to combinations of mechanical loadings, including static, fatigue, and impact loadings. Therefore, the need for high performance adhesive joints is very crucial.

The main objective of this work is to develop CFRP adhesive joints with high mechanical performance for the wind-lens and other similar structures. This is to be done by either improving the current joints and/or developing new adhesive joints. First, the emphasis will be given to develop new joints. Then subsequent improvements on these joints will be done. All CFRP joints and fabrics will be made using VARTM manufacturing process.

1.3. Scope and Organization of the thesis

According to Figure 1.6, the remainder of this thesis is organized as follows: Chapter 2 introduces five new adhesive joints, divided into two types: the first type is constructed between dry carbon and CFRP fabrics, and the second is constructed with two dry carbon fibers. These CFRP joints were made in our laboratory using VARTM manufacturing techniques. Specimens were prepared for tensile testing to measure joint performance. The next chapters introduce subsequent improvements for both types. Chapter 3 describes the effect of using the stitching technique on the tensile strength of both CFRP adhesive joint types. Chapter 4 introduces the improvements that made for the first joint type. For this joint type, three adhesive joints were introduced: the first is the original stepped joint and the other two are improved stepped joints. Specimens were prepared for tensile testing to measure joint performance. Chapter 5 introduces the adjustments were made for type 2 joints. In this chapter the mechanical performance in terms tensile strength was measured to asses these adjustments. The adjustments were made by overlapping the two halves or adding extra carbon fiber pieces.

Four laminated joints were investigated: the original laminated joint (OLJ), two overlapped joints, O20 and O40, with overlap lengths of 20 mm and 40 mm, respectively, and a multiple-covers joint (MLJ). Specimens were prepared for tensile tests to evaluate joint performance. The fracture modes for all joints were done by optical microscopy. Finally, chapter 6 continues the improvements that made for the second joint type. These improvements include the stitching of the two halves together using carbon fiber bundles and inserting extra carbon fiber covers in the joint connection. For this joint type, three adhesive joints were studied: a conventional laminated joint and two improved laminated joints. Specimens were prepared for bending tests to evaluate joint performance. Two acoustic emission (AE) sensors were placed on the specimen to monitor fracture progress during the test. The fracture modes for all joints were done by optical microscopy and/or scanning electron microscopy SEM.

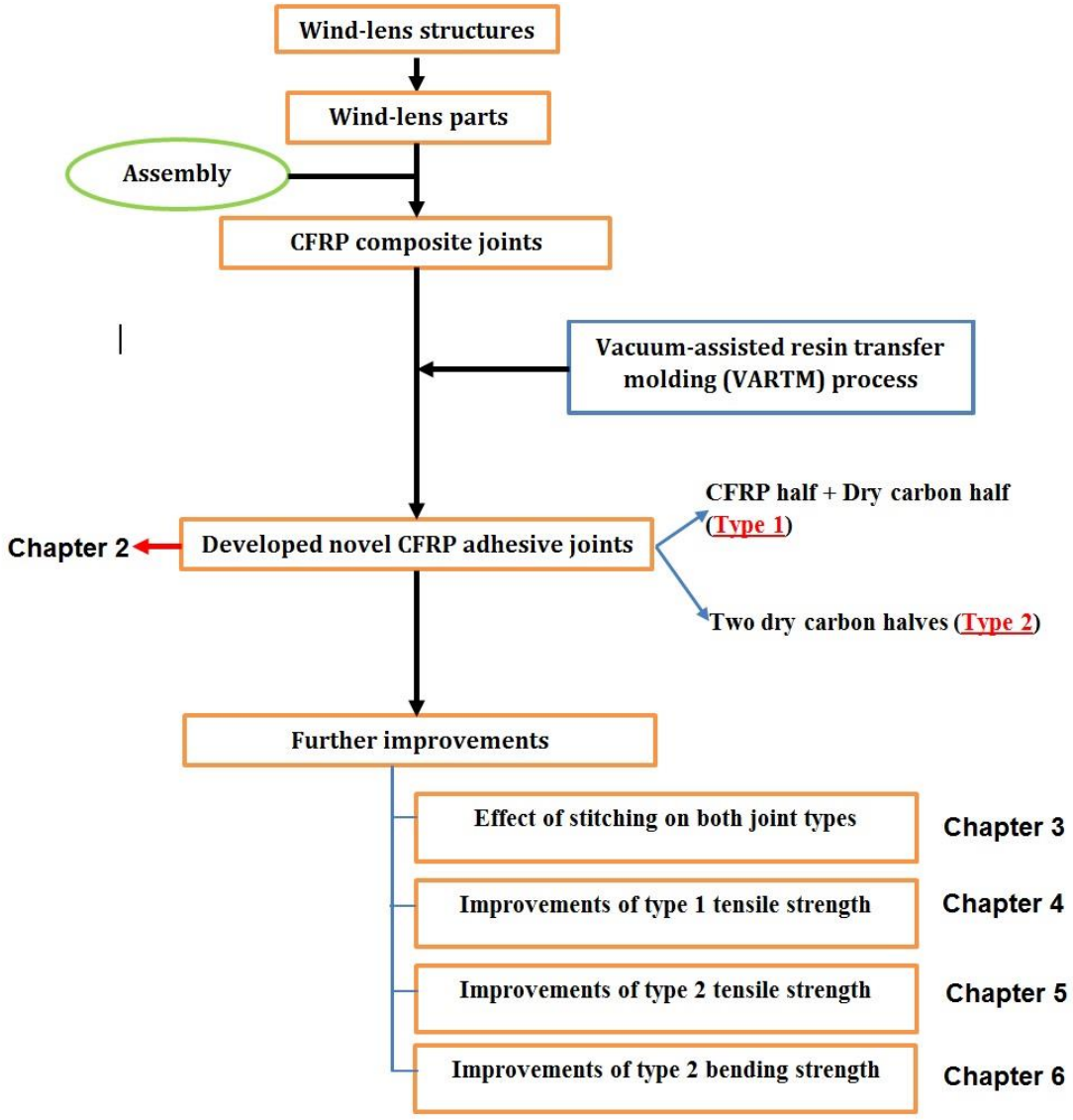

Figure 1.6: Organization of the current research work

Chapter 2
Novel CFRP Adhesive Joints for Wind-lens offshore structures

2.1. Introduction

Carbon fiber reinforced polymer (CFRP) composites are important for structural applications in the transportation industry and other areas, where lightweight design is advantageous for operational costs. When composite materials are used to fabricate a large complicated structure, joints between different parts are inevitable. As such, the structural integrity depends critically on the joint performance and not just on the basic composite structure.

This chapter introduces five new adhesive joints. These joints can be divided into two types: type 1 and type 2 joints. The first type is constructed between dry carbon and CFRP halves, and the second is constructed between two dry carbon fibers halves. These CFRP joints were made in our laboratory using VARTM manufacturing techniques. Specimens were prepared for tensile testing to measure joint performance novel adhesive bonded joints, made of CFRP, for using in offshore wind-lens structures. These newly developed joints are dedicated to the offshore wind-lens and other similar structures. The tensile strength of five joints will be assessed. All joints and CFRP material tested in this study were made using a VARTM process.

2.2. Experimental work

2.2.1. Materials

The CFRP composites consisted of carbon fabric and a resin mixture. The resin was a mixture of XNR6815 and XNH6815 at a weight ratio of 100:27. The resin mixture viscosity at 25°C was 260 mPa.s. The carbon fiber used for this work was made by Saertex GmbH & Co. KG. Table 2.1 introduces the characteristics for this carbon fiber.

Table 2.1: Characteristics of the carbon fiber used for this work

Carbon fiber designation	Style	No. of filaments	Weight	Density	Tensile strength	Tensile modulus	Elongation
			g/m^2	g/cm^3	MPa	GPa	%
STS40	UD	24,000	511	1.78	4,300	240	1.8

2.2.2. Adhesive joints

Four adhesive joints were tested. These joints were divided into two types. One was constructed using dry carbon fabrics and CFRP. In this type, the CFRP half of the joint was manufactured first, and then re-molded again with dry carbon fabric. Figure 2.1 shows two joints which represent the first joint type. These joints namely called staircase joint-1 and staircase joint-2. For both joints, a stepped CFRP part is made first. Then this part is remolded with the other dry carbon fibers half. In Figure 2.1, the left half of both joints is a stepped CFRP portion that had been molded, and the right side represents a dry carbon fabric. The major difference between the two joints is the number of CFRP steps. For instance, staircase joint-1 consists of 2 steps, while staircase joint-2 consists of 4 steps (see Figure 2.1). The second joint type was constructed with two dry carbon fiber halves; thus, the whole joint was made in a

single step. Two joints were designed and fabricated for this joint type. These joints were namely called laminated joint and multiple-covers laminated joint, respectively. Laminated joint was made by stacking the two carbon fiber halves together and a joint length of 40 mm was made (see Figure 2.2a). Each carbon fiber layer was stacked in which one half is 40 mm longer than the other half. The second joint, multiple-covers, was made by stacking the two carbon fiber halves with equal length and inserting extra carbon fiber pieces between each layer in a structural manner similar to the sandwich structures (see Figure 2.2b). Four carbon fiber layers were used for all joints.

2.2.3. Manufacturing

All CFRP fabrics were produced using VARTM process. The entire process consist of three steps: constructing a vacuum package, infusing the resin and molding. The structure of the vacuum package used in the experiment is shown in Figure 1.5a. A solid mold, covered with a piece of peel ply, was used. Four layers of stitched unidirectional carbon-fiber fabric (from Saertex GmbH & Co. KG, the carbon fiber is TENAX STS, the stitching material is PES) with 30 cm in length were laid on the peel ply and then covered by another piece of peel ply. The horizontal direction of Figure 1.5a was the fiber direction. A small piece of distribution medium, a kind of mesh, was placed on the peel ply to promote the flow of resin.

The inlet for infusion, which was composed of a rubber connecter and a segment of spiral tube, was positioned on the distribution medium. The vent for air and excess resin elimination was positioned on the other side of the inlet. Both inlet and vent were composed of a rubber connecter and a segment of spiral tube. Since inlet and

vent considered very critical points in the entire process they are tightly sealed by the sealant tape. Finally, the entire package was enclosed in a vacuum bag and sealed with tape. Figure 1.5b shows a picture of the adopted structure. After establishing a vacuum, degassed resin was infused from the inlet. After 40 min, the inlet was closed, and the vent was left open until the resin was cured. An epoxy resin that could be cured at room temperature (XNR/H 6815, supplied by Nagase & Co., Ltd.) was used in the experiment. The initial viscosity of the resin at 25^{o}C was 260 MPa s. When the resin was cured completely (about 24 h later), the CFRP laminate was removed from the mold. The thickness of the plate was about 2 mm.

2.2.4. Test procedures

Joint strength was evaluated via tensile testing using standardized test specimens [27]. Figure 2.3 shows the dimensions of the specimens; the total length was 250 mm and the width was 10 mm. Pairs of GFRP tabs were used to reduce the stress when holding each specimen. All specimens are tested using SHIMADZU DSS-5000 universal testing machine. Figure 2.4 shows the setup used for the current tensile test. The specimen was fixed between the machine's jaws, and the load-time data was recorded through a load cell mounted on the upper jaw. A real time camera connected to PC was mounted to record the deformation of the specimen during the loading.

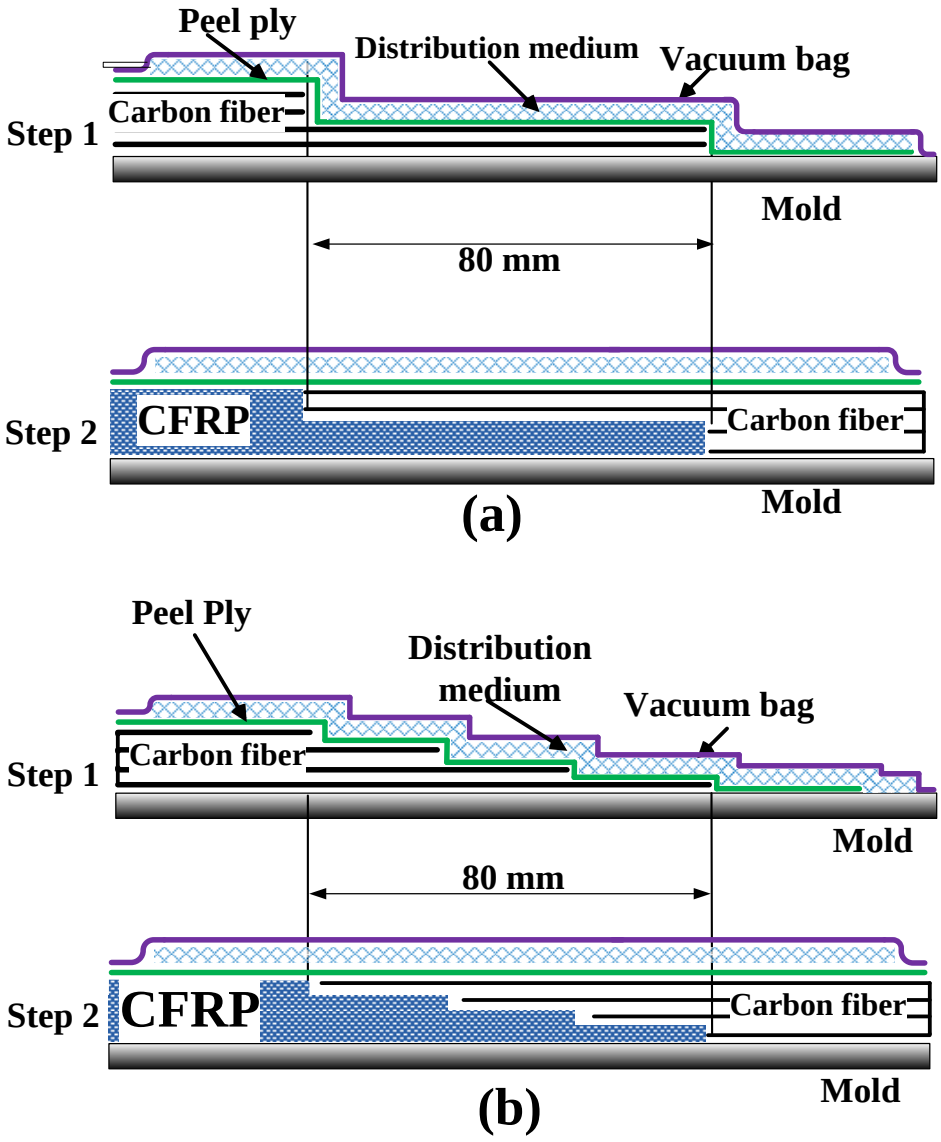

Figure 2.1: Joint group 1: (a) staircase joint-1, and (b) staircase joint-2

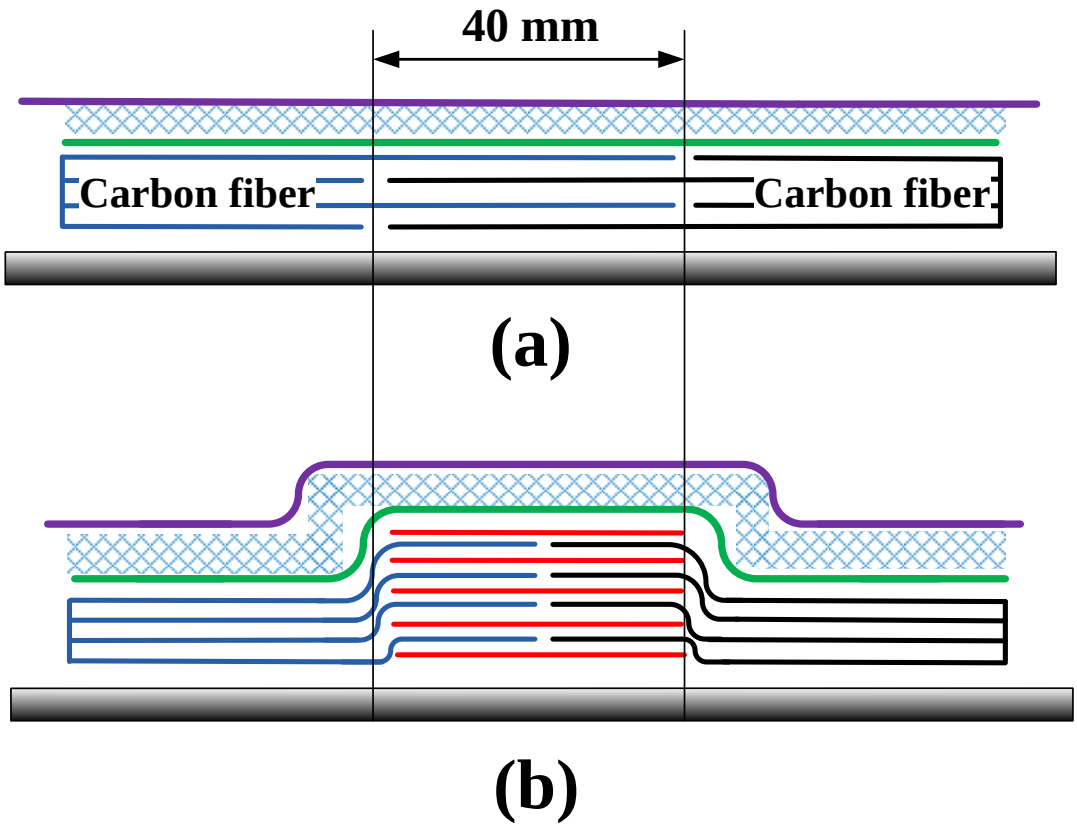

Figure 2.2: Joint group 2: (a) laminated joint-1, (b) laminated joint-2, and (d) multi-overlapped joint.

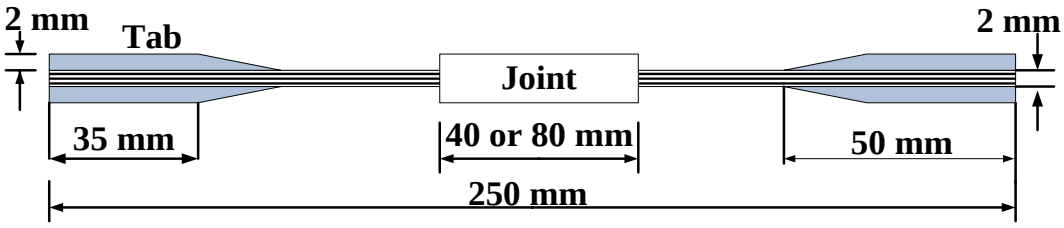

Figure 2.3: The standard specimen dimensions used for tensile testing

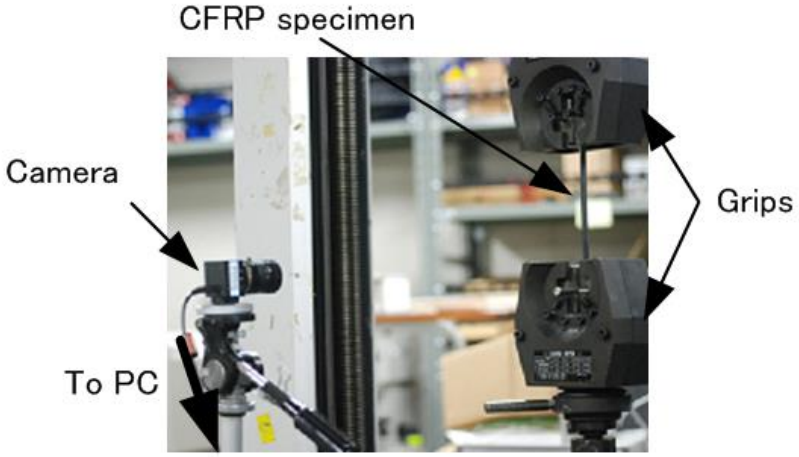

Figure 2.4: Tensile test setup for the current work

2.3. Results and discussions

The maximum tensile load was recorded as a measure of the joint's mechanical performance. First, the tensile load of the jointless CFRP samples was measured, and used as a reference for the strength of subsequent joints. The jointless CFRP achieved a failure tensile load of 34 kN (See Figures 2.5 and 2.6), indicating that the tensile strength along the fiber direction was 1.7 GPa.

Figure 2.5 shows the maximum tensile load for joint type-1 samples. The lowest joint tensile strength recorded was for staircase joint-1, with a measured strength of 8.8 kN (26% joining efficiency). However, the strength of the other staircase joint, staircase joint-2 was significantly higher (14.3 kN; 42% joining efficiency). This is in agreement with previous studies that have suggested that joining carbon fabrics and CFRP fabrics results in low strength [27]. This behavior can be attributed to two factors. First, resin residue on the CFRP surface before joining can act as an insulator. Second, the absence of overlap contact in these joints reduces the contact area, resulting in a weaker joint [8]. On the other hand, staircase joint-2 achieved a much

higher strength than joint-1. This is attributed to the three fiber layers in that joint type that contact the CFRP part, three times more than the number of layers in joint-1. Hence, joining dry carbon fabrics together resulted in generally higher strengths.

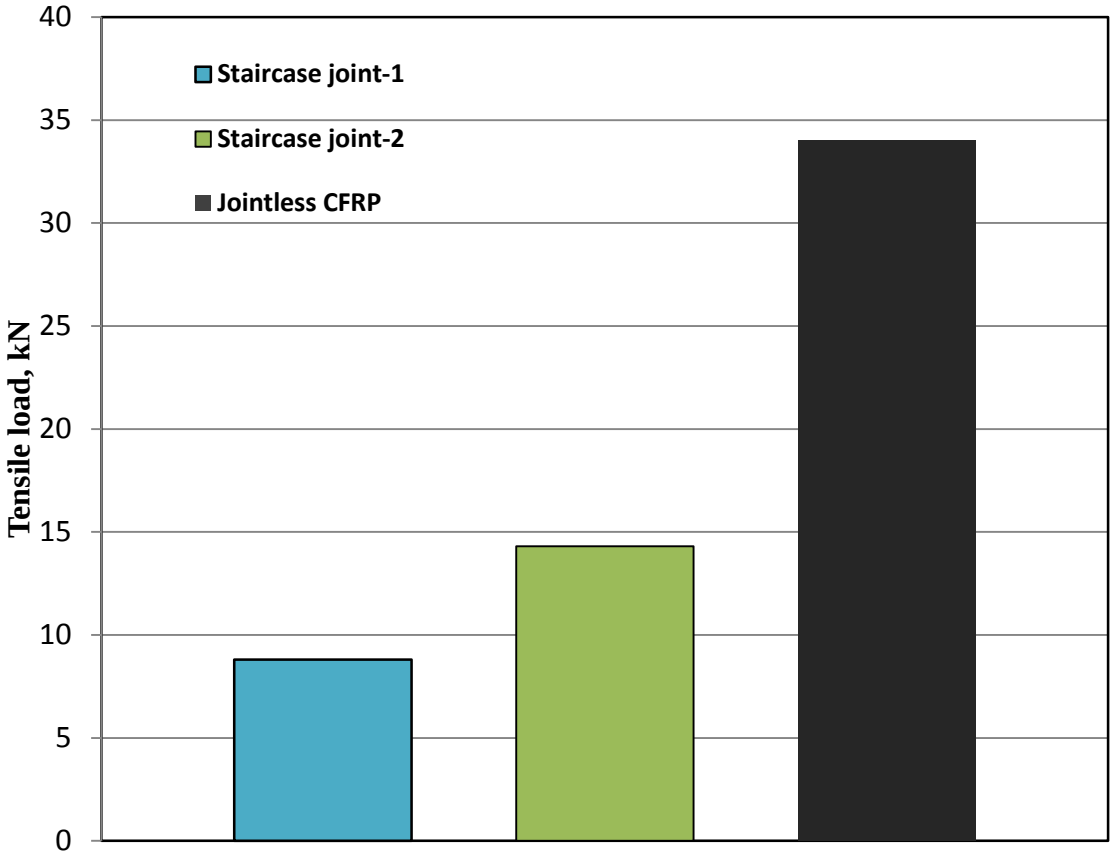

Figure 2.5: Maximum tensile load data of joint type-1 and jointless CFRP samples

Figure 2.6 shows the maximum tensile load for joint type-2 samples, the laminated joint had a tensile strength similar to that of staircase joint-2, with a measured strength of 14.7 kN. This can be attributed to the absence of overlap contact between the two halves in laminated joint, which reduces the strength and promotes crack propagation near the joint ends. The introduction of overlap areas not only increases the contact area, but also increases joint thickness. On the other hand, the

remaining two joints were much stronger than the previous four joints. Multiple-covers joint had tensile load and joining efficiency of 28.8 kN and 85%, respectively. This joint performed with the major difference being the greater thickness of the multiple-covers joint, which could be the reason for the higher observed strength. Löbel et al. [8] constructed CFRP joints based on stainless pins, which resulted in a high joining efficiency of 83%. However, the metal-to-carbon fiber contact caused galvanic corrosion of the carbon fabrics, weakening the structure over time [42].

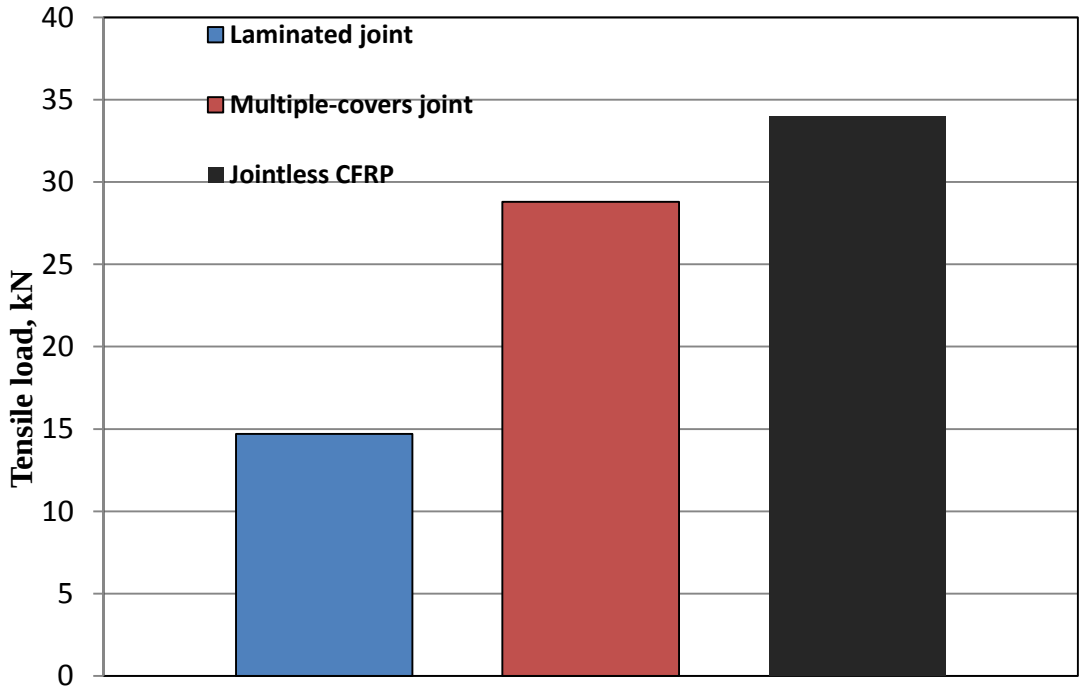

Figure 2.6: Maximum tensile load data of joint type-2 and jointless CFRP samples

Figure 2.7 shows a typical tensile load-displacement diagram combined with images that show the deforming specimen of the staircase joint-1. In staircase joint-1, an initial crack occurred near the end of the joint, which reduced the gradient of the load-displacement curve. This resulted in a linear relationship between the tensile load

and displacement. As the load increased, the crack size also increased until the specimen ultimately fractured. As noted, the initial cracking occurred at the end of the joint. This behavior can be explained as follows. In staircase joint-1, when joining the CFRP with carbon fabric, two separation lines were formed on both surface sides (Figure 2.8). These two lines were filled with resin after joining, and the crack initiated at these lines at the beginning of the tensile test. As the tensile load increases, the shear stress in the contact area increases and this causes relative motion between the CFRP portions. This leads to the enlargement of both separation lines and hence crack propagation.

The failure patterns were also investigated for other joint types. Figure 2.9 shows a typical tensile load-displacement diagram for Multiple-covers joint. Two cracks appeared near the joint ends, due to the accumulation of stress in these zones, which apparently caused a gradient change. Then the cracks propagated until specimen fracture. Figure 2.10 shows a schematic drawing of the multiple-covers joint. The possible zones of fracture are near the joint ends, where there is an accumulation off stress.

There are seven failure modes, including but not limited to the separation of the interface between the adhesive and composite, de-lamination within the composite, and a mixture of these two modes [43]. Micromechanical investigations have revealed different dominant failure modes under tensile and shear loads [36]. In addition, the strength of the interface between the adhesive and composite at a joint is a key factor determining the failure mode and the strength of a structure. In the present study, both staircase joints 1 and 2 showed separation of the interface, whereas joint group 2 showed a mixture of failure modes.

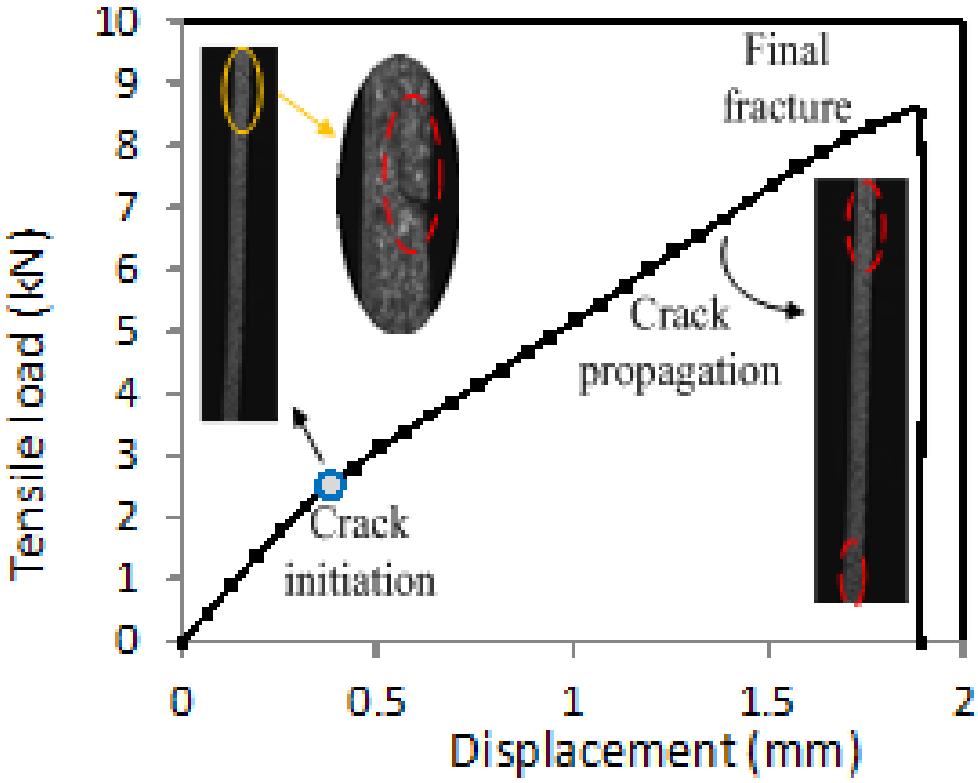

Figure 2.7: A diagram of typical tensile load-displacement, with images for staircase joint-1.

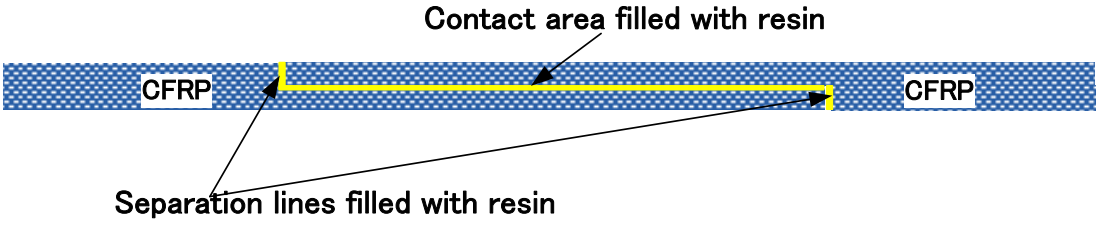

Figure 2.8: Schematic drawing of a staircase joint after bonding

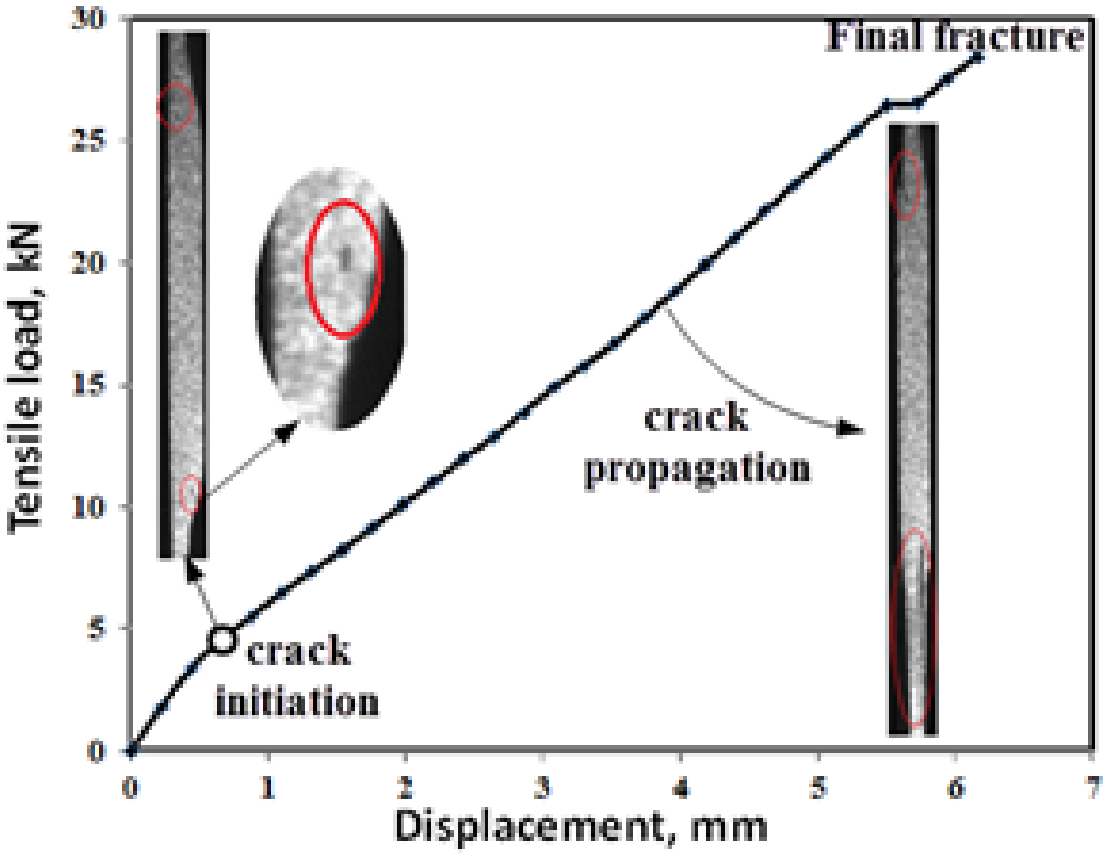

Figure 2. 9: Typical tensile load-displacement diagram with images for a multiple-covers joint

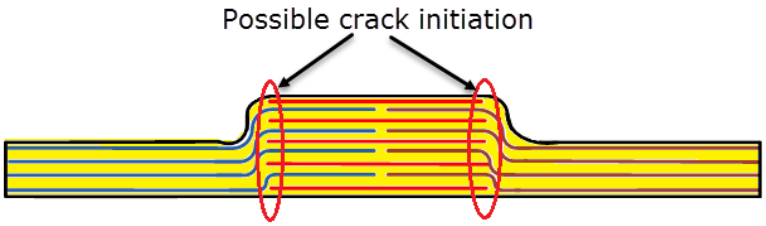

Figure 2.10: Schematic drawing of a multiple-covers joint with possible crack zones highlighted

2.4. Conclusions

Four adhesive joints were designed and fabricated using VARTM manufacturing process. The tensile test results showed low strength when one half of the joint is CFRP fabrics, which was the case for the first two developed joints, staircase joint-1

and staircase joint-2. In these joints, it was investigated that the residue resin on the CFRP half's surface worked as insulator, and hence the shear strength along the interface was reduced. On the other hand, multiple-covers joint, showed higher tensile strength. However, joining techniques that use dry carbon fibers are still limited for simple shapes, so there are some difficulties for applying these techniques for complex curved shapes like wind blades and lens as well.

To sum up, type 1 joints are weaker, longer fabrication time. But, it's more practical and can be used to join complex shapes. In contrast, type 2 joints are stronger, shorter fabrication time, but it's more complex. Therefore, both joint types should be considered for the future improvements.

Chapter 3
Effect of stitching on the tensile strength of the current novel joints CFRP adhesive joints

3.1. Introduction

In chapter 2, two CFRP adhesive joint types were introduced. Joint type 1, which is constructed between CFRP fabric and dry carbon fibers halves. This joint was represented by two staircase joints named staircase-1 and staircase-2. Joint type 2 is fabricated by stacking two dry carbon fibers halves. This joint represented by two joints called laminated and multiple-covers joints. Compared to joint type 1, joint type 2 was stronger and shorter fabrication time. However, joint type 1 is more practical and less complex. Therefore, when applying further improvements, both joint types should be considered.

In CFRP composite structures, joints are crucial load-carrying elements, and the mechanical performance of the whole structure depends on the joining efficiency. In other words, the strength of the CFRP composite structure is equal to the strength of its joint. Therefore the improvement of CFRP adhesive joints is very crucial. There remains significant scope for improvement in the strength and durability of bonded joints [8]. Stitching is considered to be an effective method of forming strong bonded composite joints [8], and Hes et al. [44] and Dransfield et al. [45] showed that this technique could enhance the fracture toughness of composites under peel load conditions.

This chapter studies the effect of stitching on both CFRP joint types, which introduced in chapter 2. The stitching technique will be applied for two joints, staircas

e joint-2 and multiple-covers joint. For the staircase joint-2, the original staircase joint -2 was put in comparison with the adjusted one. The adjustment was applied by stitching with carbon fiber bundles (see Figure 3.1 a-c). Similarly for multiple-covers joint, its original form was put in comparison with its stitched form (see Figure 3.2 a-c).

3.2. Experimental Methods

3.2.1. Materials

The CFRP composites consisted of carbon fabric and a resin mixture. The resin was a mixture of XNR6815 and XNH6815 at a weight ratio of 100:27. The resin mixture viscosity at 25°C was 260 mPa.s. The carbon fiber used for this work was made by Mitsubishi Rayon Co. LTD. Table 3.1 introduces the characteristics for this carbon fiber. Five unidirectional carbon fabric layers were stacked and molded together to form 1.5-mm-thick plates.

Table 3.1: Characteristics of the carbon fiber used in this work

Carbon fiber designation	Style	No. of filaments	Weight	Density	Thick.	Tensile strength	Tensile modulus	Elongation
			g/m^2	g/cm^3	mm	MPa	GPa	%
TRK976P QRW	UD	12,000	317	1.82	0.33	4,900	253	1.9

3.2.2. Adhesive joints

Two different types of joint were used with the stitching technique. One joint was constructed using dry carbon fiber fabric and CFRP. A stepped CFRP fabric was manufactured first, which was then re-molded with dry carbon fiber fabric. This joint is called staircase joint. Figure 3.1a shows a schematic top view of the VARTM mold for all staircase joints. Figure 3.1b shows the original staircase joint. The stitching was

applied perpendicularly through both CFRP and dry carbon fibers halves using carbon fiber bundles. The stitches compose a matrix in which its rows are in the fiber direction (resin flow direction), and the columns are in the other perpendicular, see Figure 3.1a. The stitch length is 8 mm, and the distance between columns is 10 mm, see Figure 3.1c.

The other joint type was constructed using two dry carbon fiber halves. With this joint, two five-layer carbon fiber sheets were stacked. This joint is termed multiple-covers joint. Figure 3.2a shows a schematic top view of the VARTM mold for all multiple-covers joints. The original form for this joint is shown in Figure 3.2b. In this joint, the separation between the two mated carbon layers was covered using two 40-mm-wide carbon fiber pieces. The second form for multiple-covers joint is shown in Figure 3.2c. With this joint, we used stitching with carbon bundles of the same carbon fiber type, which were applied perpendicular to the plane of the laminate [44-45]. All joints were formed using a single VARTM process.

3.2.3. Manufacturing

All CFRPs' parts were formed using VARTM, which is a variation of the resin transfer molding (RTM) technique, in which a solid mold with a flexible tape-sealed vacuum bag is used instead of a closed mold. In the VARTM process, reinforcements are stacked on a solid mold, which is treated with a mold-releasing agent and covered with a peel-ply and a distribution medium. These are enclosed in a vacuum bag, which has an inlet and a vent, and which is sealed using gum tape, as shown in Figure 3.3.

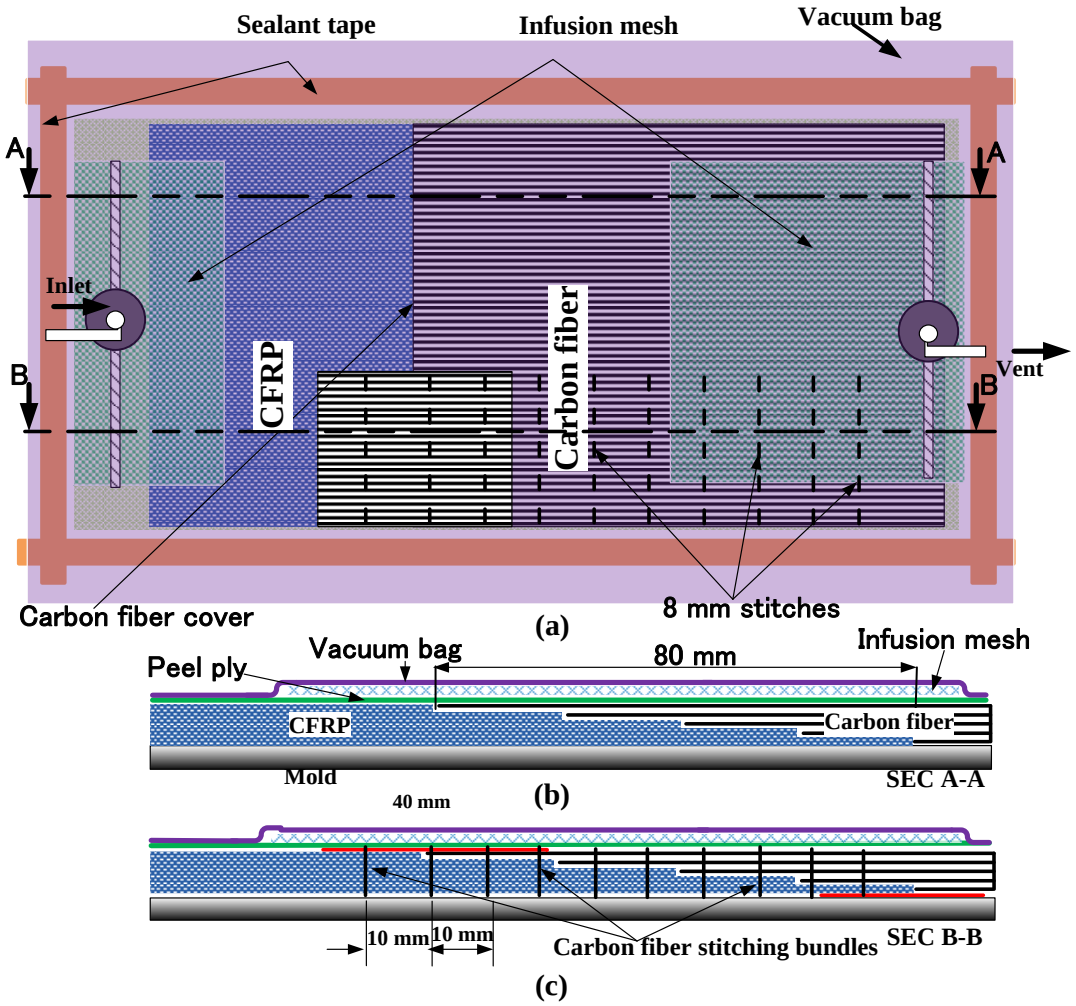

Figure 3. 1: (a) Schematic top view of the staircase joints: (b) original staircase and (c) stitched staircase joints

3.2.4. Test procedures

The strength of the joints was evaluated via tensile testing using standardized test specimens [27]. Figure 3.4a shows the dimensions of the specimens; the total length was 250 mm and the width was 10 mm. Pairs of CFRP tabs were used to reduce the stress when holding each specimen, as shown in Figure 3.4b.

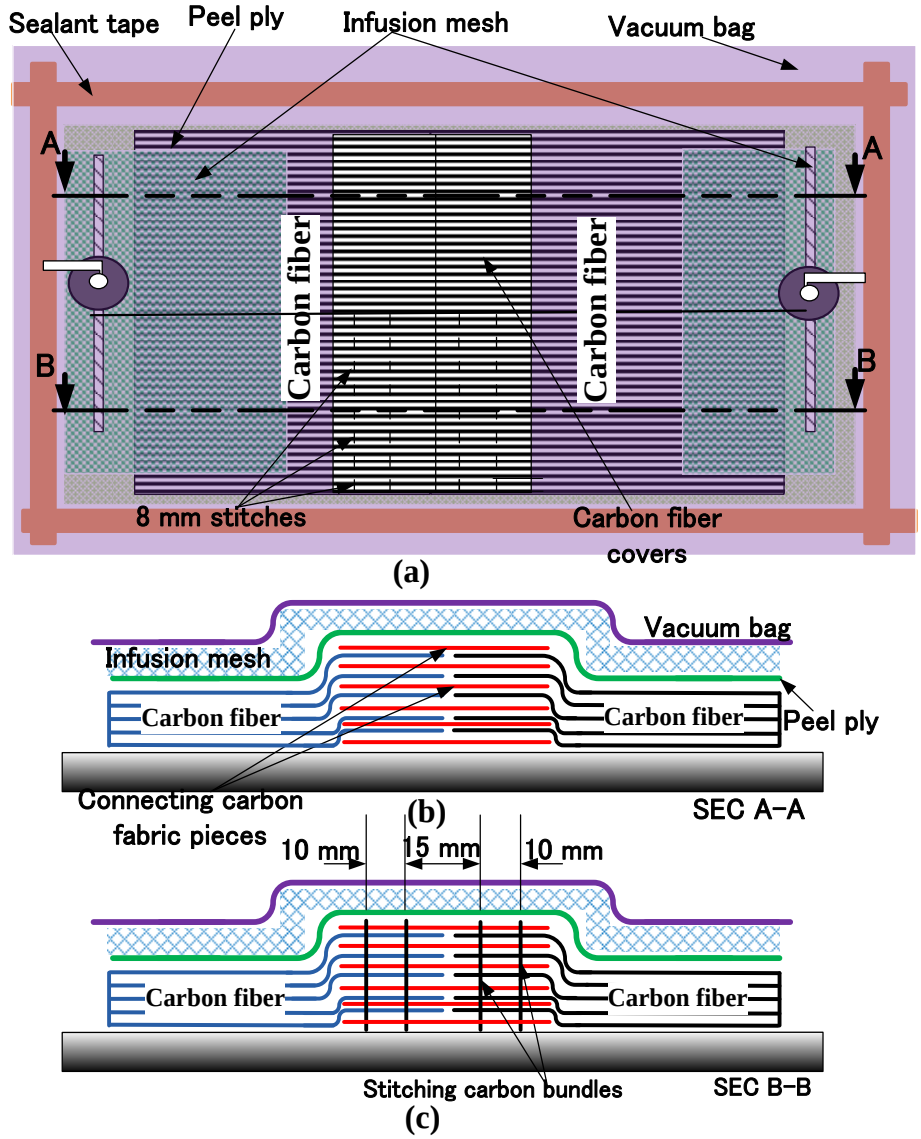

Figure.3. 2: (a) Schematic top view of all multiple-covers joints (b) original multiple-covers, and (c) stitched multiple-covers joints

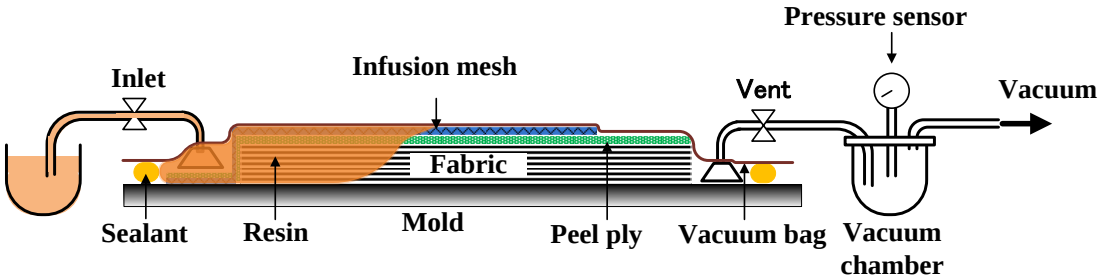

Figure.3. 3: Schematic diagram of the VARTM process used in this work

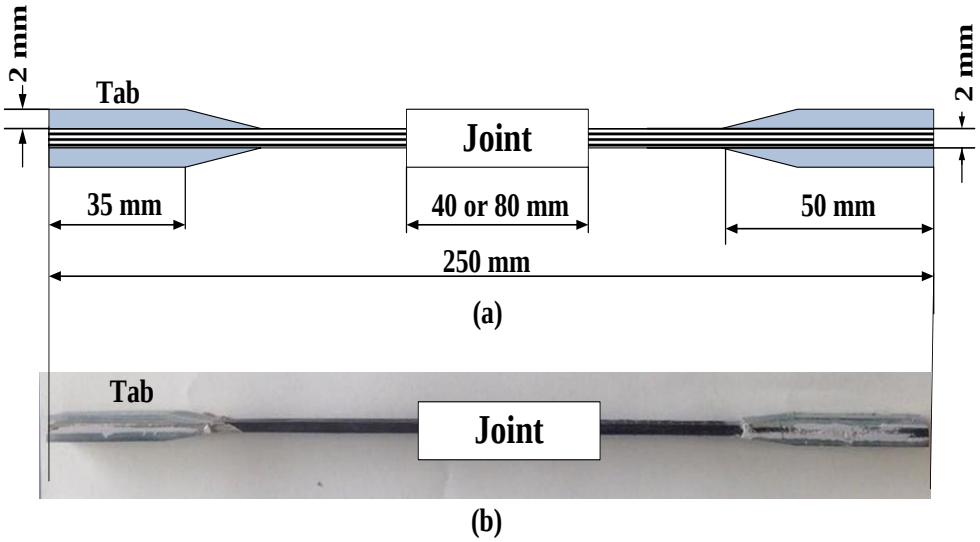

Figure 3. 4: Standard specimen dimensions used for tensile testing and (b) an image of a specimen used in a tensile test

3.3. Results and Discussions

All tests were carried out according to the ASTM standard D3039/D3039M, with a constant crosshead speed of 2 mm/min at a room temperature (i.e., 23ºC). The tensile tests were performed at least three times and the average value of the three measurement values was used as representative. The results showed a maximum error of 15%. Figure 3.5 shows the tensile load of the multiple-covers joint in both original and stitched forms. The tensile load of the original CFRP without joint is also indicated in the figure as the maximum value that logically all joints cannot exceed. The load of the unstitched multiple-covers joint was 17.2 kN, and that of the stitched multiple-covers joint was 20.8 kN (i.e., 21% stronger). This can be attributed to two factors. First, the use of additional carbon bundles results in an increase in the average thickness of the joint. Second, the stitching direction was perpendicular to the

laminate, so that it functions as an additional carbon lamina, forming a bidirectional composite.

Figure 3.6 shows the tensile load of all staircase joints combined with vertical error bars. The strength of the staircase joint was only 9.5 kN. This is consistent with previous studies showing that joining carbon fabrics and CFRP fabrics results in low-strength joints [26]. This can be attributed to two factors. First, resin residue on the CFRP surface prior to joining can act as an insulator. Second, the absence of overlap in these joints reduced the contact area, resulting in a weaker joint [8].

Figure 3.7 shows a typical tensile load–displacement curve combined with images that show the original staircase joint at various stages of the test. An initial crack occurred near the end of the joint, which reduced the gradient of the load–displacement curve. This resulted in a linear relationship between the tensile load and the displacement. As the load increased, the crack grew, until the specimen fractured. The initial crack occurred at the end of the joint. This can be explained as follows. When joining the CFRP with the carbon fabric, two separation lines were formed on the two surfaces of the part. These two lines were filled with resin after joining, and the crack initiated at these lines. As the tensile load increased, the shear stress in the contact area increased, which caused relative motion between the two CFRP portions, and led to enlargement of both separation lines, and hence crack propagation.

On the other hand, stitched staircase joint achieved a small increase in the strength. The tensile load of the stitched staircase joint was 9% higher than that of the original staircase joint. However, it is believed that this increase was caused by addition of two carbon fiber pieces near the joint ends. These two pieces were put

before applying the stitching to cover the gaps at the joint ends. Oppositely, the fracture analysis shows a weakened structure because of stitching. First, the stitches over the CFRP fabric result in gaps between the mold and the CFRP part, as shown in Figure 3.8a. These gaps were filled with resin during molding. In addition, due to the position of these gaps, it was difficult to remove voids in the resin that filled the gaps (see Figure 3.8b). Second, stitching produced notches in the CFRP part, which weakened the structure after molding. LÖbel et al. [8] showed that the existence of holes in CFRP fabrics results in peaking the stress around these holes, and hence a weaker CFRP structure. Figure 3.9 shows a typical tensile load–displacement curve, combined with images that show the deformed stitched staircase joint at various stages of the test. The crack initiated and propagated at the end of the joint, yet the specimen failed at the location of the notches caused by stitching.

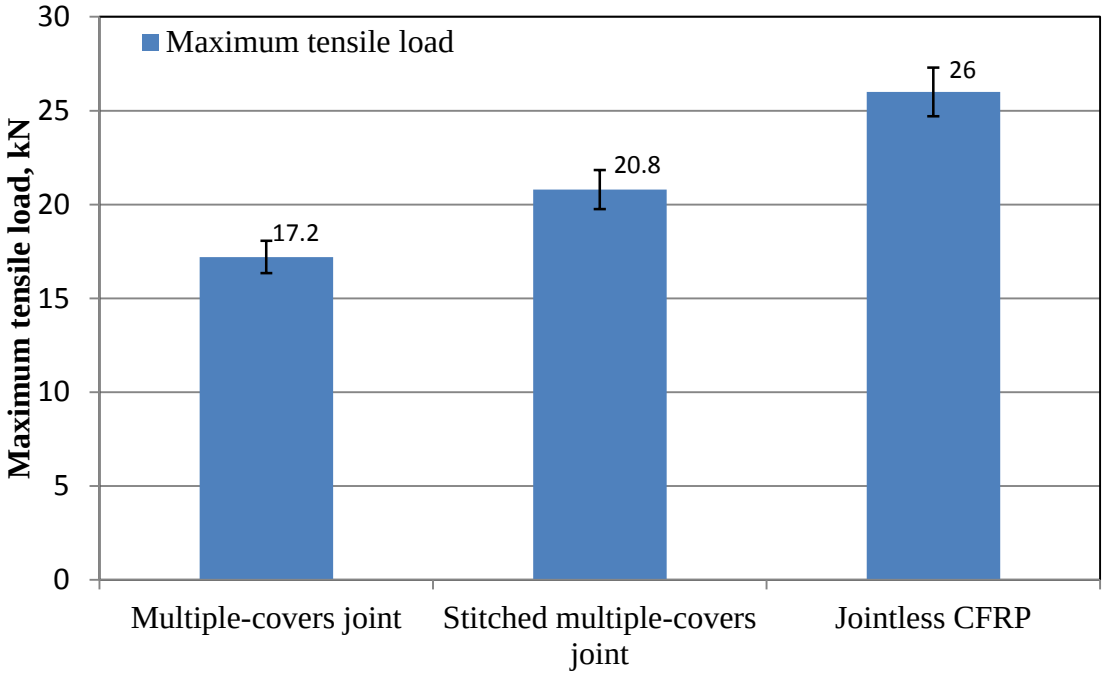

Figure 3. 5: Tensile loads of the two multiple-covers joints

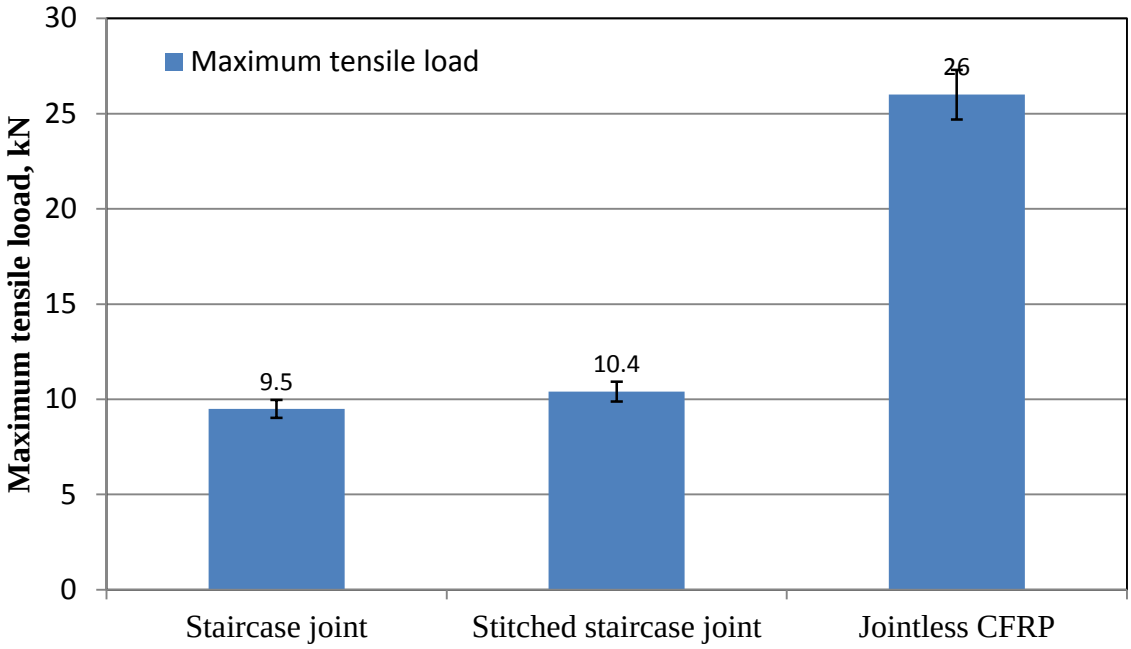

Figure 3.6: Tensile loads of the staircase joints

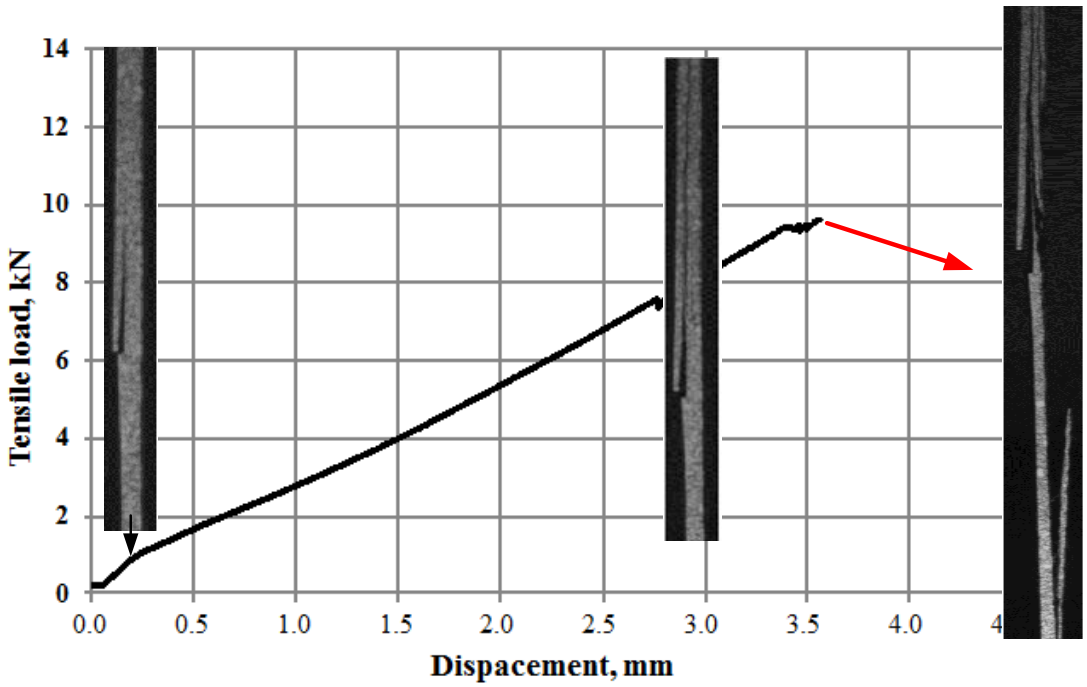

Figure 3.7: Typical tensile load–displacement curve, with images of the staircase joint at different stages of the test

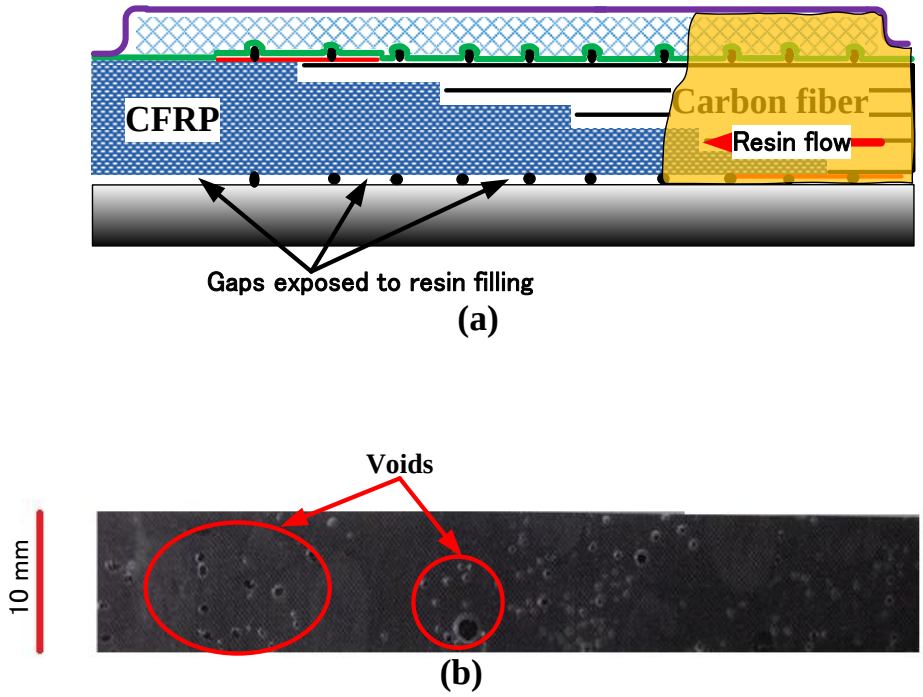

Figure 3.8**:** (a) Schematic diagram of the resin flow for stitched staircase joint, and (b) images of voids formed at the bottom of the joint

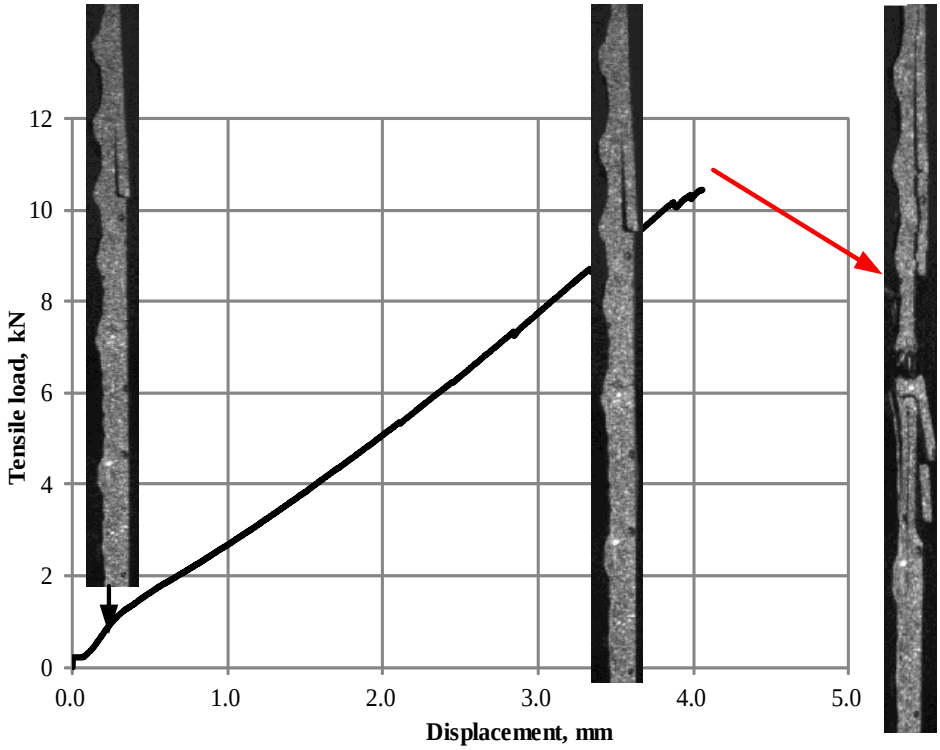

Figure 3.9: Typical tensile load–displacement curve, with images of the stitched staircase joint at different stages of the test

3.4. Conclusions

We have described four adhesive joints formed using VARTM, two adhesive joints in their original and improved forms. Tensile testing was applied to measure the joint mechanical performance. Tensile test results revealed improved strength when stitching was applied to the multiple-covers and staircase joints. The improvement achieved for multiple-covers joint higher than that for the staircase joint. For the staircase joint, the strength improvement caused by the extra carbon fiber pieces which were put at the joint ends not by applying the stitching technique. The fracture analysis using images taken by in-situ monitoring camera showed the following:

1- For the original staircase joint, all fracture progress steps, crack initiation and propagation and final fracture, occurred near the joint ends
2- For the stitched staircase joint, crack initiation and propagation occurred near the joint ends. However, the final fracture occurred at the middle of the specimen

Chapter 4
Improvement of an adhesive joint constructed from carbon fiber-reinforced plastic and dry carbon fiber laminates

4.1. Introduction

Today, adhesive composite joints today play an important role in aerospace, turbine, and ship designs [6]. CFRP type 1 adhesive joints, which are constructed from at least 50% CFRP fabric, include conventional joints such as single-lap [25, 28], double-lap [29, 47], and stepped [31, 32] joints. Various experimental studies have been reported to improve the strength of these conventional joints [8, 44-45, 62]. However, developing and improving novel adhesive joints still limited.

In chapter 3, the stitching technique was applied to both joint types (type 1 and 2). This technique achieved improved tensile strength for joint type 2 samples (multiple-covers laminated joint). However, there is no noticed improvement achieved for the first joint type (staircase joint). In this chapter, we introduce three staircase joints. The first is the original and the other two are proposed improvements. The improvements included adding two carbon fiber pieces at the joint ends and overlapping the dry carbon fiber halve over the CFRP halve. The main objective of this work was to achieve improved tensile strength in the joint. All joints and CFRP materials tested in this study were made using the VARTM manufacturing process.

4.2. Experimental work

4.2.1. Staircase adhesive joints

As it was described in chapters 2 and 3, the staircase joint [26] is an adhesive joint constructed using stepped CFRP fabric, half molded with dry carbon fibers. To fabricate the staircase joint, the VARTM process is applied twice. First, the VARTM process was used to fabricate the CFRP fabric half. Figure 4.1a shows the stacking system of five carbon fiber layers for the joint's first half. The carbon-fiber layers are stacked together, and the joint length (80 mm) is divided into equal stairs. Some staples were used to hold all the carbon fabric in position and prevent any relative movement during mold preparation.

Figure 4.1a shows a detailed drawing of the VARTM manufacturing process used to produce this CFRP part. Following the steps explained above, the mold was prepared. Figure 4.1b shows a real image of the mold used. After resin filling, the pump was stopped and the mold was left for 24 h for resin curing, and the first CFRP half was successfully fabricated. Figure 4.1c shows the first half of the staircase joint. This CFRP part was then used for the fabrication of the staircase joints.

The VARTM manufacturing process was used again to accomplish the fabrication of the staircase joints. After fabrication of the first half, it was necessary to remold this part again after stacking the carbon fabrics, which represents the second half. An additional step was needed before remolding this part. To obtain a better staircase joint bond, any surface resin at the contact length had to be removed from the first half. Generally, the staircase joint strength is sensitive to the existence of any resin at the contact surface of the first half before remolding. In fact, this resin layer acts as an insulator and thus a weakened joint will result. To remove the resin layer, a

sand-blasting process was applied using a Hozan shot blast SG-106 (Hozan Tool Ind. Co., Ltd, Osaka, Japan). Before applying sand blasting, the surface was treated with some sand paper.

In this chapter, we describe three staircase joints: the first is the original staircase joint and the others are proposed improvements. These joints were made in one mold (Figure 4.2a). Figure 4.2b shows the original staircase joint. In this joint, the first CFRP half is remolded with another identically stacked carbon fiber half. For the second joint, the staircase joint with covers, two additional carbon fiber pieces, 40 mm in length, were put on the joint ends. These carbon pieces were added intentionally to cover the joint ends (Figure 4.2c). Figure 4.2d shows the third joint, which is called an "overlapped staircase joint." In this joint, the contact lines were covered using a mating carbon fiber layer.

4.2.2. Materials and testing

Joint strengths were evaluated via tensile testing using standardized test specimens [26]. Figure 4.3 shows the dimensions of the specimens; the total length was 250 mm and the width was 10 mm. Pairs of CFRP tabs were used to reduce the stress when holding each specimen. All specimens were tested using a Shimadzu DSS-5000 universal testing machine (Shimadzu Corp., Kyoto, Japan). For all experiments, the composite material was CFRP. Table 4.1 shows the detailed constituents for the given CFRP fabric.

Table.4. 1: CFRP composite material constituents

Carbon fabric type (Density)	Resin/Hardener	No. of carbon fiber layers	CFRP thickness, mm
Mitsubishi Rayon UD 1M (317 g m-2)	XNR6815/XNH6815	5	1.5
Mitsubishi Rayon UD 1M (317 g m-2)	XNR6815/XNH6815	7	2.0

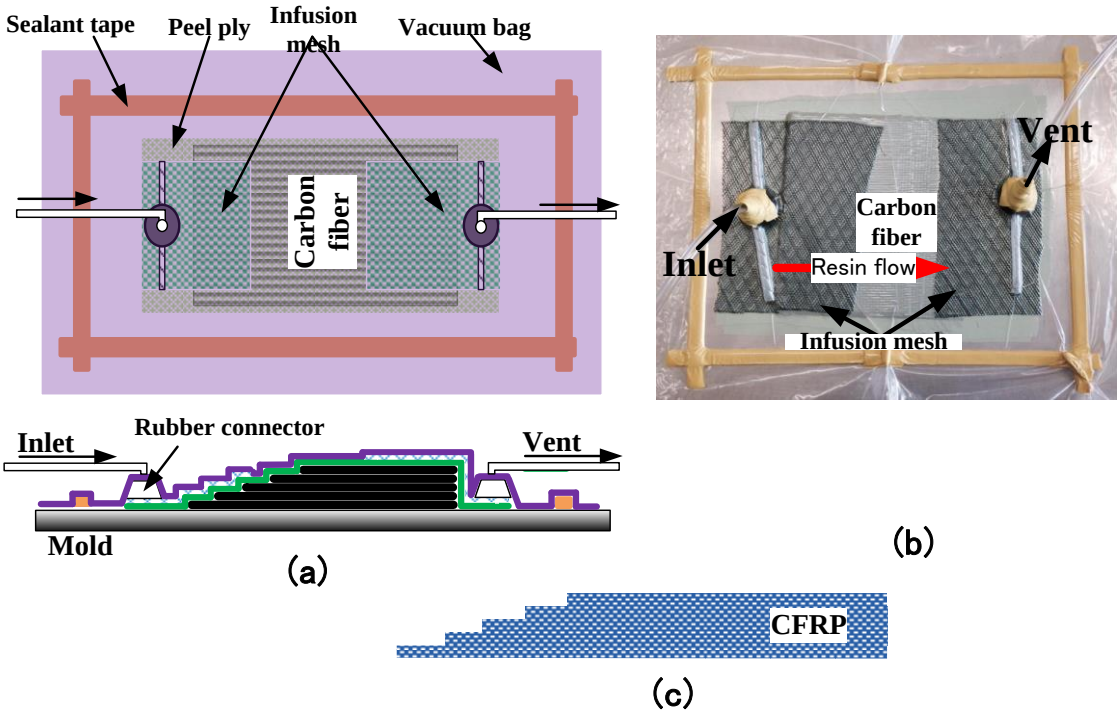

Figure 4. 1: (a) Schematic view of the manufacturing of the carbon fiber-reinforced plastic (CFRP) part. (b) Photograph of the fabrication of the CFRP part. (c) Schematic drawing of the resulting CFRP fabric part.

4.3. Results and discussions

All tensile tests were carried out according to the ASTM D638-03, with a constant crosshead speed of 2 mm/min at room temperature (23°C). Figure 4.4 shows the tensile strength results for all joints and the original CFRP. First, the tensile loads for five- and seven-carbon-fiber layer CFRP were 26 and 28 kN respectively, showing that the tensile strengths in the fiber direction were 1.7 and 1.4 GPa, respectively. Both tensile loads coincided with the CFRP tensile load range of 1.2–2 GPa [8, 27, 47].

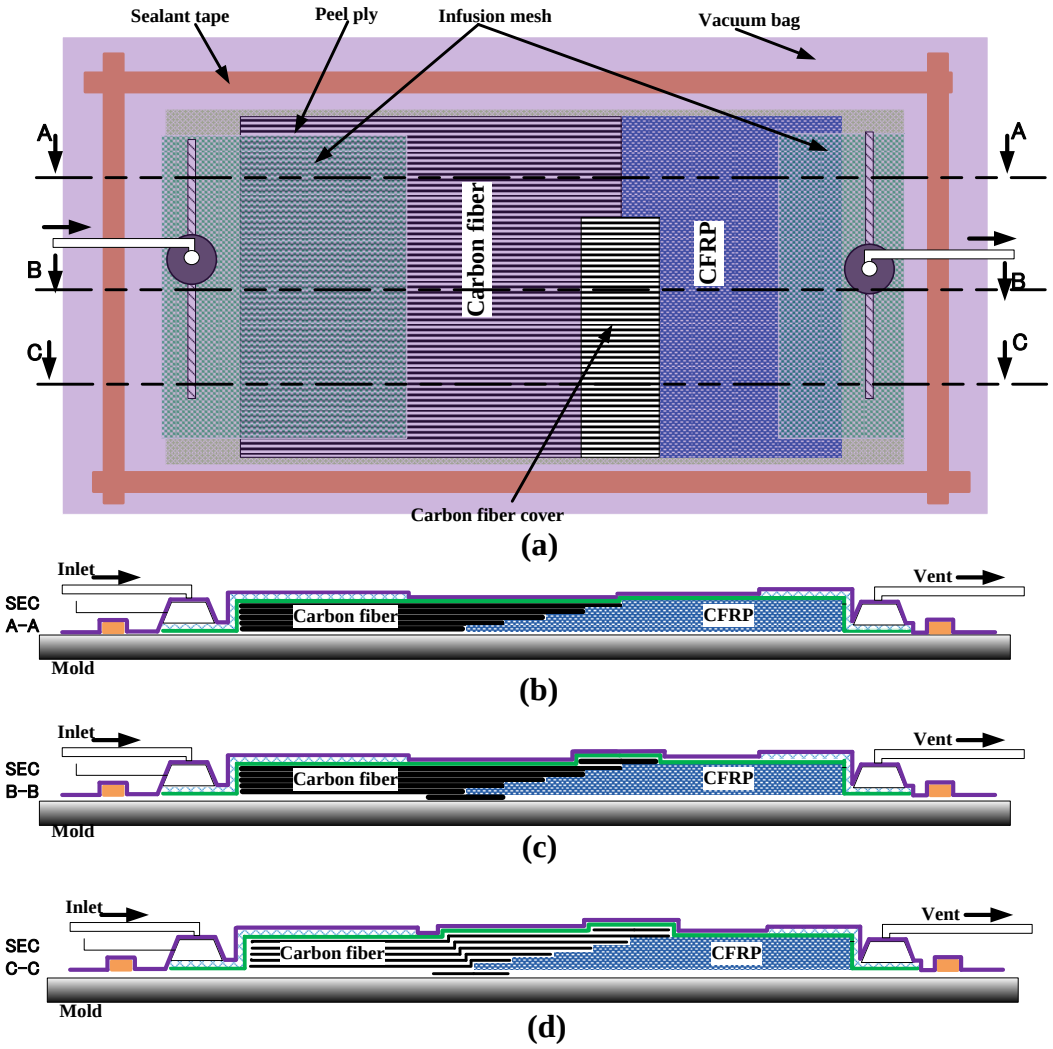

Figure 4.2: (a) Schematic view of the joints. (b) Sectional side view of the original staircase joint. (c) Sectional side view of the staircase joint with covers. (d) Sectional side view of the overlapped staircase joint.

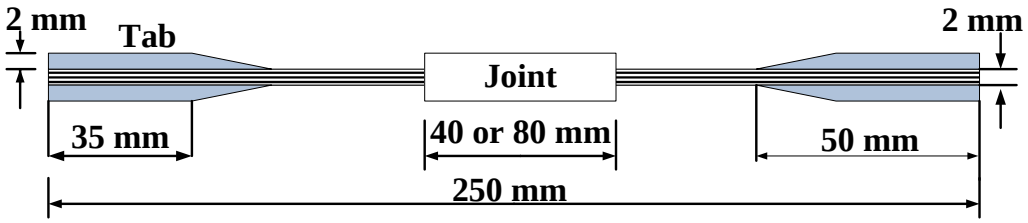

Figure 4. 3: Standard specimen dimensions used for tensile testing.

The tensile results showed a recorded tensile load of 9.5 kN for the original staircase

joint of five carbon fiber layers, which represents 36.5% joining efficiency. The seven-carbon-fiber joint recorded a tensile load and joining efficiency of 14.5 kN and 52%, respectively. The reason for this higher tensile load and joining efficiency is not only the higher number of carbon fabric layers but also the higher number of stairs [26]. This is in agreement with previous studies that have suggested that joining carbon fabrics and CFRP fabrics results in low strength [26]. Abusrea et al. [26] has explained the reasons for this limited strength. The behavior can be attributed to two factors. First, resin residue on the CFRP surface before joining can act as an insulator. Second, the absence of overlap contact in these joints reduces the contact area, resulting in a weaker joint. However, this strength is still relatively high compared with conventional adhesive joints. For example, a double-lap joint achieved a tensile strength of 7.1 kN [8, 27].

The second joint, the staircase joint with covers, showed an improved tensile load. For this joint, the five-carbon-fiber-layer fabric achieved a tensile load of 11.7 kN, which represents a 23% increase versus the original staircase joint. In addition, this value represents a joining efficiency of 45%. This improved strength may be due to the addition of the extra carbon fiber pieces, which helped in resisting crack initiation. Furthermore, the addition of carbon fiber pieces on the joint ends is helpful for reducing the peak stresses at the joint ends [50]. A similar idea was used to improve the single-lap joint. For example, Tsai et al. [51] performed a finite element (FE)

analysis to study the strain/stress distributions in laminated composite single-lap joints with and without a spew fillet [51, 52].

For the third joint, the overlapped staircase joint, the tensile load recorded for five carbon fiber layers was 13.2 kN, which represents a 39% increase and 51% joining efficiency. Additionally, the load for seven carbon fiber layers was as high as 15.6 kN, representing a further 14% increase and 59% joining efficiency. In this joint, beyond the covering of the joint ends, the overlapping helped in covering all contact lines between the stairs of the CFRP and the mated carbon fabric layers. In fact, overlapping is one of the most important techniques used to improve the performance of adhesive joints [8, 27]. Furthermore, the overlap length is the main factor that affects how much improvement is achieved. Lobel et al. [8] studied the effect of overlap length for the double-lap joint and reported two findings. First, the strength of the double-lap joint was increased by 20% when the overlap length increased from 40 to 80 mm. Second, no observed improvement was achieved for an overlap length that was more than 80 mm. In our overlapped staircase joint, the overlap length was determined by the stair length, which was equal to 40 mm (double stair length). Consequently, this overlap length is sufficient to achieve a reasonable improvement in the staircase joint.

Thickening the joint using dry carbon fabrics, by stitching [44, 45] overlapping mated dry carbon fabrics [27], or inserting extra dry carbon fabrics [26], may improve the joint strength. Abusrea et al. [26] proposed novel joints that were improved by inserting additional carbon fabric pieces.

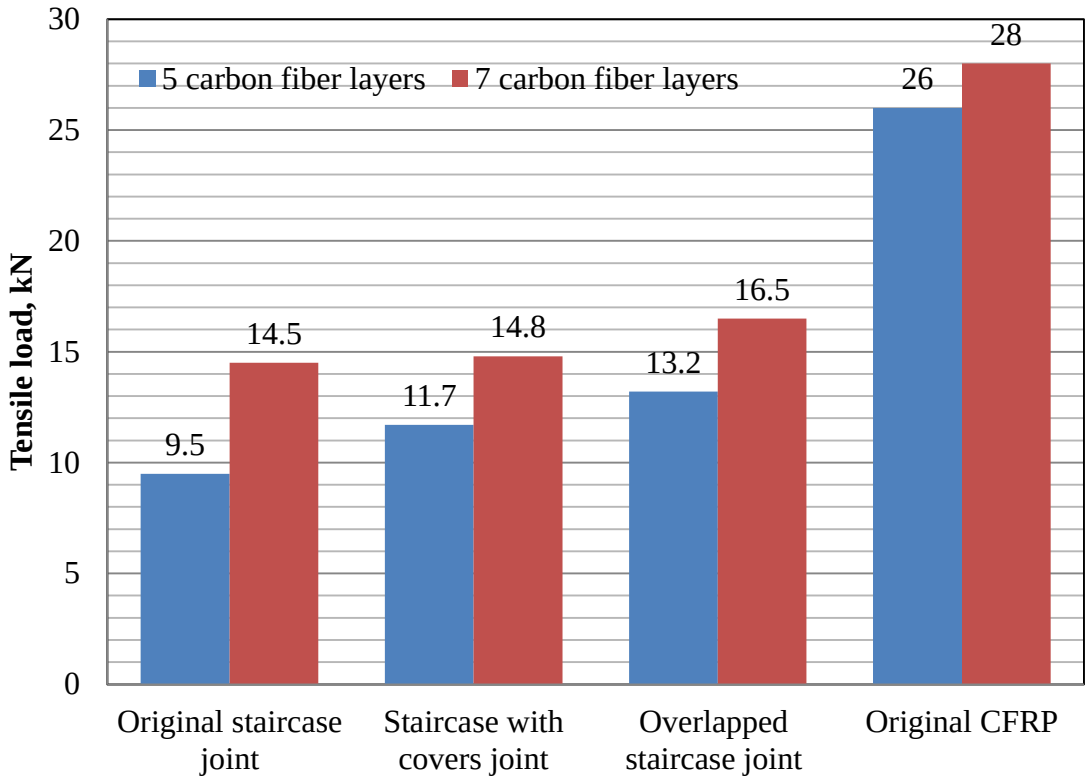

Figure 4.4: Tensile loads of all joints compared with the original CFRP.

Figure 4.5a shows the stress-strain curves for the five-carbon-fiber-layer joints. Unlike the tensile load readings, the stress-strain curves indicate different behaviors of joints. It can be seen that the stress level is lower for the improved joints. For example, the stress level for the original staircase joint was the highest among the three joints. The reason for this behavior can be further explored. First, the stress calculations are based on the maximum thickness within the specimen. As explained in the previous section, one of the main reasons for getting a higher tensile load for the adjusted joints is the increase in thickness. Furthermore, the increase in the tensile load did not recover the thickness increase. The same trend for stress-strain behavior was observed for the seven carbon fiber layers (Figure 4.6).

Figure 4.5b shows a typical fracture scenario for the second joint at the given positions in Figure 4.5a. First, a crack initiated at the joint end, then it propagated in the direction of the joint length, and finally the specimen fractured [26, 27]. The same fracture scenario was observed in the other joints.

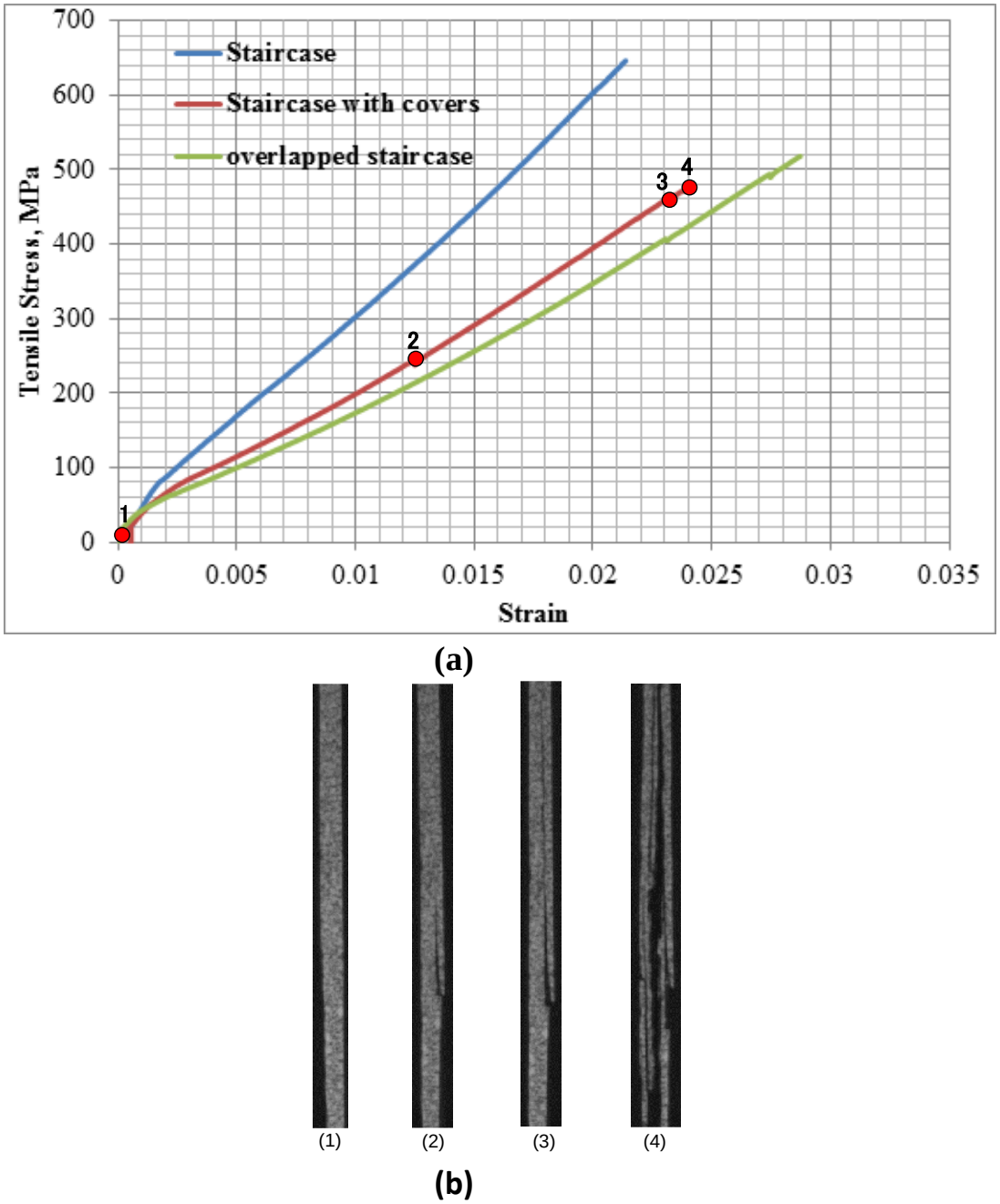

Figure 4. 5: (a) Stress-strain curves for all joints with 7 layers and (b) A typical fracture scenario for the staircase with covers joint at the given positions.

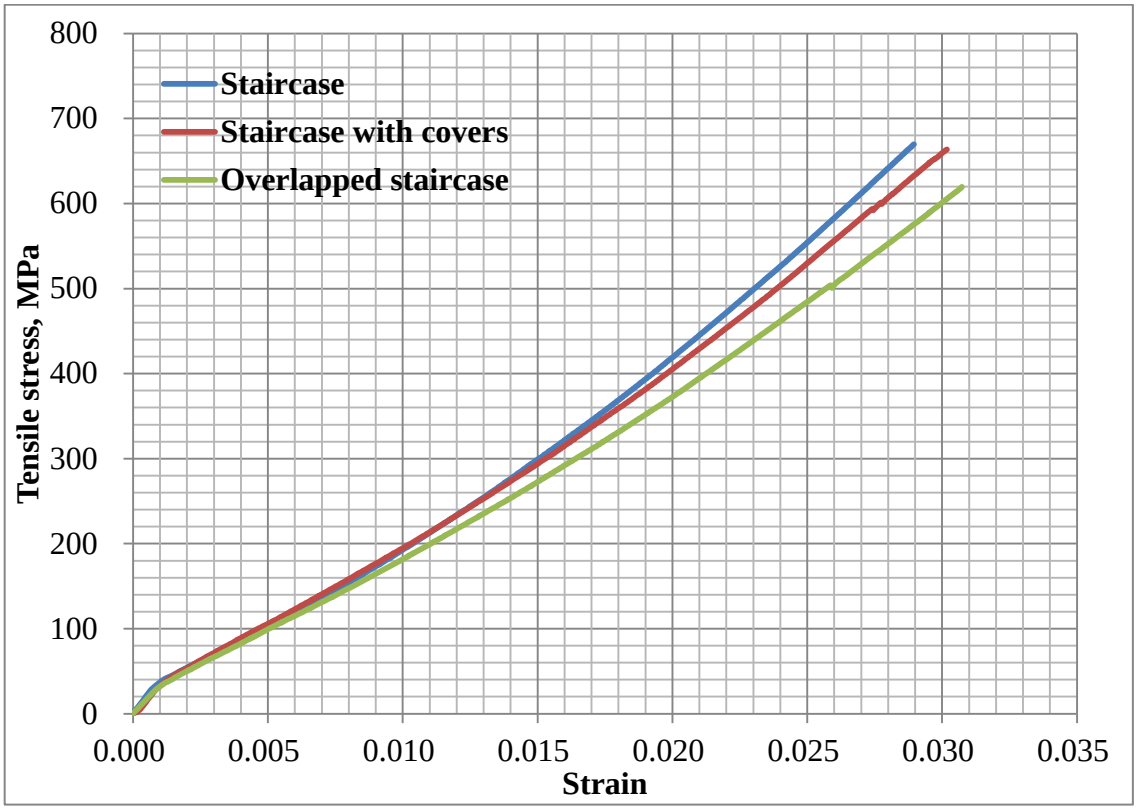

Figure 4. 6: Stress-strain curves for all joints with 7 layers.

To highlight the failure behavior of the current joints, failure analysis using optical microscopy was performed [54]. In optical microscopy, the fractured part is photographed, as shown in Figure 4.7a, and the part is then scanned to identify the images that are to be analyzed further.

Figure4. 7b–d shows typical optical microscopy analysis of the 7-carbon-fiber joints. As shown, the end of each CFRP joint was imaged. The analysis of the original staircase joint showed a uniform mixture of resin and fiber. There were no overlaps in this joint, and failure was due to the separation of the carbon fibers and stairs, as shown in Figure 4.7b. Figure 4.7c shows the images taken of the second joint. These images demonstrate fiber alignment with some pits and scratches caused by the sanding and sand blasting processes that were previously used to remove the surface

resin. Consequently, the tensile load increase at this joint was caused by the representation of more joint zones. Fiber breakage was observed near to the end of the overlapped staircase joint. For this reason, the overlapped joint exhibited the greatest tensile load, as shown in Figure 4.7d.

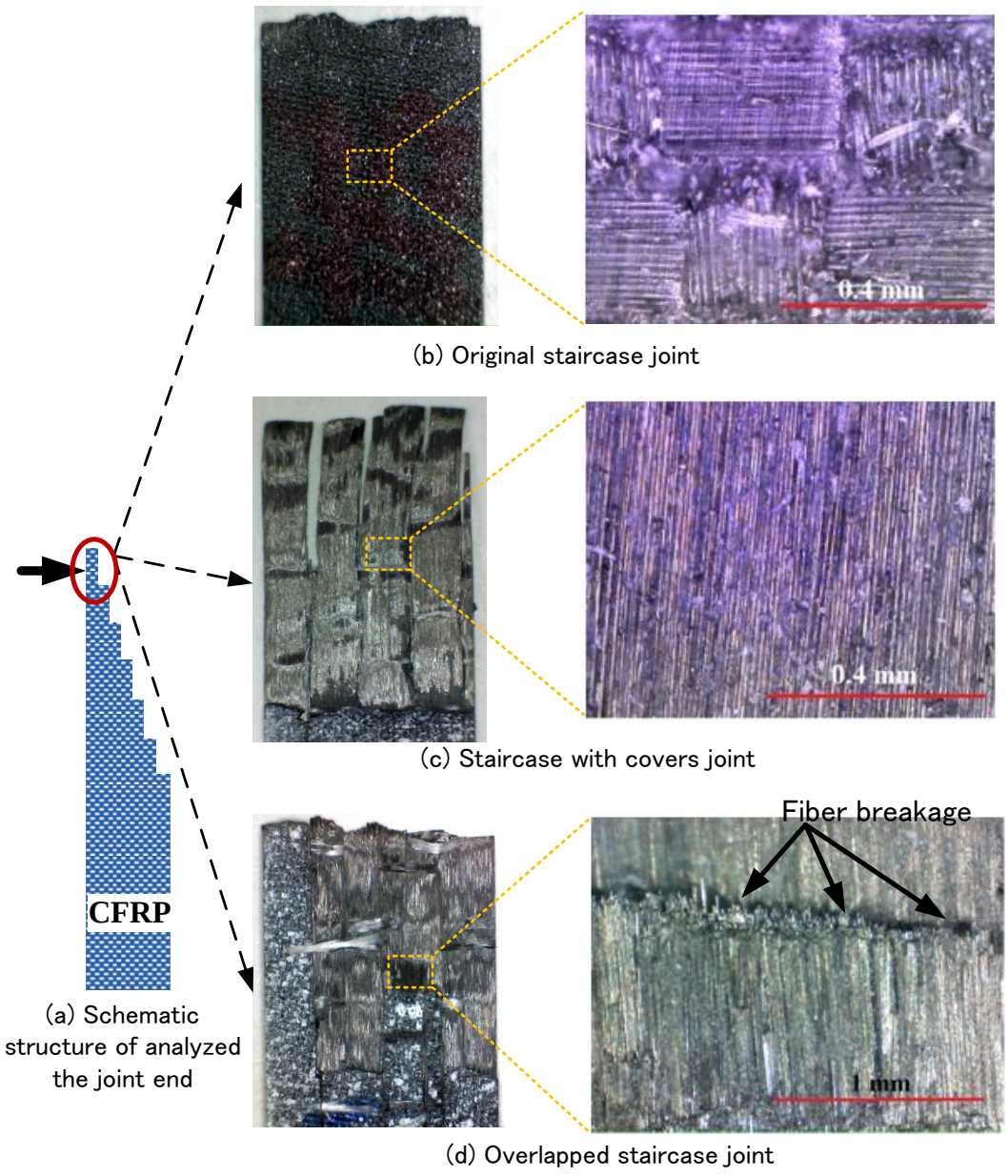

Figure 4. 7: Typical optical microscopy analysis for the 7-carbon-fiber joints

4.4. Conclusions

A stepped CFRP half for all staircase joints was made using a manufacturing process developed from VARTM. This CFRP part was remolded with another carbon fiber half to make the staircase joints. Three staircase joints were molded via the VARTM process. The first was the original staircase and the other two were improved staircase joints. The results showed an enhanced tensile load for the modified staircase joints. The percentage increase depended on the number of carbon fiber layers. For example, the total percentage increase in the tensile load recorded was 39% for the five-carbon-fiber- layer CFRP, with a further 14% increase for the seven carbon fiber layers. The final joining efficiencies reached 51% and 59% for five- and seven-carbon-fiber-layer CFRP fabrics. Finally, the fracture scenarios observed were consistent with previous work.

Chapter 5
Tensile strength enhancement of adjusted novel CFRP composite laminated joints fabricated by vacuum-assisted resin transfer molding VARTM

5.1. Introduction

Composite joints work as structure-critical load-carrying elements. Thus, the design and analysis of composite joints have attracted much attention in a series of light-weight, low-cost, and efficient composite integration projects [65]. Conventional mechanical fasteners, such as bolts, pins, and rivets, have been used to join CFRP structures [22-23, 66]. This joining technique is generally characterized by simplicity and such joints can typically be disassembled [24]. However, drilling holes in composite parts before fastening may cause problems due to stress concentration and weight increases. In contrast, adhesively bonded joints have mechanical advantages over bolted joints because the fibers are not cut, and stresses are transmitted more homogeneously [25].

Recently, CFRP composite adhesive joints have been used extensively in numerous composite structures, such as in aerospace, turbine, and ship designs [6]. These joints include ‘traditional’ adhesive joints, such as single-lap [25, 28], double-lap [29-30], stepped [31-32], and scarf-lap [67-69] joints. These engineering structures are subjected to various combinations of mechanical loadings, including static, fatigue, and impact loadings. Many studies have characterized and improved the mechanical performance of these adhesive joints.

Studies on traditional adhesively bonded joints have been reported by many researchers [67, 70-73]. In chapter 4, the improvements on joint type 1 (CFRP + dry carbon fiber joints) were introduced. A maximum of 40% improvement in the tensile load was achieved by overlapping the carbon fiber half on the CFRP part. This chapter describes the improvements that made for the second joint type. Two improvements were made to the joint. The first was done by overlapping the two halves with overlap lengths of 20 mm and 40 mm (overlapped laminated joints O20 and O40, respectively). The second was made by the addition of carbon fiber pieces (i.e., a multiple-covers laminated joint, MLJ). Figure 5.1a–e show the joints assessed in the current research. These joints were subjected to uniaxial tensile tests. The main objective of this work was to characterize and improve the tensile strength of the laminated joint. All CFRP joints and fabrics were made in our laboratory using a composite-manufacturing technique, referred to as vacuum-assisted resin transfer molding (VARTM; Figure 1.5)

5.2. Materials and Fabrications

5.2.1. Materials

The CFRP composites and their joints consisted of carbon fabric and a resin mixture (Denatite XNR6815/XNH6815) [10]. The resin mixture viscosity at 25°C was 260 mPa·s. The carbon fiber used in this work was made by Mitsubishi Rayon Co. Ltd. Table 5.1 lists the characteristics of the carbon fiber used herein.

Table 5.2: Characteristics of the carbon fiber used in this work

Type	Carbon fiber designation	Style	Weight	Density	Thickness	Tensile strength	Tensile modulus	Elongation
			g/m^2	g/cm^3	mm	MPa	GPa	%
1	TRK976PQRW	UD	317	1.82	0.33	4,900	253	1.9

5.2.2. Adhesive joints

The original laminated joint OLJ proposed in this work is a composite adhesive joint, constructed of two 6-layer dry carbon half fabrics stacked together (Figure 5.1b). A 40-mm joint length was made (Figure 5.1b). To achieve this joint length of 40 mm, each carbon fiber layer was stacked, in which one half was 40 mm longer than the other. Further improvements were made by overlapping the two halves or adding extra carbon fiber pieces. For the overlapping technique, to emphasize the effect of overlap length, two different overlap lengths were used: 20 and 40 mm. Figures 5.1c–d show the two overlapped laminated joints with 20 mm (O20) and 40 mm (O40) overlap lengths. As stated above, the second improvement was made by adding extra carbon fiber pieces (40 mm in length). One joint considered for this improvement was named the multiple-covers joint-1 (MLJ). For the MLJ, the extra carbon fiber pieces were all of the same carbon fiber as used in the fabrics, so it is expected that the thickness of the joint will be double the adherend thickness (Fig. 5.1e).

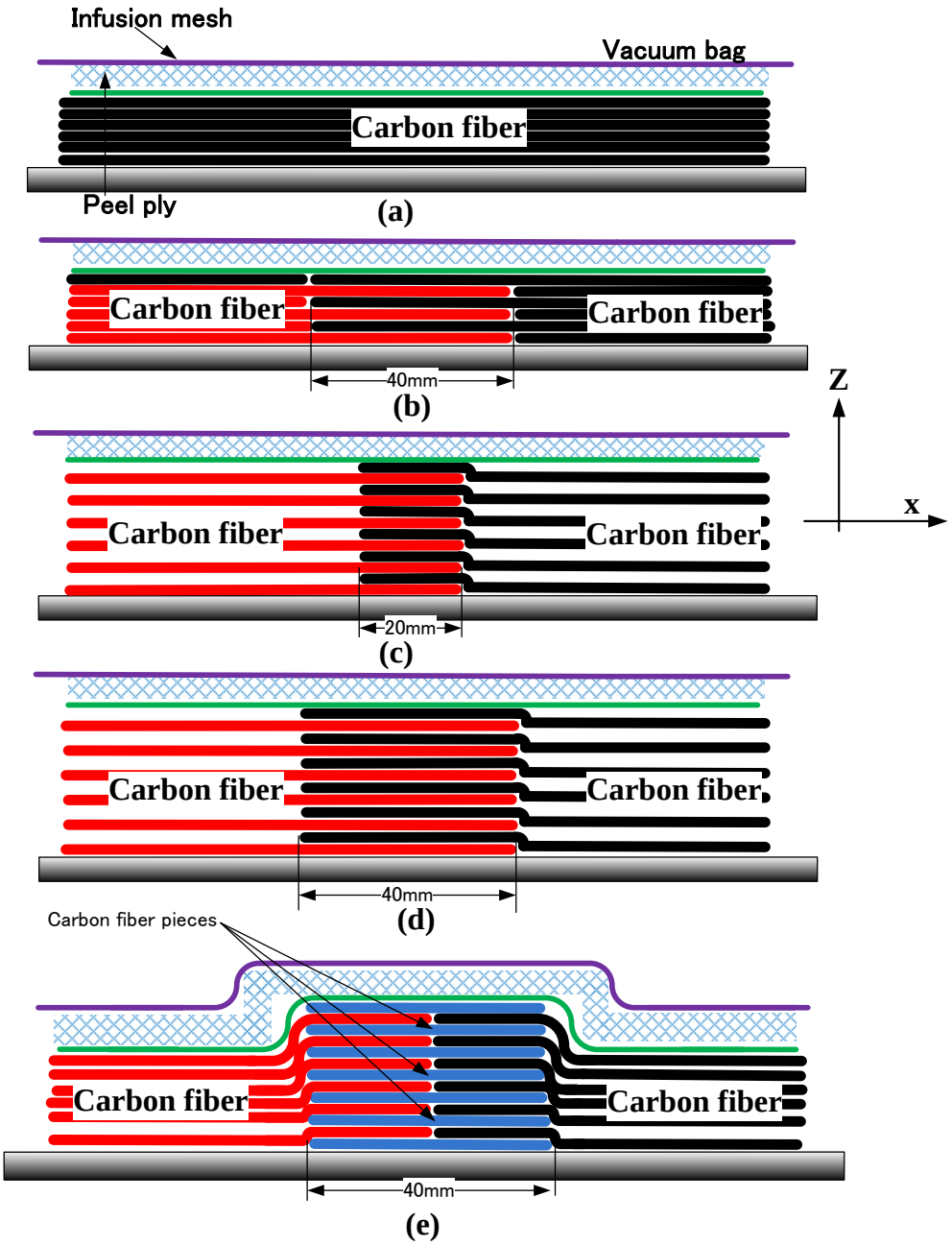

Figure 5.1: (a) Jointless CFRP, (b) Laminated joint, (c) Laminated joint with 20 mm overlap, (d) Laminated joint with 40 mm overlap and (e) Multiple-covers laminated joint

5.2.3. Test procedures and specimens

Joint strengths were evaluated via tensile testing using standardized test specimens [19]. Figure 5.2a shows the dimensions of the specimens; the total length was 250 mm and the width was 10 mm. Pairs of GFRP tabs were used to reduce the stress when holding each specimen. Figure 5.2b shows a real image of the tensile specimens for all joints. All samples were tested using a MTS 810 (100 kN capacity; MTS Corp.) universal testing machine.

Test samples were divided into five test series, representing the various joint types. Five samples were assigned to each test series. Tables 5.2 show the specimen details for all tests. The samples were coded in the form AAA-B-CC, where AAA refers to the joint type, e.g., JOS for jointless CFRP and OLJ for laminated joint, B refers to the type of testing, e.g. T for tensile testing, and CC refers to the sample number (01–05).

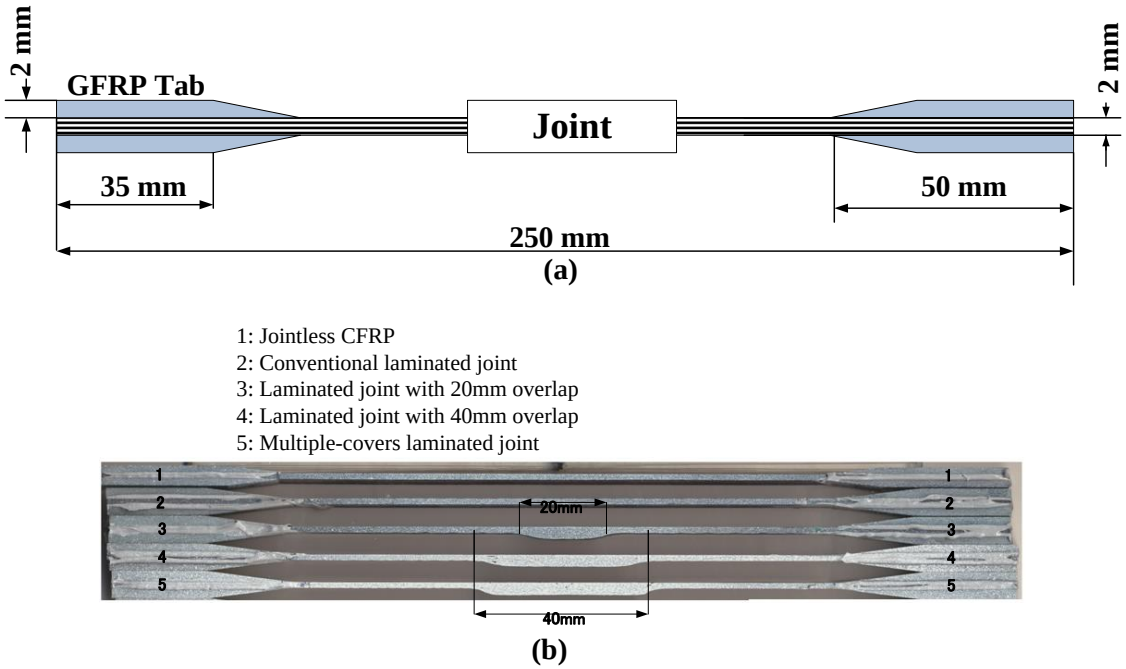

Figure 5.2: (a) Standard specimen size used in this work and (b) Image for all joints

Table 5.3: Specimens' details for tensile test

Tensile test samples							
SN	Test series	Joint type	Specimen code	SN	Test series	Joint type	Specimen code
1	1	Jointless CFRP	JOS-T-01	16	4	Laminated joint with 40 mm overlap	O40-T-01
2			JOS-T-02	17			O40-T-02
3			JOS-T-03	18			O40-T-03
4			JOS-T-04	19			O40-T-04
5			JOS-T-05	20			O40-T-05
6	2	Laminated joint	OLJ-T-01	21	5	Multiple-covers laminated joint	MLJ-T-01
7			OLJ-T-02	22			MLJ-T-02
8			OLJ-T-03	23			MLJ-T-03
9			OLJ-T-04	24			MLJ-T-04
10			OLJ-T-05	25			MLJ-T-05
11	3	Laminated joint with 20 mm overlap	O20-T-01	26			
12			O20-T-02	27			
13			O20-T-03	28			
14			O20-T-04	29			
15			O20-T-05	30			

5.3. Results and Discussions

5.3.1. Ultimate Tensile failure load

All tensile tests were carried out according to ASTM D638-03, with a constant crosshead speed of 1 mm/min at room temperature. Figure 5.3 shows the maximum tensile failure load and standard deviations for all samples. The failure load for jointless CFRP samples was 32 kN, showing that the tensile strength in the fiber direction was 1.84 GPa [19]. The failure load values for the subsequent joints can be linked to this failure load by the joining efficiency data. The OLJ achieved a maximum failure load of 14.3 kN. This failure load is considered high when compared with literature reports [67]. This OLJ was developed in Chapter 2. In Chapter 6, further improvements will be done to this kind of joint to emhance its bending strength.

The overlapped laminated joints, O20 and O40, achieved higher failure loads in this study. The laminated joint with a 20 mm overlap length achieved a higher failure load, of 20.7 kN, representing a 45% increase compared with the OLJ. The laminated joint with a 40 mm overlap length showed a failure load of 22.3 kN, a 56% increase versus the OLJ. The effect of overlap length was studied by previous researchers for traditional adhesive joints, such as SLJs and DLJs. Li et al. [67] investigated the effect of overlap length on the tensile performance of SLJs and DLJs under static conditions. As the overlap length increased, the ultimate failure load and equivalent stiffness also increased. In contrast, the overlap lap shear strength decreased with longer overlap lengths. Evaluating the surfaces of the tested joints, the fracture modes changed from

cohesive in the adhesive to cohesive in the adherend with increased overlap length. Araújo et al. [64] studied the effect of overlap length on failure load under quasi-static and impact conditions. Increased overlap length resulted in an increase in the failure load under both conditions. According to [64], the failure mode was independent of the overlap length under quasi-static conditions. However, the failure mode varied depending on the overlap length under impact conditions. Abusrea et al. [19] investigated the effect of overlapping on a stepped joint, called a staircase joint, which was constructed between CFRP and dry carbon halves. The overlapped staircase joint achieved about a 40% increase over the original staircase joint.

The ultimate failure load for the MLJ was 19.9 kN, a 40% increase versus the OLJ. Insertion of extra carbon pieces at the connection between the two joint halves is an improvement technique developed by [19, 26]. The MLJ showed an increase in the flexural loading capacity, ranging from 48 to 112%, depending on the number of carbon fiber layers.

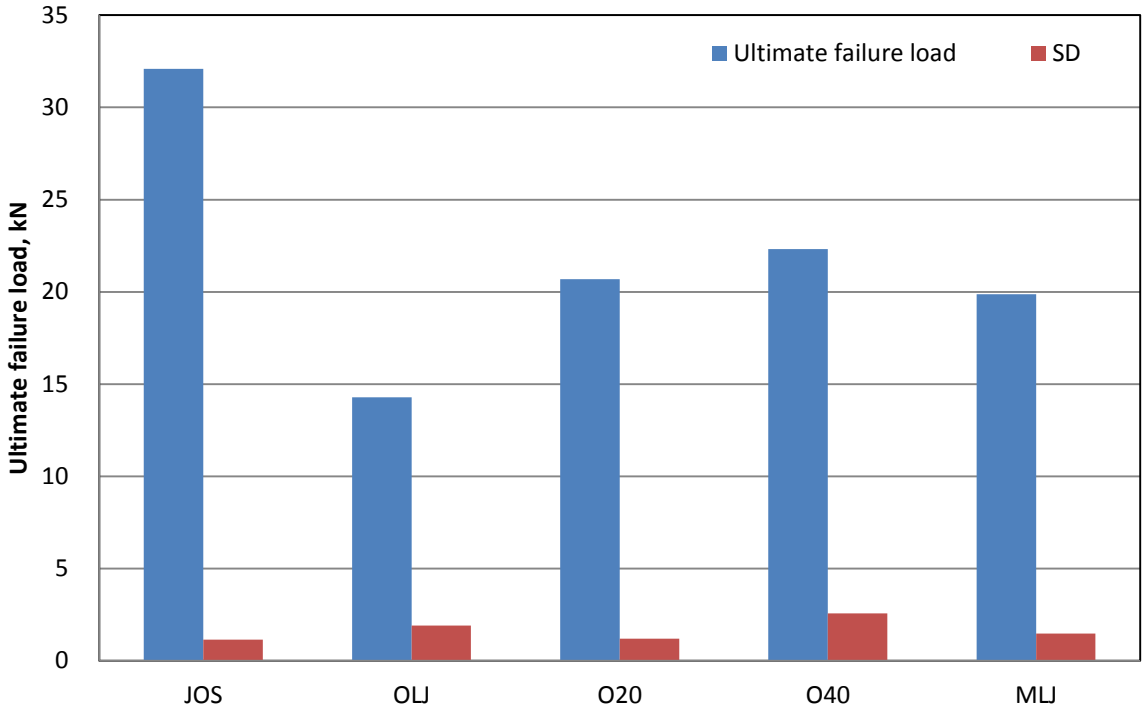

* JOS: Jointless , OLJ: laminated joint, O20: 20mm overlapped laminated joint, O40: 40mm overlapped laminated joint and MLJ: Multiple-covers laminated joint

Figure 5.3: Ultimate failure load data for joinltess CFRP and joints

5.3.2. Load-Displacement curves

Typical load-displacement curves for specimens with differing overlap lengths are presented in Figures 5.4–5.7. The load-displacement curve showed crack initiation and propagation. Figure 5.4 shows a typical load-displacement curve for the OLJ. Crack initiation can be seen with the 4 kN load. The load-displacement curve for this joint can be divided into three stages. The first stage ends with the crack initiation, and then the crack starts to propagate during the second stage, known as “steady-state crack propagation.” Linear load-displacement curves were detected in both stages. The third stage then showed a non-linear load-displacement relationship.

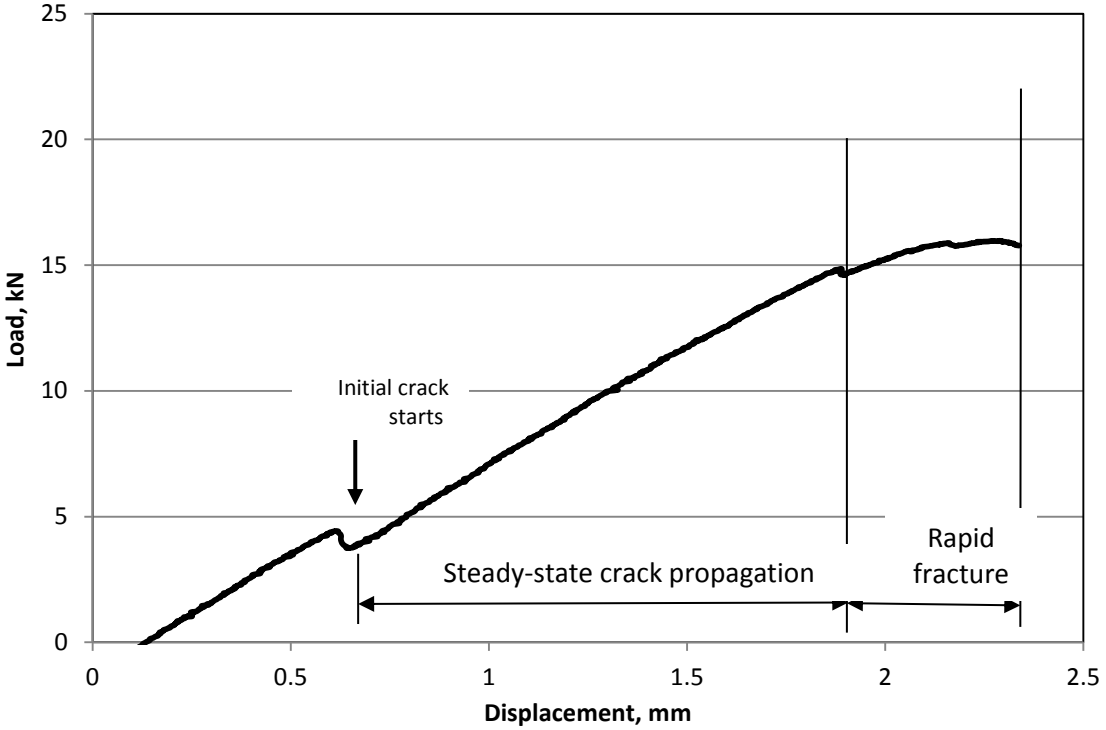

Figure 5.4: A typical load-displacement curve for the laminated joint OLJ

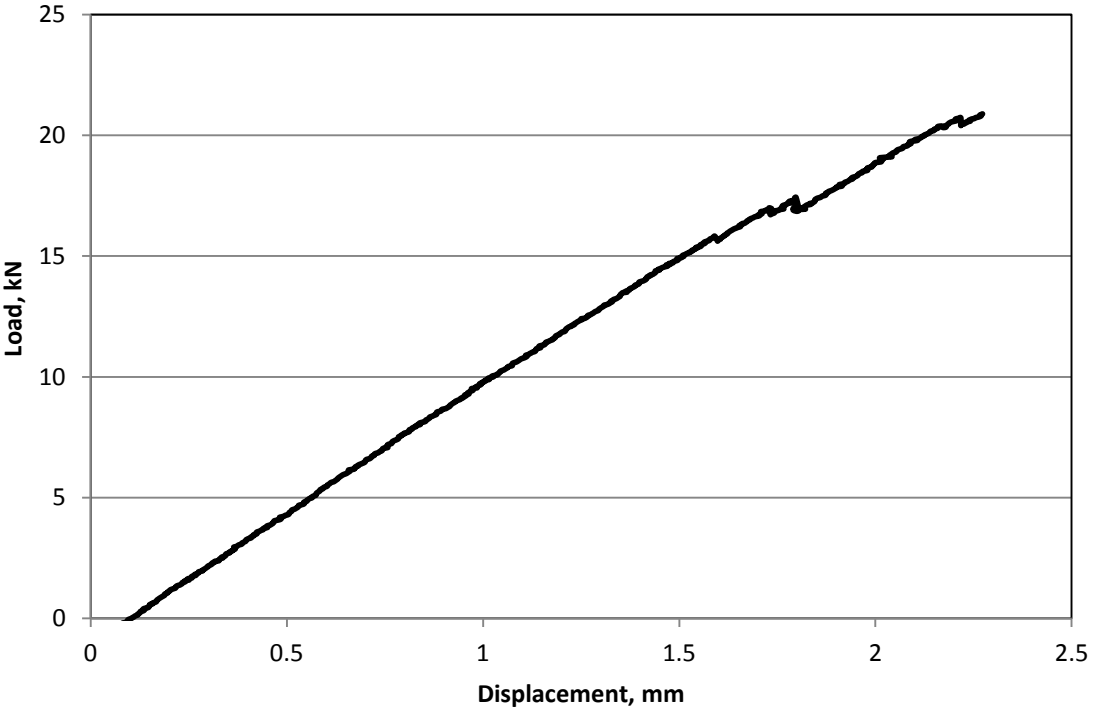

Figure 5.5: A typical load-displacement curve for the overlapped laminated joint O20

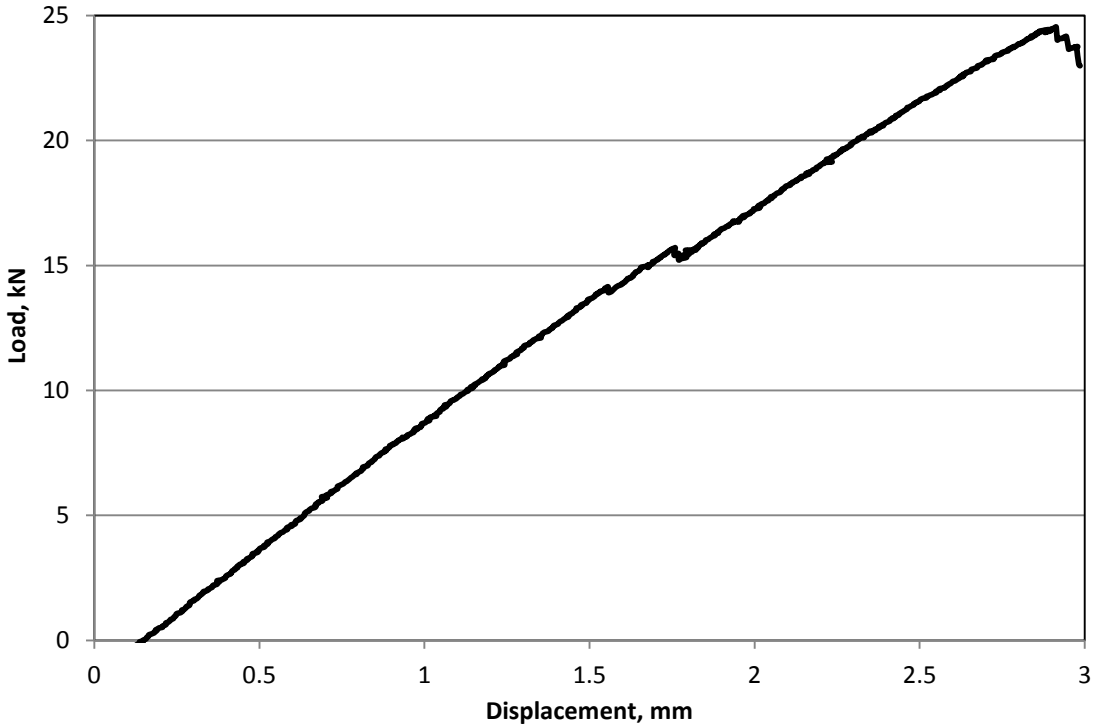

Figure 5.6: A typical load-displacement curve for the overlapped laminated joint O40

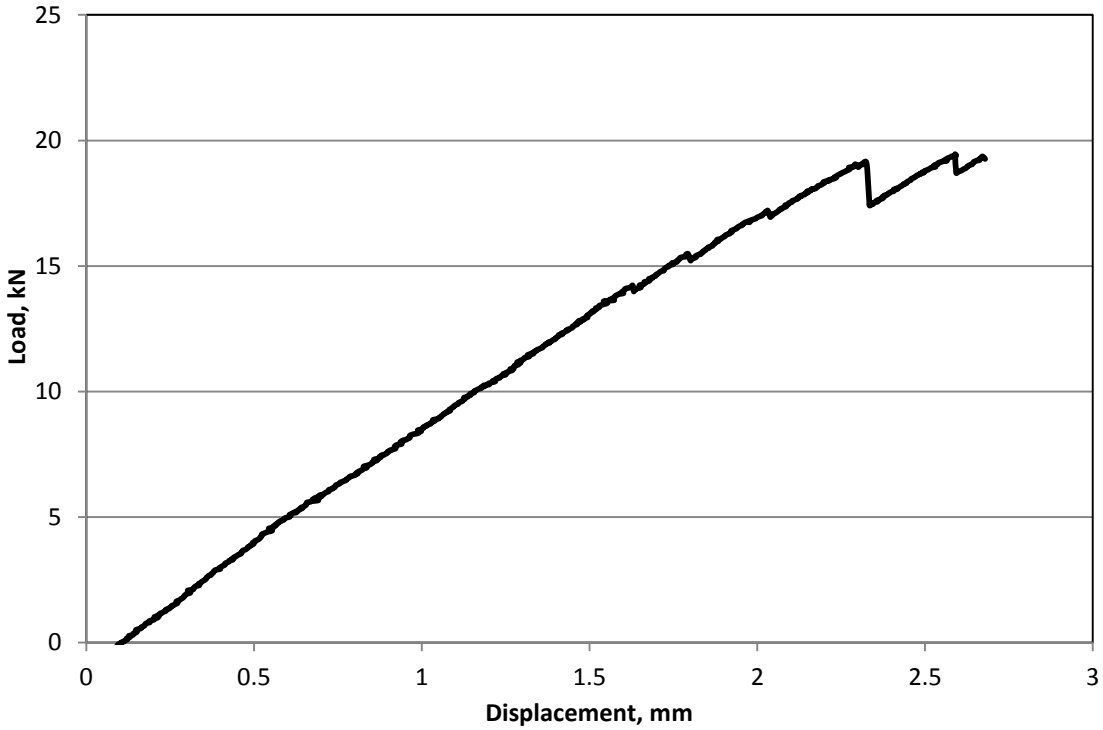

Figure 5.7: A typical load-displacement curve for the multiple-covers laminated joint MLJ

Figures 5.5–5.7 show the load-displacement curves for the improved laminated joints. Compared with the OLJ, the load-displacement curves of the improved joints showed linear relationships over the entire curve. Additionally, the first crack started to appear later. From these curves, it seems that no clear crack propagation occurred after the first crack appeared. Instead, some additional cracks appeared later, possibly due to fiber breakage and/or delamination. Traditional SLJs showed a linear relationship between the load and displacement at different overlap lengths [64, 67]. However, composite-to-aluminum single-lap joints showed a non-linear relationship [75]. It was suggested that this was due to plastic deformation of the aluminum adherend.

5.3.3. Joining efficiency

The joining efficiency was calculated by dividing the ultimate failure load for the joint by that for the jointless CFRP. Figure 5.8 shows the joining efficiency for all joints. The joining efficiency results showed the same trend as the ultimate failure load results. The joining efficiency data were considered as a measure of drop-down in the tensile loading capacity due to the existence of a joint in the engineered CFRP composite structure. The OLJ achieved 44.5% joining efficiency. This corresponds to a more than 50% drop-down in the structure tensile loading capacity, due to the existence of the laminated joint, which is considered to be of low efficiency. The overlapped joints, O20 and O40, achieved improved joining efficiencies, of 64.5% and 69.5%, respectively. The joining efficiency for the MLJ was 62%. Most previous

research did not measure joining efficiency, instead focusing on the absolute load and stress, and did not compare obtained values to those of the original jointless composites. The joining efficiencies of these improved joints are considered reasonable compared with literature reports [19, 26]. The overlapped staircase joint achieved ~59% joining efficiency [19].

5.3.4. Maximum tensile stress

Figures 5.9 and 5.10 show the maximum stress for jointless CFRP JOS and all of the tested joints. The engineering stress in tensile tests is calculated by dividing the load by the original area of the sample. For the jointless CFRP and laminated joint samples, the maximum tensile stress was calculated simply by dividing the ultimate failure load by the sample cross section area. In Figure 5.9, the maximum stresses for the jointless CFRP and OLJ were 1,840 and 840 MPa, respectively.

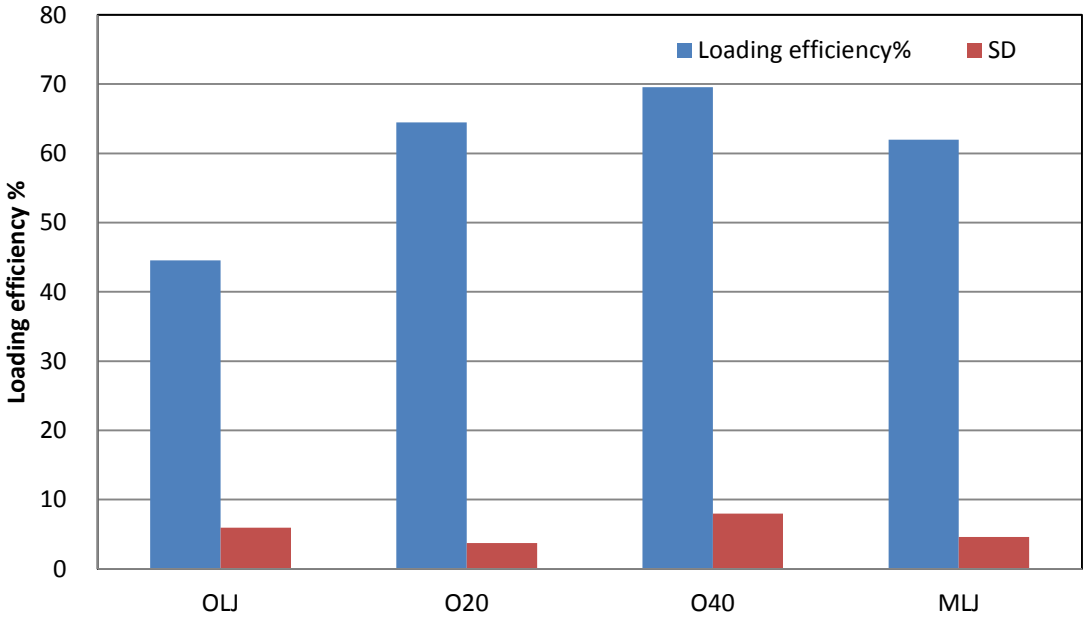

Figure 5.8: Joining efficiency data for all joints

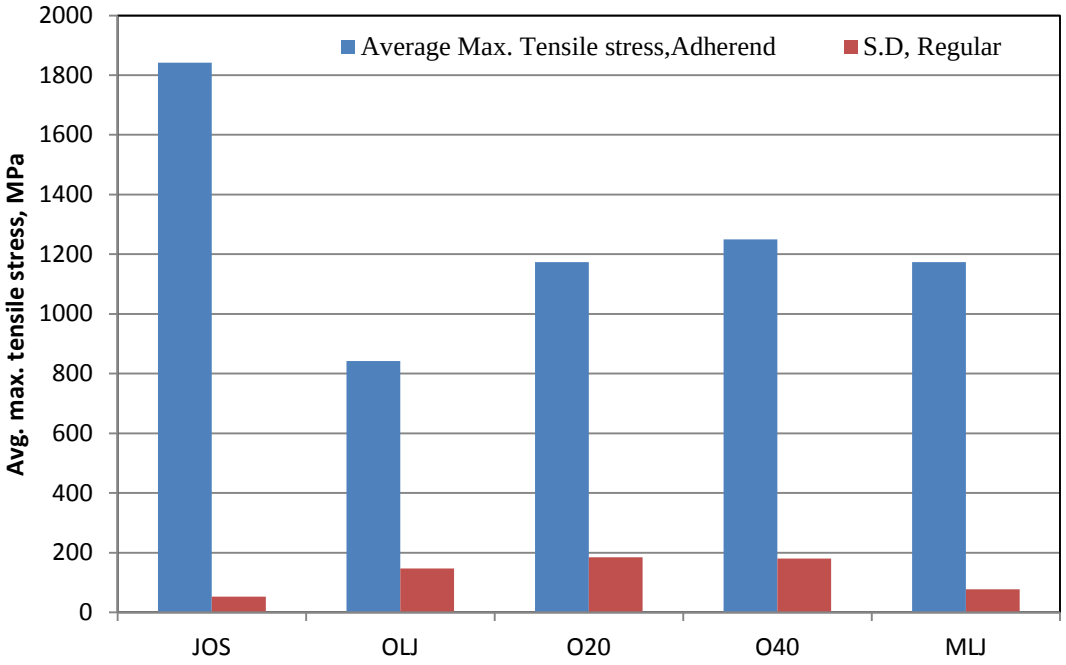

Figure 5.9: Maximum tensile stress based on the adherend thickness

For the improved joints, there are two different thickness measurements: the adherend and joint thicknesses. For all improved joints, the joint part was thicker than the adherend. The maximum tensile stress was calculated based on the adherend thickness and the joint thickness. Figure 5.9 shows the maximum stress based on adherend thickness. The stress data showed the same trend as the ultimate failure load data: the 40 mm overlapped laminated joint (O40) achieved the highest stress value, of 1,250 MPa. However, an opposite pattern for the maximum tensile stress was seen when stress was calculated based on the thicker part of the joint. The OLJ achieved the highest stress value, of 842 MPa, while the joint O40 showed a maximum stress value of 617 MPa. This may be due to the increase in the joint part thickness due to overlapping the two halves not being recovered by the same increase in the ultimate failure load. Li et al. [67] investigated the effect of overlap length in single and double lap joints DLJs. They showed that ultimate failure load increased when the overlap

length increased. However, the lap shear strength decreased with increased overlap length. This phenomenon could be due to the increase in bonding area, but this increase did not cause the same compensatory increase in ultimate failure load.

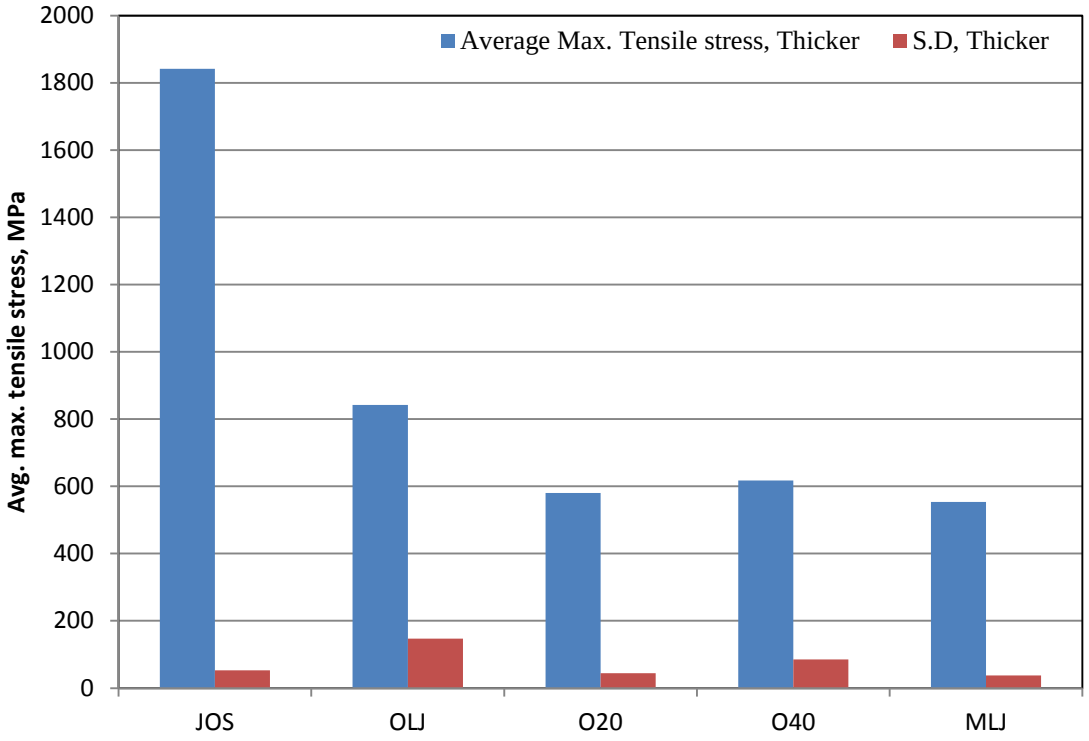

Figure 5.10: Maximum tensile stress based on the joint thickness

5.3.5. Fracture mode

Photomicrographs of the fractured samples showed different fracture modes. Figures 5.12–5.16 show photographs of fractured samples. Figure 5.11 shows the fractured sample of the jointless CFRP. It can be seen that fiber breakage failure mode occurred along the whole sample (100% fiber breakage). This fracture mode usually indicates high strength [19]. Figure 5.12 shows photographs of the fractured sample of the OLJ. A delamination fracture mode was observed for this joint. The fracture started at the joint end and propagated along the joint.

Figures 5.13–5.14 show the fractured samples for the overlapped joints O20 and O40. According to these figures, the fracture mode was different for these joints. In the case of joint O20, delamination fracture of the carbon fiber layers was observed, except for the first layer. A fiber breakage fracture mode was observed for the first layer (Fig. 5.13). When the overlap length increased to 40 mm, i.e., joint O40, the fracture mode was a combination of delamination and fiber breakage (Fig. 5.14). Li et al. [67] investigated the fracture mode of single-lap joints with differing overlap lengths. They showed that the failure modes of the single-lap joints varied by overlap length. When the overlap length was small, the adhesive was the weak part of the joint, and the crack initiated and propagated in the adhesive. Consequently, the joint showed adhesive shear failure mode (100% of the failure area). When the overlap length increased, adhesive shear failure could still be observed (23.2% of the failure area). Additionally, adherend failure, mainly in the form of delamination (76.8% of the failure area) between the layers, was also found. In cases with larger overlap lengths, the failure mode was quite different: delamination (100% of the failure area) was widely observed, and the ultimate failure was dictated by the composite adherend.

Figure 5.15 shows the fractured sample of the MLJ. It shows the same fracture pattern as joint O40. This is reasonable given the identical joint length: both joints have lengths of 40 mm. Additionally, the ultimate failure load of the MLJ was close to that of the O40 joint.

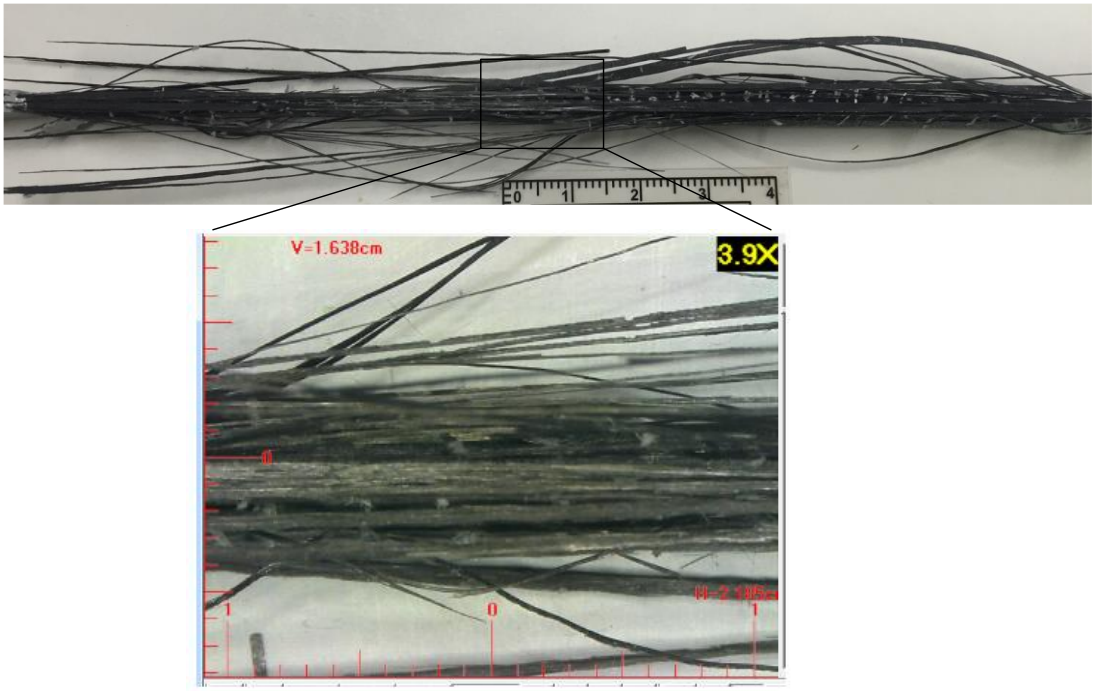

Figure 5.11: Typical microscopic photographs of the jointless CFRP sample

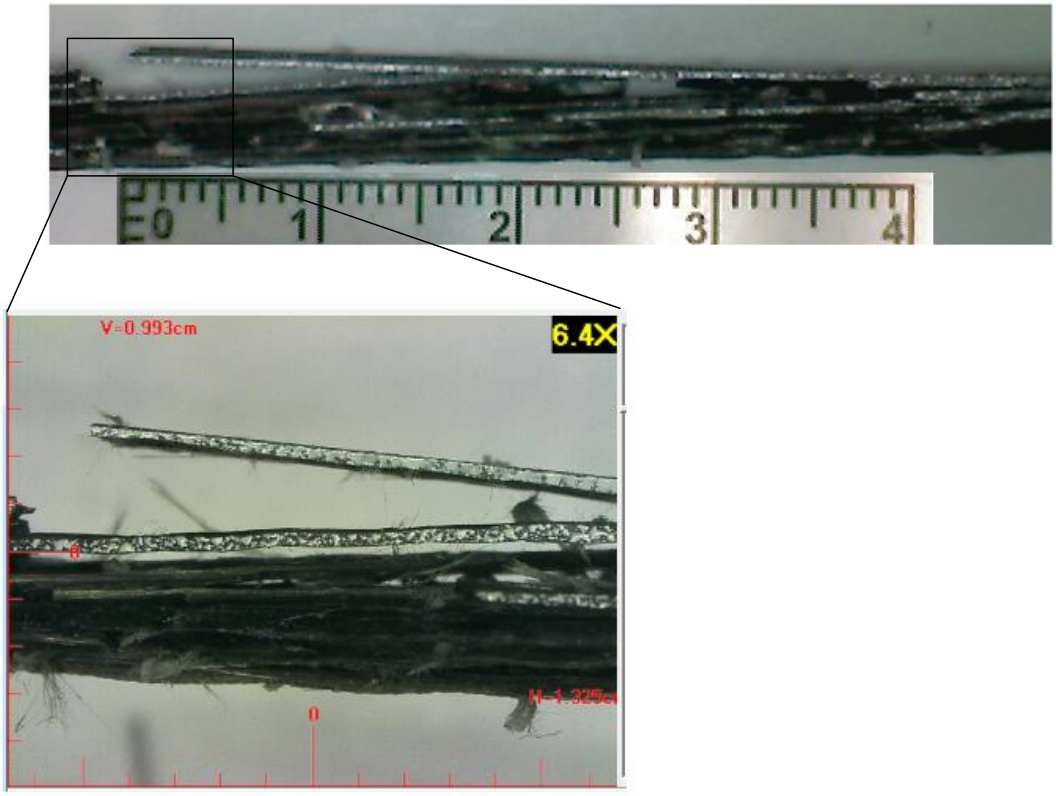

Figure 5.12: Typical microscopic photographs of the laminated joint OLJ

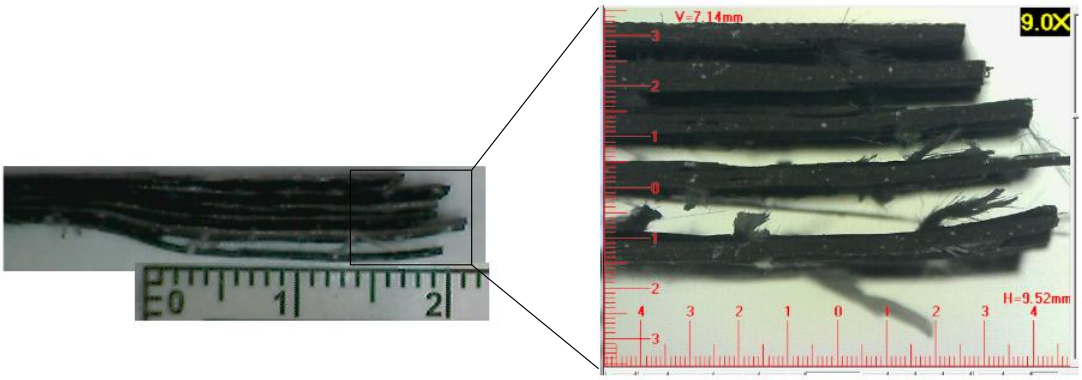

Figure 5.13: Typical microscopic photographs of the overlapped laminated joint O20

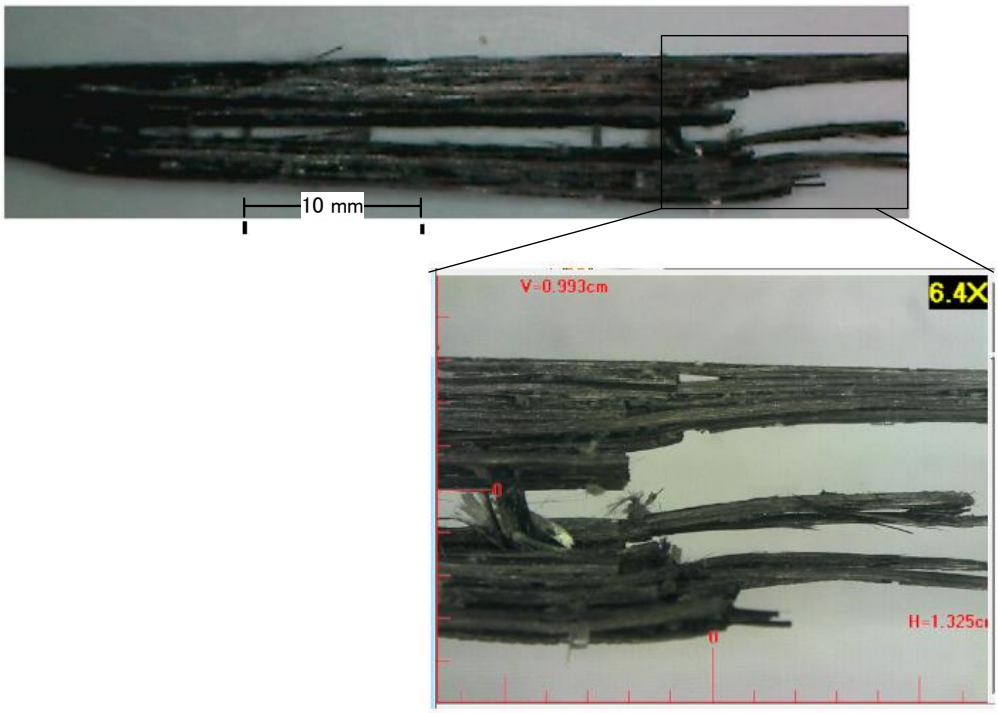

Figure 5.14: Typical microscopic photographs of the overlapped laminated joint O40

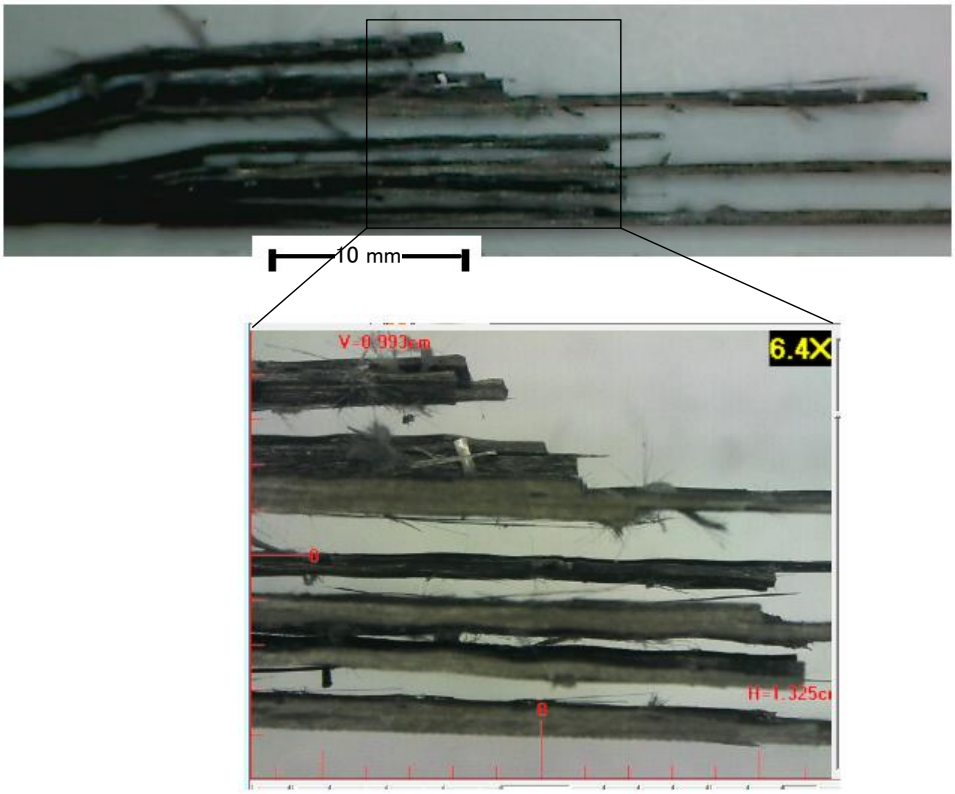

Figure 5.15: Typical microscopic photographs of the multiple-covers laminated joint MLJ

5.3.6. Thickness profile

To achieve an improved laminated joint, a thickness of the joint part versus the adherend was ensured, where the number of carbon fibers at the joint exceeded the number of carbon fiber layers used for the adherend. These excess carbon fibers were caused by either overlapping of the two carbon fiber halves or addition of extra carbon fiber pieces. The thickness of the joint part should be at least twice that of the adherend. Thickness variation occurred along the upper surface of the joint during contact because the reinforcements were placed on a rigid flat surface of the mold (Fig. 5.1c-e). Figure 5.16 compares the thickness profiles over 80 mm length for all samples. All tested joints were compared with an ideal 6-layer CFRP fabric.

It was important to create joint profiles to measure joint quality, by showing the extent to which joint thickness precision was affected by the adjustments made. In Figure 5.16, the jointless CFRP and OLJ showed thickness deviations, caused by the presence of infusion mesh. These deviations normally occur in fabrics made by a VARTM manufacturing process [27]. A much larger thickness increase was observed for the O20, O40, and MLJ. The thickness reached 3.5 mm for the O20 and O40 joints.

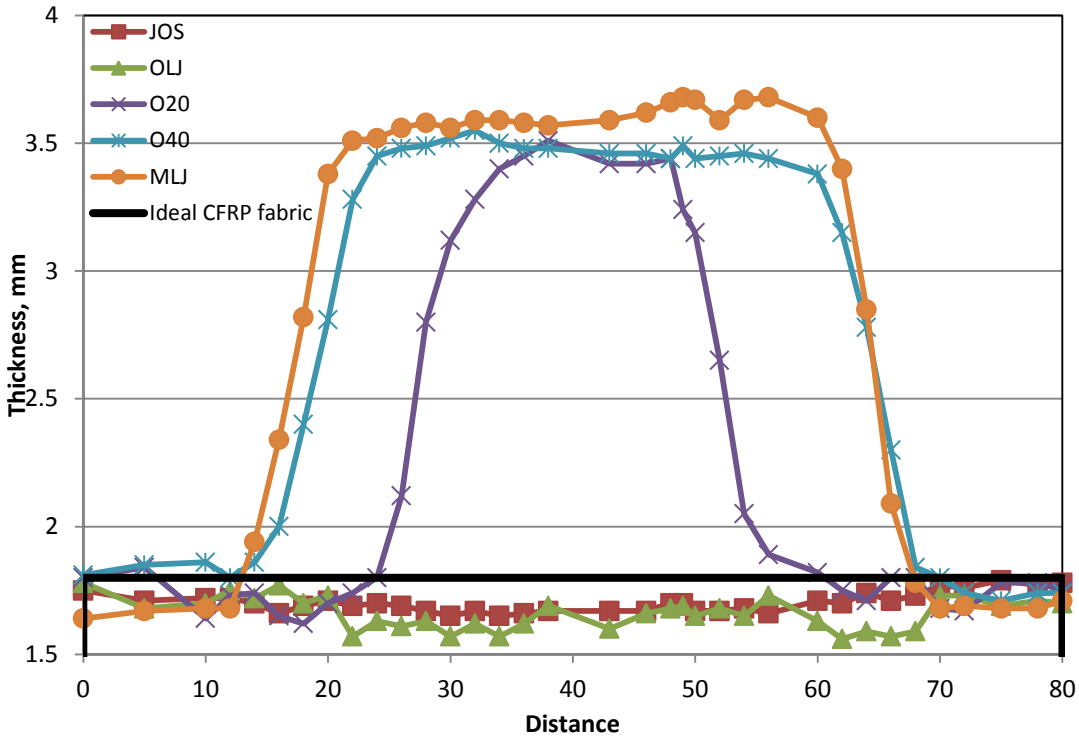

Figure 5.16: Typical thickness profiles for the three joints and the jointless CFRP fabric.

5.4. Conclusions

The laminated joints presented herein (both the original and improved types) are novel and were fabricated using a VARTM process. Four laminated joints were described. The first was the OLJ and the other three were improved joints. All samples were subjected to tensile tests to evaluate their tensile strength.

Tensile testing showed the following:

1- A maximum ultimate failure load of 22.3 kN was observed for the 40 mm overlapped laminated joint, O40. This represented a 56% increase in the failure load over the OLJ. Generally, the improved laminated joints showed 40–56% increases in ultimate failure load.

2- The load-displacement curve for the OLJ differed from those of the improved joints. It showed a linear relationship, with earlier crack initiation, in the first two stages, before changing to a non-linear relationship in the third stage. For the improved joints, the entire load-displacement curve showed a linear relationship and later crack appearance.

3- The joining efficiency showed the same trend as the ultimate failure load. The maximum joining efficiency of 69.5% was achieved with the 40 mm overlapped joint, O40, and the joining efficiency ranged from 44.5% to 69.5% for all joints.

4- The ultimate stress data, based on adherend thickness, showed the same trend as the ultimate failure load data. The highest stress value, of 1,250 MPa, was recorded for the 40 mm overlapped joint, O40. However, the stress results showed a different trend when they were calculated based on the thicker part of the joint. The ultimate stress decreased to half for joint O40 when it was calculated based on the thicker part of the joint, and the stress value for the OLJ was the highest stress value.

Failure analysis of all samples was performed using optical photomicrographs. Fiber breakage failure mode was observed for the jointless CFRP fabric. However,

delamination failure was observed for both the OLJ and overlapped joints. Combining the load-displacement curve with the photomicrographs, it was found that the delamination fracture in the OLJ started with earlier crack initiation than in the 20 mm overlapped joint, O20. Finally, a mixture of delamination and fiber breakage failure modes was observed for joint O40 and multiple-cover joints.

Chapter 6
Bending strength of novel CFRP composite adhesive joints fabricated from two dry carbon halves using vacuum assisted resin transfer molding

6.1. Introduction

The previous chapters focused on improving the tensile strength of the developed CFRP adhesive joints. However, the CFRP composite structures such as wind-lens turbine and other similar applications are subjected to a combination of mechanical loadings such as axial, flexural, fatigue, and impact loadings. The main objective of the research work in this chapter is improve the flexural properties of the laminated joint is previously introduced in chapter 2.

In this chapter improvements are made for the second joint type (laminated joints). These improvements include the stitching of the two halves together using carbon fiber bundles and by inserting extra carbon fiber covers in the joint connection. For this joint type, three adhesive joints were studied: a conventional laminated joint and two improved laminated joints. The samples were prepared for bending test. The 3-point bending loading system was used to measure the bending load capacity for all joints. The fracture was investigated during and after testing. All joints were designed and fabricated using VARTM manufacturing technique.

6.2. Materials and Fabrications

6.2.1. Materials

The CFRP composites consisted of carbon fabric (Mitsubishi Rayon UD 1M; 317 g/m2, see table 6.1) and a resin (Denatite XNR6815/XNH6815) [19]. The resin

was a mixture of XNR6815 and XNH6815 at a weight ratio of 100:27. The resin mixture viscosity at 25°C was 260 mP.s.

Table 6. 1: Detailed information of the used carbon fabric [76]

Carbon fiber designation	Style	No. of filaments	Weight	Density	Thickness	Tensile strength	Tensile modulus	Elongation
			g/m^2	g/cm^3	mm	MPa	GPa	%
TRK976PQRW	UD	12,000	317	1.82	0.33	4,900	253	1.9

6.2.2. Adhesive joints

The laminated joint proposed in this work is a composite adhesive joint constructed of two dry carbon halves that are stacked in mating together. The fiber volume fraction measured for this joint was approximately 26%. In this joint, the joint length was 40 mm and the total specimen length was 80 mm (Figure 6.1b). The first improvement to this joint was made by applying a stitching technique. We used stitching with carbon bundles of the same carbon fiber type, which were applied perpendicular to the plane of the laminate [44, 45]. Figure 6.1c shows the stitched laminate joint (SLJ). Abusrea and Arakawa [55] showed a weakened stepped joint in which stitching was applied; the tensile strength of the stitched stepped joint was 26% lower. However, it showed improved tensile strength when the stitching was applied to the dry carbon-to-dry carbon joints. The second improvement was made by adding carbon fiber pieces of 40 mm in length. These carbon fiber pieces were put between the carbon fiber layers and covered the contact between the two joint halves. Figure 6.1d shows the multi-covered laminate joint (MCLJ).

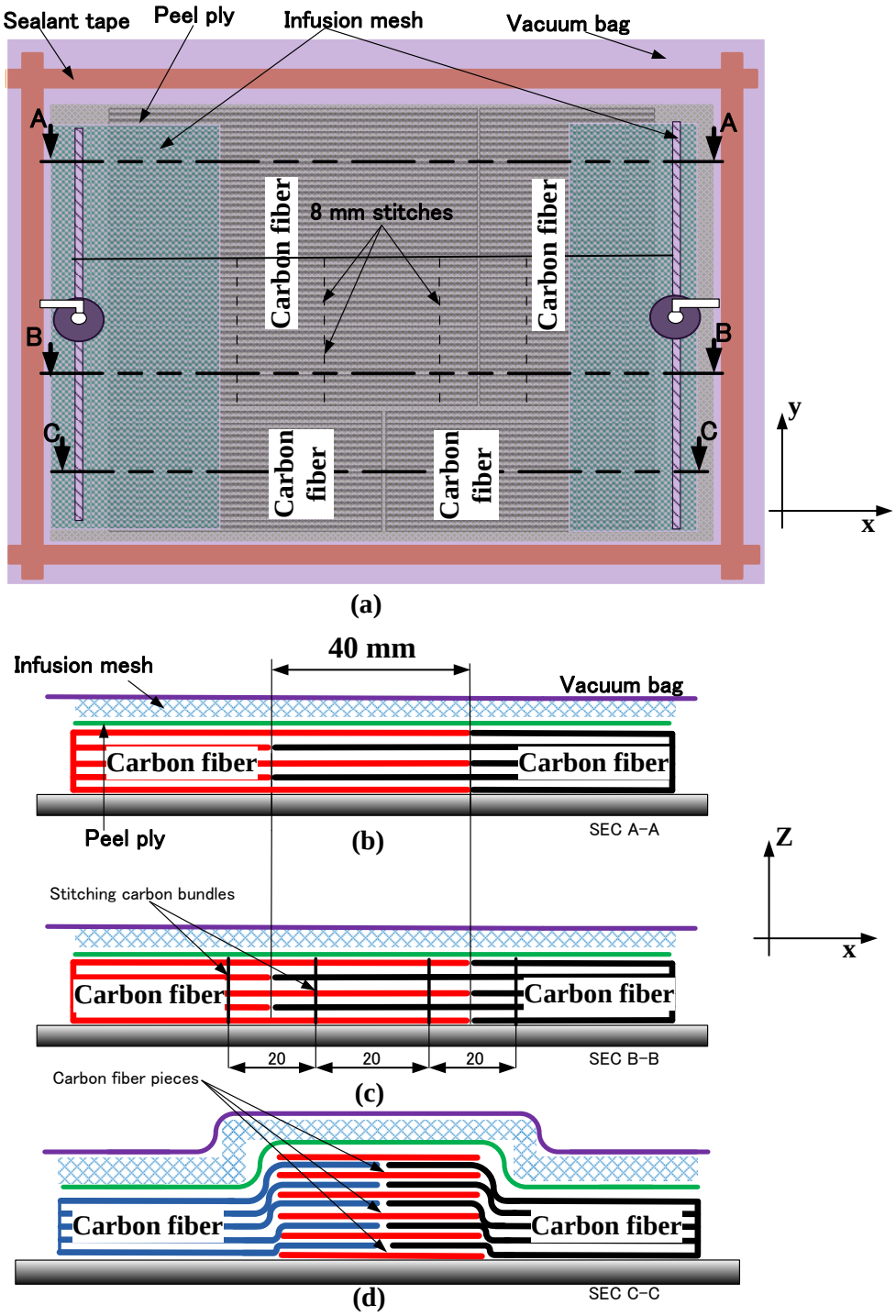

Figure 6. 1: (a) Schematic view of the joints. (b) Sectional side view of the laminated joint (LJ). (c) Sectional side view of the stitched laminated joint (SLJ). (d) Sectional side view of the multiple-cover laminated joint (MCLJ).

In this work, we chose four different numbers of carbon fiber layers for all joints.

We assigned 5, 6, 7 and 10 carbon fiber layers as these are commonly used. For the

first conventional laminated joint, two different cases were used; therefore, we divided the four carbon fiber layers into two combinations, which were 6&10 and 5&7 carbon fiber layers. Two cases were examined for the laminated joint: a 'normal case' laminated joint (NCLJ) and a 'shifted case' laminated joint (SCLJ). For NCLJ, the carbon fiber layers were stacked and arranged 'correctly' in their positions; that is, there was no gap at the joint ends (Figure 6.2a). We used 6 and 10 carbon fiber layers as examples. In the SCLJ, the carbon fiber layers were shifted to create a gap at the joint ends (Figure 6.2b). Because carbon fiber layer movement may occur during mold preparation with this kind of joint, the SCLJ was used to examine the effects of any such movement on final product quality, in terms of thickness variation, and mechanical performance, in terms of bending strength. For the SCLJ, 5 and 7 carbon fiber layers were stacked.

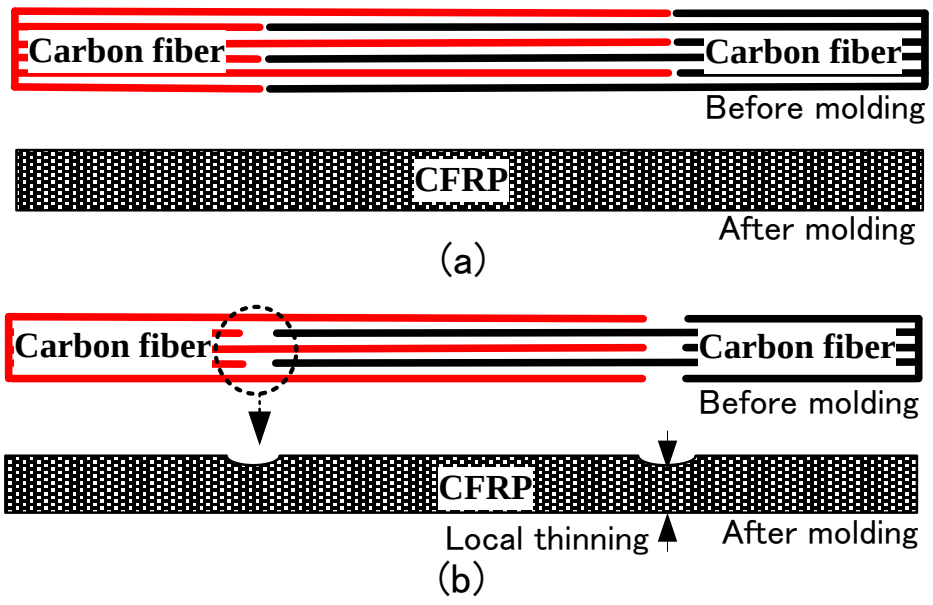

Figure 6. 2: Schematic drawing before and after molding for the (a) normal-case laminated joint (NCLJ) and (b) shifted-case laminated joint (SCLJ).

6.2.3. Testing procedure

The CFRP joints were sectioned to form specimens for the three-point bending tests, with the geometry shown in Figure 6.3. Five specimens were prepared for each condition. During the test, the specimen was monitored with AE measurements. The bending tests were carried out with a universal testing machine (Zwick 250, testXpert, ver. 11.02) at room temperature with a crosshead rate of 3 mm/min. Fracture processes were examined in real time using two AE sensors (micro30, Physical Acoustic Corp.), marked as S1 and S2, which were attached to the bending specimens using vacuum grease and mechanical fixation. The two acoustic emission sensors were put 46 mm apart, each one is 23mm distant from the specimen center. They were put in such positions close to the joint ends. A two-channel AE detection system (MSTRAS 2001, Physical Acoustic Corp.) was used to record the AE data, and the AE measurement conditions were a 40dB pre-amp, a threshold level of 40 dB, and a sampling rate of 4 MHz. The threshold level of 40 dB was put to filter the noisy sounds coming from other emission sources. A band-pass filter (range, 1 kHz to 1 MHz) under software control was used for signal gain for specific frequencies. Three AE parameters were investigated: amplitude, energy, and the frequency spectrum of the AE signals obtained using an FFT. AE analysis can provide a way to identify and differentiate fracture sources. Consistent with Yoon et al. [30], we assumed that the distance between the sensor and the crack was sufficient to measure the AE characteristics. Considering the attenuation problems at high frequencies, we focused primarily on frequency bands below 400 kHz for verification of the fracture mechanism. Fractographic analyses were also performed on the fracture surface of the

test specimens using optical microscopy and scanning electron microscopy (SEM). The fractographic results were used for quantitative and qualitative analyses.

6.3. Results and discussion

Many previous researches [8, 28-32, 44-46, 77-84] have investigated the mechanical performance of adhesively bonded and also z-pinned and stitched bonded joints. However, they didn't take into consideration the joint quality in terms of thickness accuracy. The current research presents, beside the bending strength, the thickness measurements at the joint area. Table 6.2 shows thickness data obtained for the NCLJ. The average thicknesses were 1.83 and 3.04 mm for 6 and 10 layers, respectively. The minimum thickness and the max thickness deviation were recorded as measures of product quality. Table 6.2 shows that the minimum thicknesses were 1.78 and 2.93 mm for 6 and 10 layers, respectively. Furthermore, the thickness deviation ranged from 2.8% for 6 layers to 3.5% for 10 layers.

For the SCLJ, Table 6.3 shows that the average thicknesses for 5 and 7 carbon fiber layers were 1.46 and 2.02 mm, respectively. The minimum thicknesses were 1.15 and 1.55 mm for 5 and 7 layers, respectively. However, the thickness deviation was as high as 23%. The minimum thickness and the thickness deviation indicated the degree of local thinning for the SCLJ.

The strength in terms of maximum bending load or maximum bending strength was measured [56] to evaluate the joints' mechanical performance [85]. Figure 6.5 shows the average maximum bending loads for the NCLJ and SCLJ. For the NCLJ, the bending loads for 6 and 10 carbon fiber layers were 604 and 1326 N, respectively. Lower bending loads were recorded for the SCLJ. For example, the bending loads for

5 and 7 carbon fiber layers were 280 and 535 N, respectively. Figure 6.4 shows the maximum bending strength for the NCLJ and SCLJ. The bending strength of 5 and 7 carbon-layers SCLJ showed a low strength of 206 and 256 MPa, respectively. On the other hand, the bending strength for the 6 and 10 carbon-layers NCLJ showed a much higher strength of 1072 and 873 MPa, respectively.

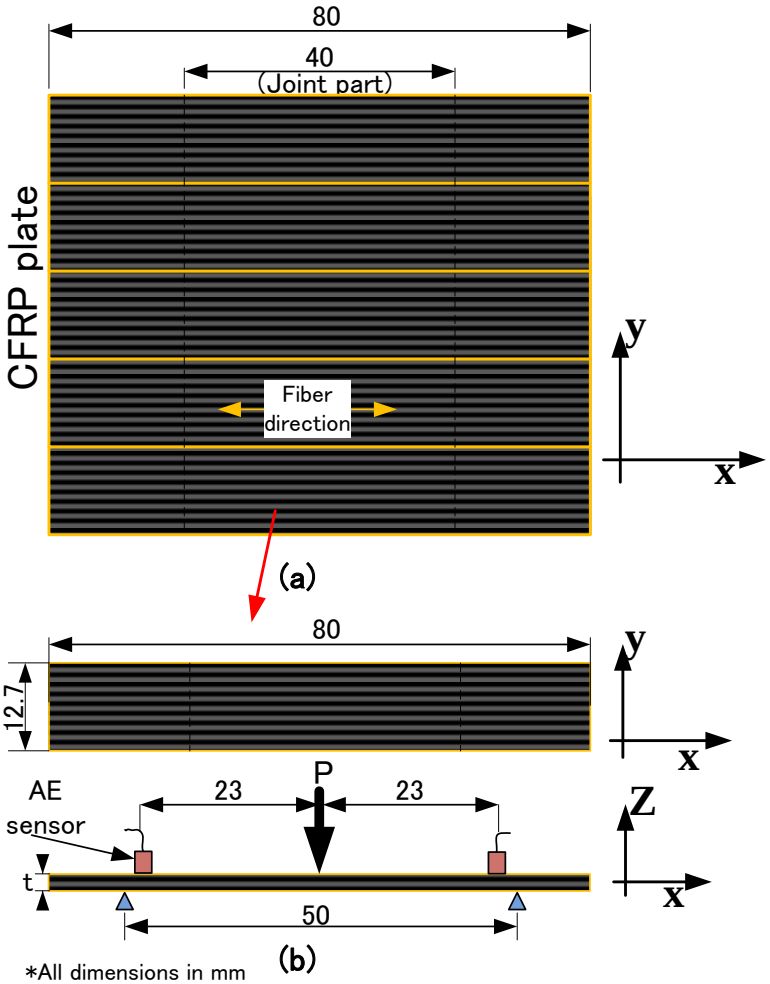

Figure 6. 3: Specimen preparation. (a) Location of specimens taken from the CFRP plate and (b) an illustration of the specimen for the three-point bending testing with acoustic emission (AE) monitoring

Table 6. 2: Thickness measurements for the NCLJ

	Thickness, mm	minimum thickness, mm	% max thickness deviation
6 layers	1.83(0.04)	1.78	2.8
10 layers	3.04(0.07)	2.93	3.5

Table 6. 3: Thickness measurements for the SCLJ

	Thickness, mm	minimum thickness, mm	% max thickness deviation
5 layers	1.46(0.08)	1.15	21
7 layers	2.02(0.08)	1.55	23

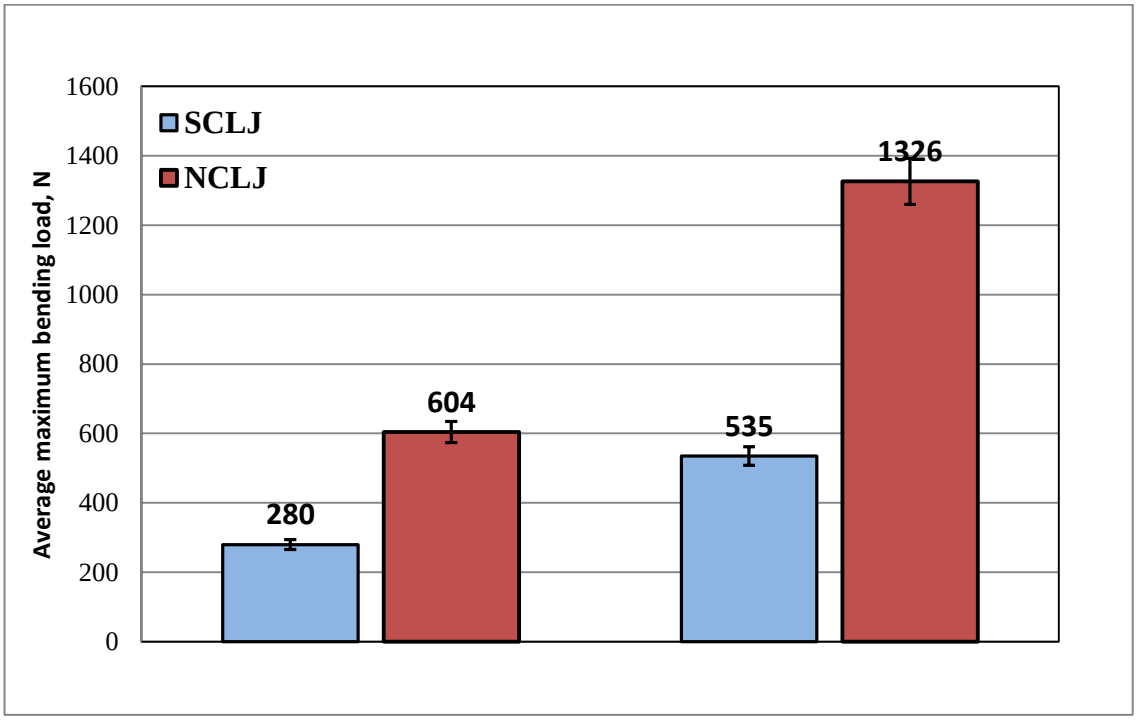

Figure 6. 4: Bending load data for the NCLJ and SCLJ

The bending strength was markedly affected by the placement of carbon fiber layers. This behavior can be examined using AE, optical microscopy, and SEM techniques. Figures 6.5a-b and 6.6a-b show typical three-point bending stress behaviors with accompanying amplitude distributions of the AE signals as functions

of time for the NCLJ and SCLJ, respectively. For NCLJ, the bending strength, σ_1, is given by:

$$\sigma_1 = 3PL/2Wt^2, \qquad (1)$$

Where P is the maximum load point on the load-deflection curve, L is the span length, W is the specimen width, and t is the specimen thickness. For SCLJ, the bending strength of a specimen, σ_2, is given by:

$$\sigma_2 = 3Pb/Wt_c^2, \qquad (2)$$

where b is the distance between the specimen end and the thinner section, and t_c is the thickness of the specimen at the thinner section.

In Figures 6.5a-b and 6.6a-b, the stress behavior can be separated into two stages. In the first, the stress increased until the peak, along with few AE pulses. After reaching the peak, extensive amplitude pulses were generated with the stress drop-down. For NCLJ, the 6-layer joint reached a maximum stress level of 1200 MPa and generated amplitude pulses of 83 dB. Furthermore, there were a few high-amplitude pulses of 90 dB, followed with a sudden stress drop to 600 MPa. The NCLJ with 10 layers reached a higher maximum stress of 2000 MPa. After that, the stress decreased gradually to 1500 MPa, emitting large AE amplitude pulses of 95 dB.

SCLJs with 5 and 7 layers showed similar stress and AE patterns to the NCLJ with 6 layers. In this case, stress was calculated based on the minimum thickness using Eq. (2).

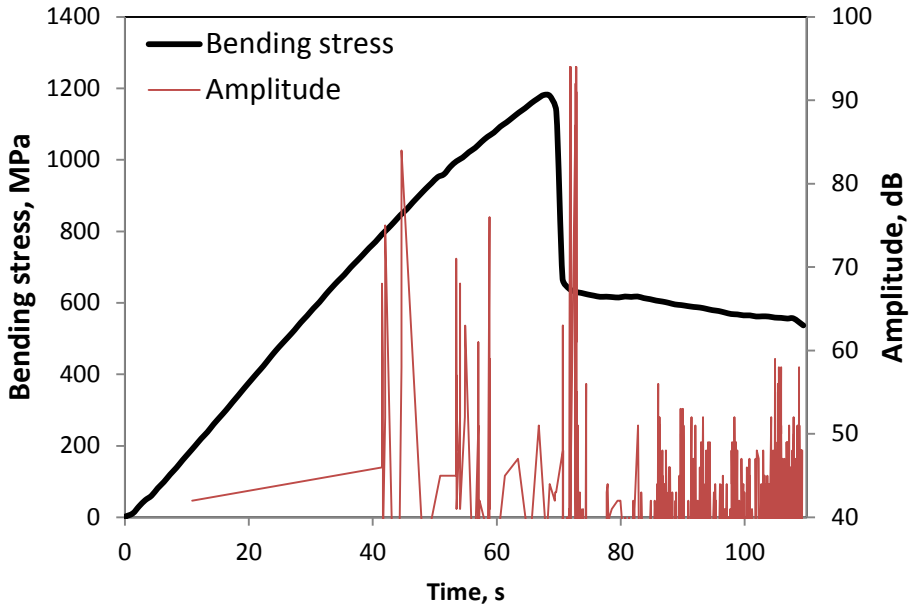

(a)

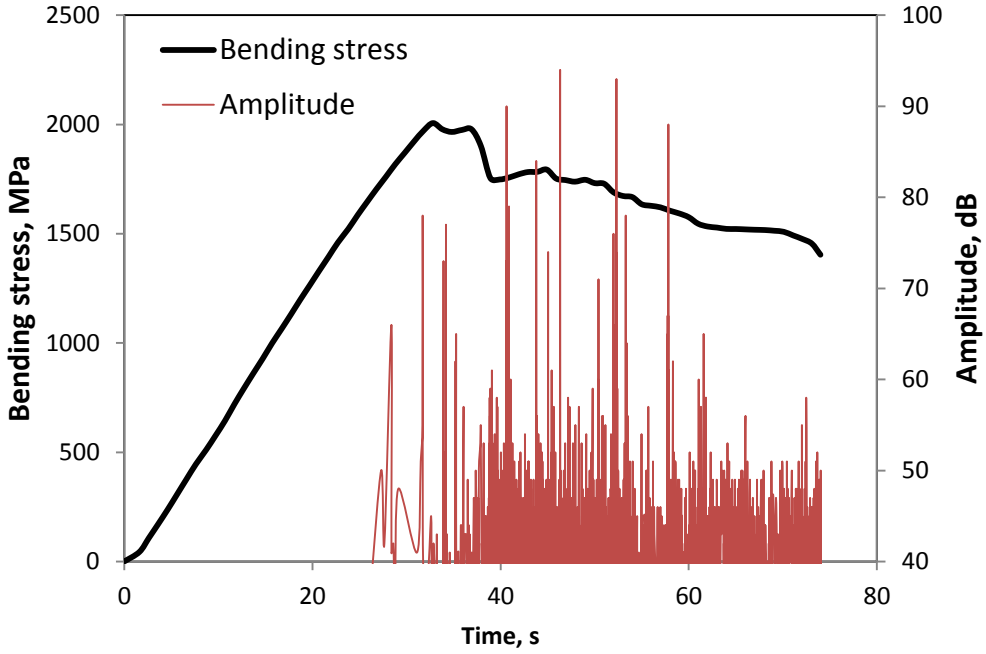

(b)

Figure 6. 5: Bending stress-time diagram with accompanying AE amplitude for NCLJ: (a) 6 carbon fiber layers and (b) 10 carbon fiber layers

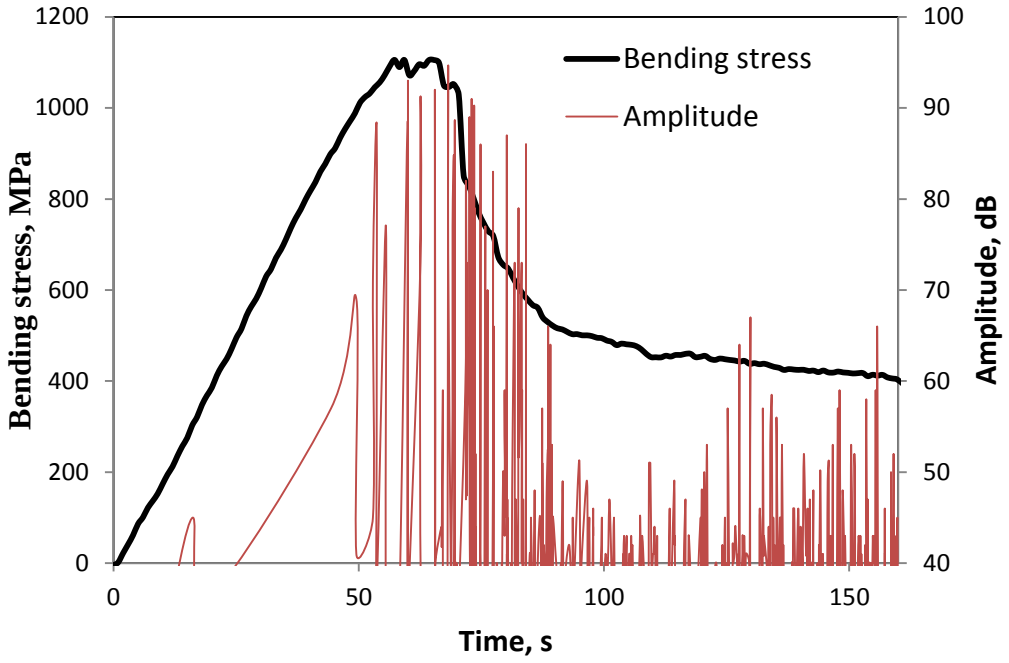

(a)

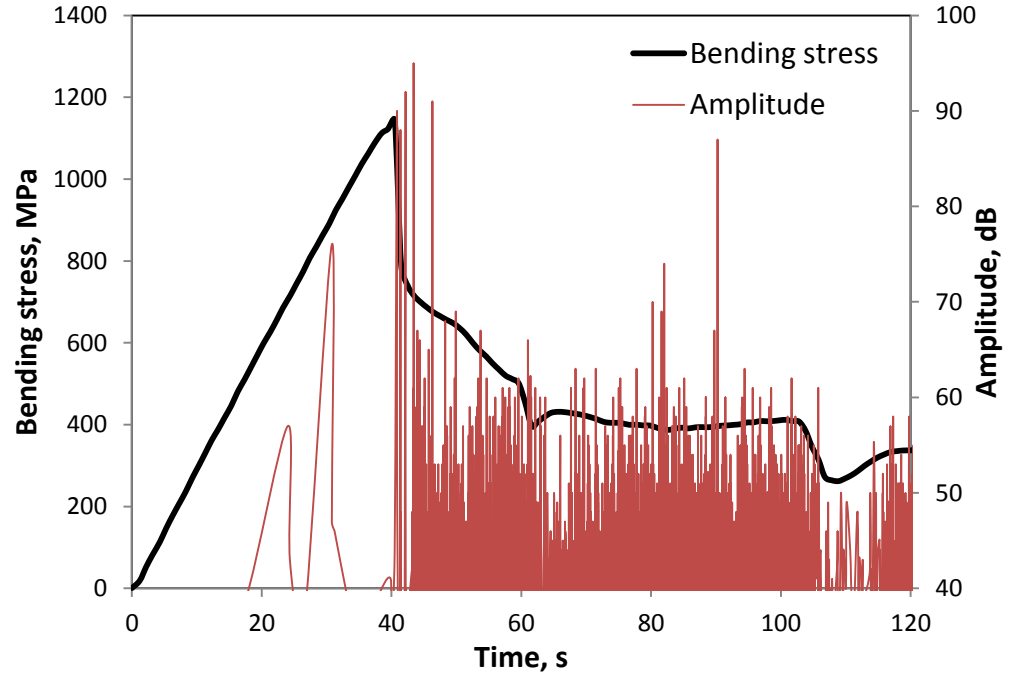

(b)

Figure 6. 6: Bending stress-time diagram with accompanying AE amplitude for SCLJ: (a) 5 carbon fiber layers and (b) 7 carbon fiber layers

To clarify the fracture behavior under a bending load, we classified the AE features according to the fracture mode on the basis of previous studies in which

spectral features below 160 kHz corresponded to resin matrix fracture, spectral features in the range of 160-240 kHz corresponded to matrix-fiber mixed fracture, and features above 240 kHz were associated with fiber fracture [56,57]. Figure 6.7 shows the percentage of AE energy at these frequency bands. The AE energy spectra occurred mostly in the third frequency band (f > 240 kHz). The percentage of AE energy ranged from 85% for the NCLJ with 10 layers to 90% for 6 layers. Thus, the predominant fracture mode in the tests was fiber fracture.

To confirm the failure behavior of NCLJs, additional failure analyses using optical microscopy and SEM were performed. Figure 6.8 shows typical optical micrographs and an SE micrograph of the NCLJ with 10 layers. A bending fracture occurred at the center of the specimen, not at the joint ends. This indicated that the joining efficiency was at least 80% because, at the same bending load, the bending stress at the joint ends approximated 80% of the bending stress at the middle of the specimen.

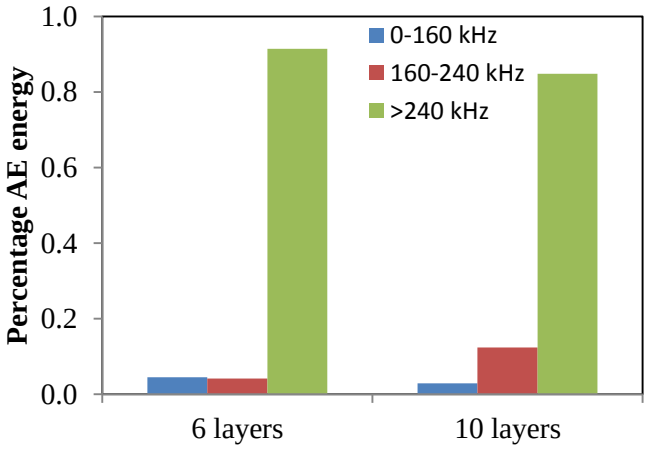

Figure 6. 7: Typical percentage AE energy data for the three frequency bands for NCLJ

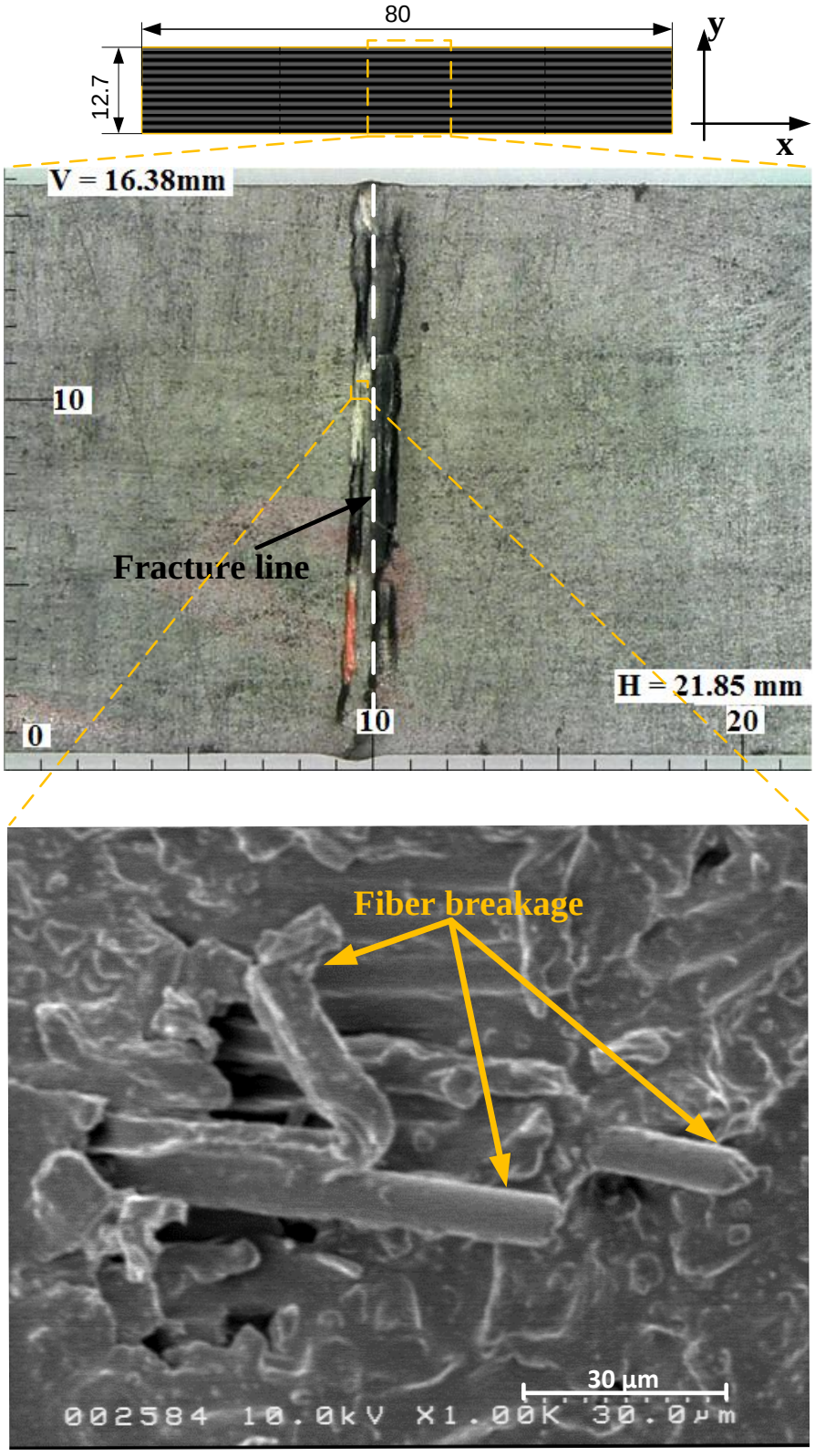

Figure 6. 8: Typical optical microscopy and SEM micrographs for the fracture of NCLJ with 10 layers

In contrast, AE and SEM analyses for the SCLJ showed different failure behavior. Figure 6.9 shows the percentage of AE energy at the adopted frequency bands for the SCLJ. A higher fraction of the AE energy spectrum occurred in the first frequency band (f < 160 kHz). This indicated that the fracture occurred due to resin failure. This behavior was confirmed by optical microscopy, as shown in Figure 6.10. For the SCLJ with 5 layers, a crack was initiated at the joint end and then propagated at the laminate interface until the final rupture.

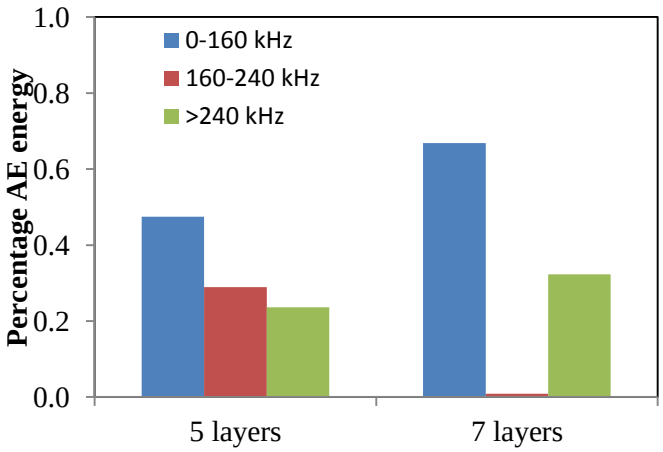

Figure 6. 9: Typical percentage AE energy data for the three frequency bands for SCLJ

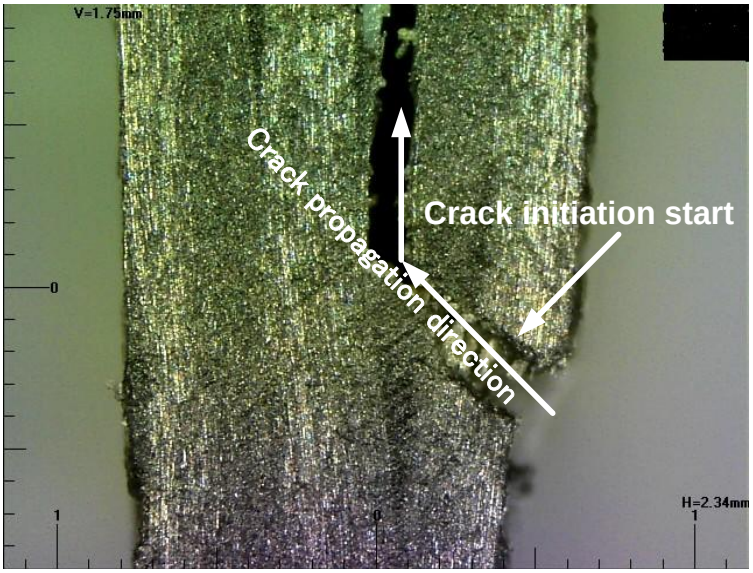

Figure 6. 10: Typical optical micrographs for the fracture of the 5-layer SCLJ

For the second joint, the stitched laminated joint, an improved bending load resulted versus the conventional laminated joint. The bending load for an SLJ with 6 layers was 771 N. This represents a considerable increase, 27%, over the conventional laminated joint (Figure 6.11). Plain and Tong [58] used a stitching technique to improve mode I and II fracture toughness for laminated composites. Velmurugan et al. [59] showed retarded crack initiation, followed by gradual crack propagation, when stitching was applied to a cylindrical shell subjected to axial compression. For bending, Chung et al. [60] found that the stitching improved the strength of CFRP and KFRP composites under 4-point bending, by ~25%. Adanur and Tsao [61] reported an improvement in the flexural properties of KFRP and CFRP even when stitched at a comparatively low density. However, at higher stitch densities, the properties deteriorated.

Stitched laminated joints were analyzed by AE, optical microscopy, and SEM. Figure 6.12 shows typical percentages of AE energy in the three frequency bands for stitched laminated joints with 5, 6, and 7 layers. The SLJ showed a higher percentage of AE energy in the third frequency band (> 240 kHz). This behavior indicated fiber-dominated breakages. This fracture behavior was confirmed by the optical microscopy and SEM analyses (Figure 6.13).

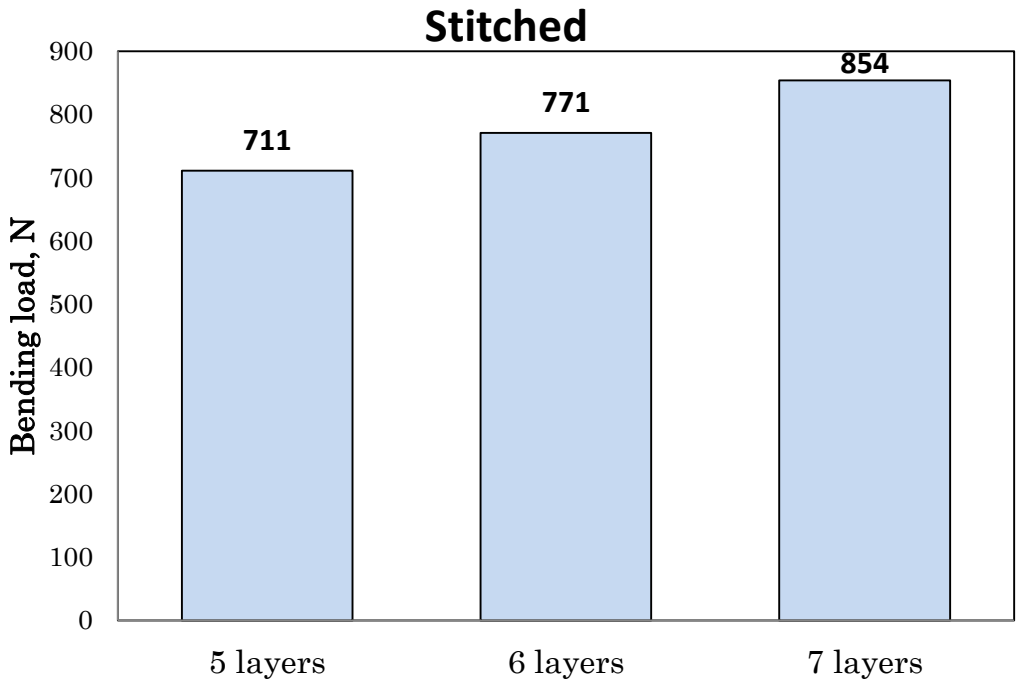

Figure 6. 11: Bending load data for the SLJ with different layer numbers

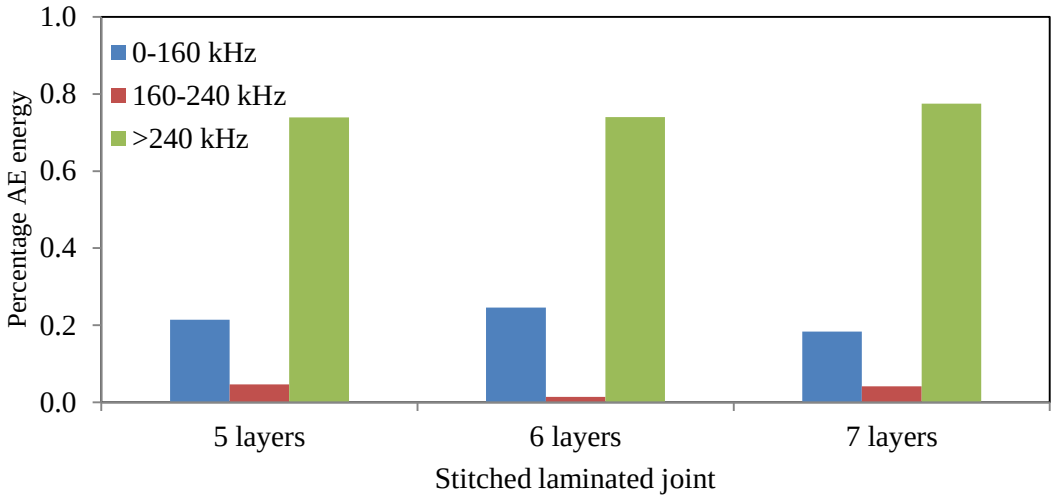

Figure 6. 12: Typical percentage AE energy data for the three frequency bands for SLJ

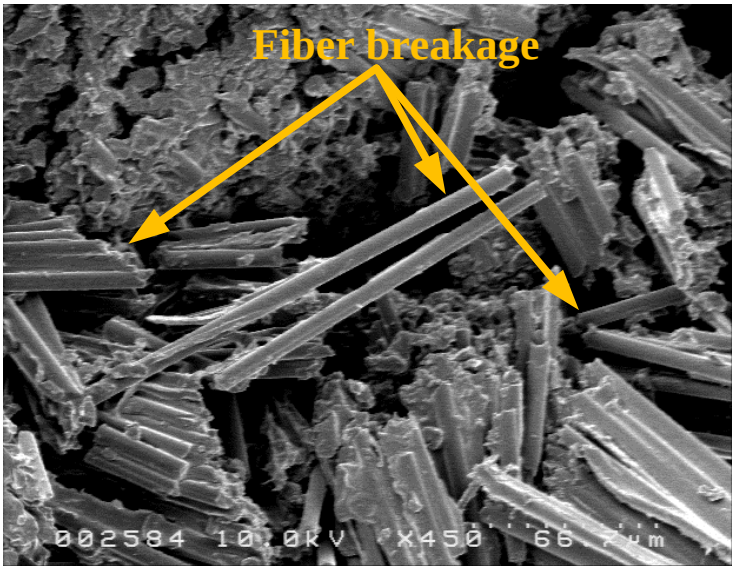

Figure 6. 13: Typical SEM micrograph for the fracture of the 6-layer SCLJ

For the third joint type, the multiple-cover laminated joint, a greater thickness for the joint part than for the adherend was observed. This joint was characterized by extra inserted carbon fiber pieces. The number of additional carbon fiber pieces exceeded the number of carbon fiber layers for the adherend. Thus, the thickness at the joint part should be at least twice the thickness of the adherend. This thickness difference occurred in the specimen length direction because all carbon fibers, including the additional carbon fiber pieces, were placed on a rigid flat surface of the mold (Figure 6.1d). Thus, a thickness difference was observed at the upper surface of the joint in contact with the flexible vacuum bag. The positioning of this joint specimen during the test might affect its bending strength. Figure 6.14 compares the specimen thickness of the three joints, NCLJ, SLJ, and MCLJ, for 6 layers of fabric in comparison with an 'ideal' 6-layer jointless CFRP. The stitched joints showed higher thickness deviation, especially at the stitches. The thickness deviation was

about +0.45 mm. A much greater thickness increase at the joint part was observed for the third joint, the MCLJ. The thickness at the joint part, 40 mm, recorded around 3.6 mm, was double the ideal thickness.

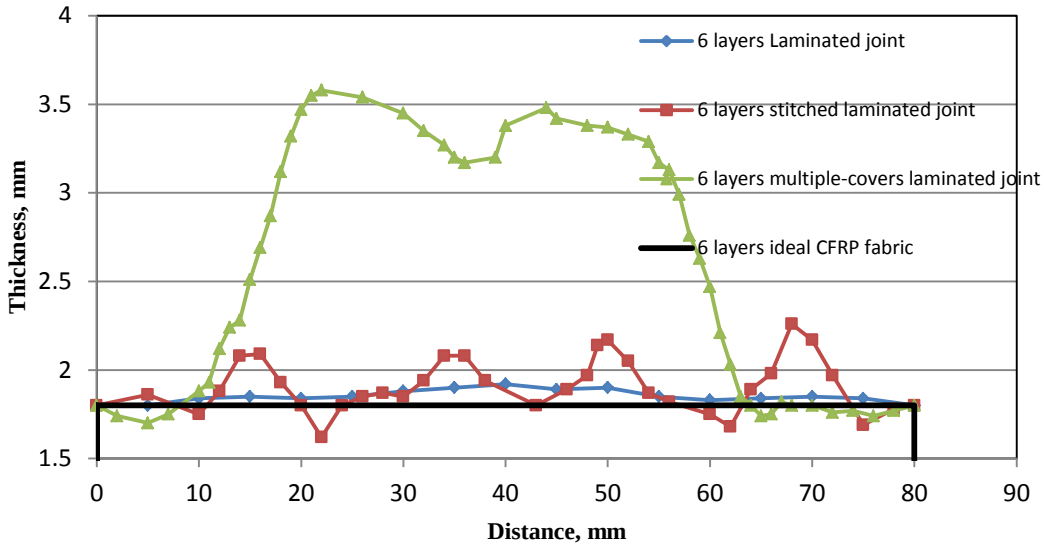

Figure 6. 14: Typical thickness profiles for the three joints and the jointless CFRP fabric

For the bending test results, the MCLJ achieved much higher bending loads than the conventional laminated joint and the stitched laminated joints. For example, the MCLJ with 6 layers showed a bending load of 1280 N, representing increases of 112% and 66% versus conventional laminated and stitched laminated joints. The MCLJ with 10 layers achieved 1958 N, an increase of 58% (Figure 6.15).

Similar to the SLJ, the MCLJ showed dominant fiber breakage, as confirmed in the percentage AE energy in the third frequency band, > 240 kHz (Figure 6.16), and many broken fibers on the surface (Figure 6.17).

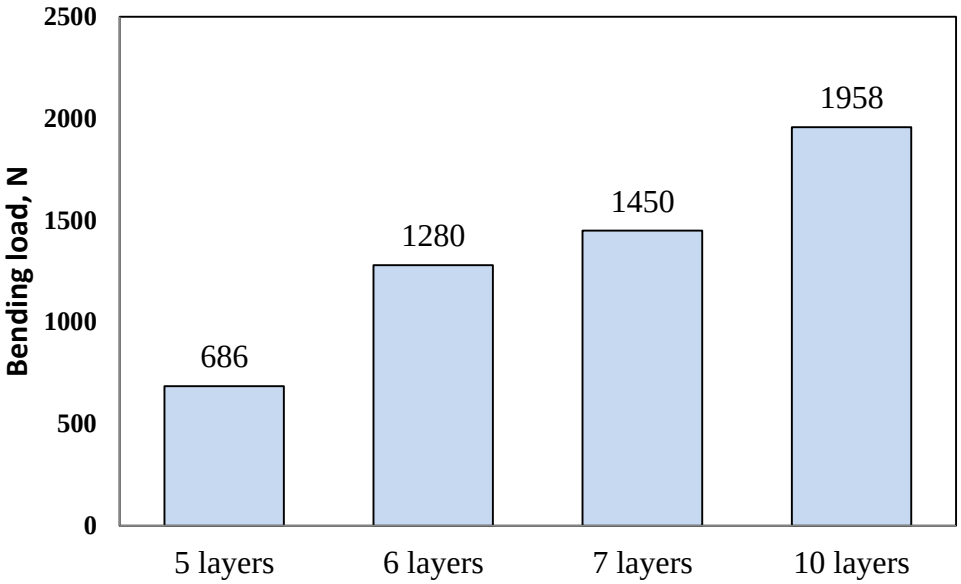

Figure 6. 15: Bending load data for the MCLJ with different layer numbers

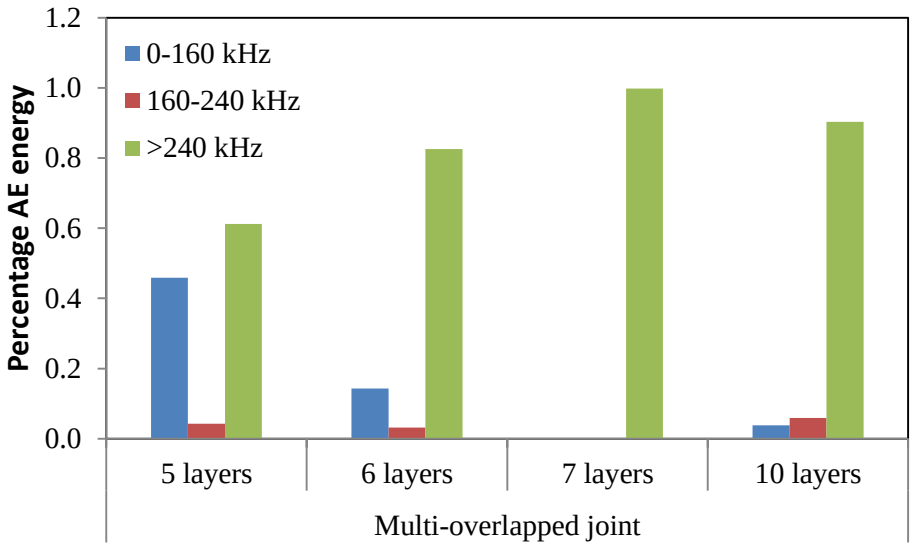

Figure 6. 16: Typical percentage AE energy data for the three frequency bands for MCLJ

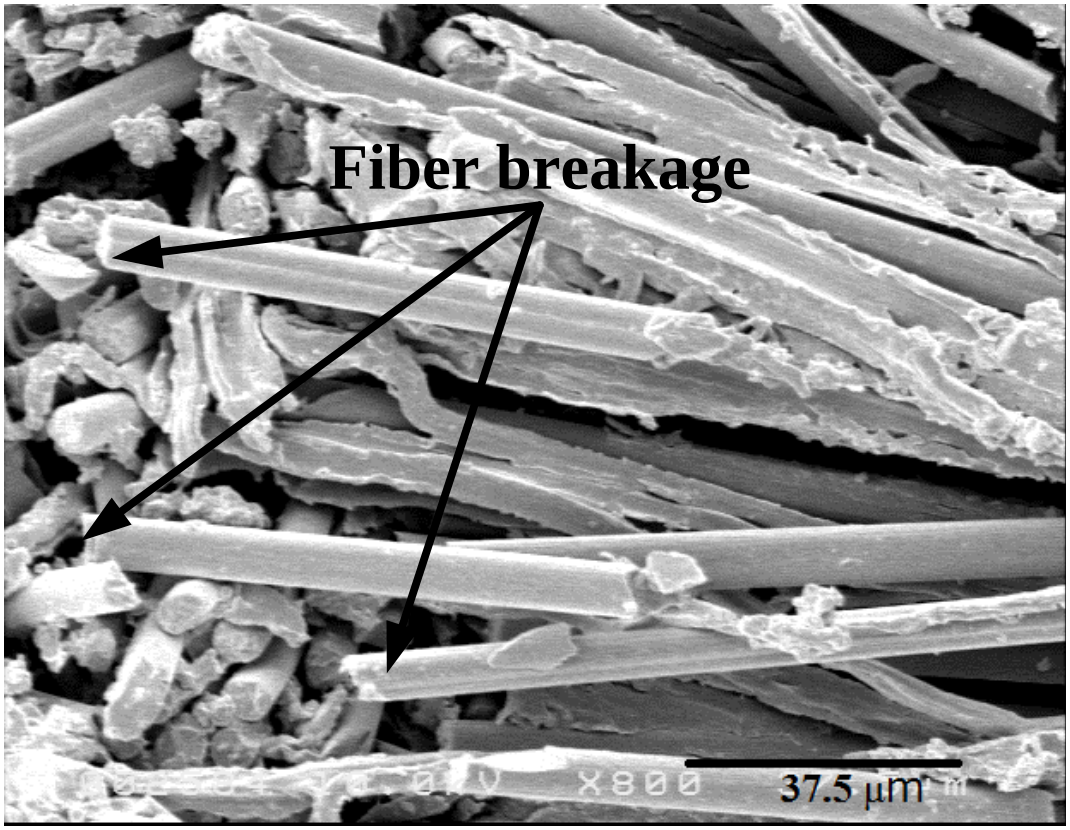

Figure 6. 17: Typical SEM micrograph for the fracture of the 10-layer MCLJ

6.4. Conclusions

The laminated joints presented in this paper are novel and fabricated completely by VARTM process. Three laminated joints were introduced in this work. The first was a conventional laminated joint and the other two are the improved joints. All samples were tested under 3-point bending to evaluate their flexural strength in terms of bending load as well as bending strength.

For the conventional laminated joint, to emphasize the effect of the carbon fiber shifting, two cases were recorded; normal case laminated joint NCLJ and shifted laminated joint SCLJ. The thickness measurements and the bending test results showed the following characteristics:

1. The NCLJ showed a much higher bending load than the SCLJ. For instance, the 6 layers NCLJ achieved double bending load of the 5 layers SCLJ and the 10 layers achieved 2.5 times the bending load of the 7 layers SCLJ
2. The bending strength for NCLJ increased by 5 times over the SCLJ
3. The thickness readings showed a higher thickness deviation of about 23% for the SCLJ samples. While the maximum thickness deviation for the NCLJ was about 3.5% for the 10 layers fabrics
4. The above results prove a high influence of the carbon fiber shifting on both the bending strength and the thickness accuracy.

For the stitched laminated joint SLJ, a wide range of bending load increase was recorded in comparison with conventional laminated joint. The 6 layers SLJ achieved 27% bending load increase over the 6 layers NCLJ. The multiple covers laminated joint MCLJ achieved a wide range of bending load increase by 48% to 171% for the 10 layers and 7 layers MCLJ, respectively. On the other hand, the thickness distribution along the samples showed a higher thickness around the stitches for the SLJ samples.

Failure analysis for the three joints was performed using in-line AE monitoring as well as fracture surface observations. Resin failure was prevalent for the SCLJ, while fiber breakage was dominant for the NCLJ. However, with any movement in the carbon fiber layers, such as in the SCLJ, the failure mode changed to resin failure, rather than fiber breakage, causing lower bending strength. Both failure behaviors, fiber and resin failures, were confirmed using post-failure analyses. Fiber breakage was dominant for the two other joint types, SLJ and MCLJ.

References

[1] Abe K-i, Ohya Y. An investigation of flow fields around flanged diffusers using CFD. Journal of Wind Engineering and Industrial Aerodynamics. 2004;92(3–4):315-330

[2] Abe K, Nishida M, Sakurai A, Ohya Y, Kihara H, Wada E, et al. Experimental and numerical investigations of flow fields behind a small wind turbine with a flanged diffuser. Journal of Wind Engineering and Industrial Aerodynamics. 2005;93(12):951-970

[3] Ohya Y, Karasudani T. A Shrouded Wind Turbine Generating High Output Power with Wind-lens Technology. Energies. 2010;3(4):634-649

[4] Brondsted P, Lilholt H, Lystrup A. COMPOSITE MATERIALS FOR WIND POWER TURBINE BLADES. Annual Review of Materials Research. 2005;35(1):505-538

[5] T. Keller, T. Vallée. Adhesively bonded lap joints from pultruded GFRP profiles. Part I: stress-strain analysis and failure modes. Composites: Part B 36 (2005), pp. 331–340

[6] F. Ascione. The influence of adhesion defects on the collapse of FRP adhesive joints. Composites: Part B 87 (2016), pp. 291-298

[7] Dvorak GJ, Zhang J and Canyurt O. Adhesive tongue-and-groove joints for thick composite laminates. Compos Sci Technol 2001; 61: 1123–1142

[8] LÖbel T., Kolesnikov B, Scheffler S, et al. Enhanced tensile strength of composite joints by using staple-like pins: working principles and experimental validation. Compos Struct 2013; 106: 453–460

[9] Shufeng L , Xiaoquan C , Qian Z, Jie Z, Jianwen B, and Xin G. An investigation of hygrothermal effects on adhesive materials and double lap shear joints of CFRP composite laminates. Composites: Part B 91 (2016), pp. 431–440

[10] L. Burns, A.P. Mouritz, D. Pook , S. Feih . Strengthening of composite T-joints using novel ply design approaches. Composites: Part B 88 (2016), pp. 73–84

[11] Jakub Korta, Andrzej Mlyniec, Tadeusz Uhl. Experimental and numerical study on the effect of humidity-temperature cycling on structural multi-material adhesive joints. Composites: Part B 79 (2015), pp. 621–630

[12] DD Chen, " Improvements of Vacuum Assisted Resin Transfer Molding Process and Applications to Composite Structures ," D. Eng. thesis (Fukuoka, Japan: Dept. of Molecular and Material Science, Kyushu University, 2014)

[13] Sang-Jae Yoon, " Acoustic Emission Analysis of Composite Materials ," D. Eng. thesis (Fukuoka, Japan: Dept. of Molecular and Material Science, Kyushu University, 2014)

[14] Simacek P, Advani SG and Iobst SA (2008). Modeling flow in compression resin transfer molding for manufacturing of complex lightweight high-performance automotive parts, Journal of composite materials, 2008;42(23): 2523-45

[15] Rachmadini Y, Tan VBC, Tay TE. Enhancement of Mechanical Properties of Composites through Incorporation of CNT in VARTM - A Review, J. Reinf. Plast. Compos. 2010;29(18):2782-807

[16] Zhao JL, Fu T, Han Y, Xu KW. Reinforcing hydroxyapatite/thermosetting epoxy composite with 3-D carbon fiber fabric through RTM processing, Mater. Lett. 2004;58:163–8

[17] Johnson R, Pitchumani R. Enhancement of flow in VARTM using localized induction heating, Compos. Sci. Technol. 2003;63(15):2201-15

[18] Ou, Y., Zhu, D., Zhang, H., Yao, Y., Mobasher, B., & Huang, L. (2016). Mechanical properties and failure characteristics of CFRP under intermediate strain rates and varying temperatures. Composites Part B: Engineering, 95, 123–136. doi:10.1016/j.compositesb.2016.03.085

[19] Abusrea, M. R., & Arakawa, K. (2016). Improvement of an adhesive joint constructed from carbon fiber-reinforced plastic and dry carbon fiber laminates. Composites Part B: Engineering, 97, 368–373. doi:10.1016/j.compositesb.2016.05.005

[20] Padhi, G. ., McCarthy, M. ., & McCarthy, C. . (2002). BOLJAT: a tool for designing composite bolted joints using three-dimensional finite element analysis. Composites Part A: Applied Science and Manufacturing, 33(11), 1573–1584. doi:10.1016/S1359-835X(02)00113-6

[21] Ueda, M., Miyake, S., Hasegawa, H., & Hirano, Y. (2012). Instantaneous mechanical fastening of quasi-isotropic CFRP laminates by a self-piercing rivet. Composite Structures, 94(11), 3388–3393. doi:10.1016/j.compstruct.2012.04.027

[22] Thoppul, S. D., Finegan, J., & Gibson, R. F. (2009). Mechanics of mechanically fastened joints in polymer–matrix composite structures – A review. Composites Science and Technology, 69(3-4), 301–329. doi:10.1016/j.compscitech.2008.09.037

[23] Friedrich, C., & Hubbertz, H. (2014). Friction behavior and preload relaxation of fastening systems with composite structures. Composite Structures, 110, 335–341. doi:10.1016/j.compstruct.2013.11.024

[24] Lee, Y.-H., Lim, D.-W., Choi, J.-H., Kweon, J.-H., & Yoon, M.-K. (2010). Failure load evaluation and prediction of hybrid composite double lap joints. Composite Structures, 92(12), 2916–2926. doi:10.1016/j.compstruct.2010.05.002

[25] Oplinger JW. Mechanical fastening and adhesive bonding. In: Peters ST, editor. Handbook of composites. New York: Springer; 1998

[26] Abusrea, M., R., Jiang, S., Chen, D., Arakawa, K., Novel CFRP Adhesive Joints and Structures for Offshore Application. International Journal of Chemical, Molecular, Nuclear, Materials and Metallurgical Engineering 9 (9), 2015

[27] Chen, D., Arakawa, K., Jiang, S., . Novel joints developed from partially un-moulded carbon-fibre-reinforced laminates. Journal of Composite Materials, 2015, Vol. 49(14) 1777–1786.

[28] Rahman, N. M., & Sun, C. T. (2014). Strength calculation of composite single lap joints with Fiber-Tear-Failure. Composites Part B: Engineering, 62, 249–255. doi:10.1016/j.compositesb.2014.03.004

[29] De Castro, J., & Keller, T. (2008). Ductile double-lap joints from brittle GFRP laminates and ductile adhesives, Part I: Experimental investigation. Composites Part B: Engineering, 39(2), 271–281. doi:10.1016/j.compositesb.2007.02.015

[30] Heim, D., Hartmann, M., Neumayer, J., Klotz, C., Ahmet-Tsaous, Ö., Zaremba, S., & Drechsler, K. (2013). Novel method for determination of critical fiber length in short fiber carbon/carbon composites by double lap joint. Composites Part B: Engineering, 54, 365–370. doi:10.1016/j.compositesb.2013.05.026

[31] Hart-Smith LJ. Further developments in the design and analysis of adhesively bonded structural joints. Joining of Composite Materials, ASTM STP 1981;749:3–31

[32] Salih Akpinar. The strength of the adhesively bonded step-lap joints for different step numbers. Composites: Part B 67 (2014) 170–178 doi:10.1016/j.compositesb.2014.06.023

[33] Lee DG, Jeong KS, Kim KS, et al. Development of the anthropomorphic robot with carbon fiber epoxy composite materials. Compos Struct 1993; 25: 313‑324

[34] Niu M. Airframe structural design. 9th printing. Hong Kong: Conmilit Press Ltd.; 1997

[35] Wang ZY, Wang L, Guo W, et al. An investigation on strain/stress distribution around the overlap end of laminated composite single-lap joints. Compos Struct 2009; 89: 589‑595. 3

[36] Liu F, Zhao L, Mehmood S, et al. A modified failure envelope method for failure prediction of multi-bolt composite joints. Compos Sci Technol 2013; 83: 54‑63

[37] Quaresimin M and Ricotta M. Stress intensity factors and strain energy release rates in single lap bonded joints in composite materials. Compos Sci Technol 2006; 66: 647‑656

[38] Al-Zubaidy H, Al-Mahaidi R and Zhao X-L. Experimental investigation of bond characteristics between CFRP fabrics and steel plate joints under impact tensile loads. Compos Struct 2012; 94: 510-518

[39] Fawzia S, Al-Mahaidi R and Zhao X-L. Experimental and finite element analysis of a double strap joint between steel plates and normal modulus CFRP. Compos Struct 2006; 75: 156‑162

[40] Fawzia S, Zhao XL, Al-Mahaidi R, et al. Bond characteristics between CFRP and steel plates in double strap joints. Int J Adv Steel Constr 2005; 1: 17‑27

[41] Banea MD, Da Silva LF. Adhesively bonded joints in composite material: an overview. J Mater Des Appl 2009;223:1‑18

[42] Wen-Xue W., Yoshiro T., Terutake M. Galvanic corrosion-resistant carbon fiber metal laminates. 16th Int. conf. on composite materials

[43] Katnam KB, Comer AJ, Stanley WF, et al. Characterising pre-preg and non-crimp-fabric composite single lap bonded joints. Int J Adhes Adhes 2011; 31: 679‑686

[44] Heb, H. and Himmel, N.: Structurally stitched NCF CFRP laminates. Part 1: Experimental characterization of in-plane and out-of-plane properties. Compos Sci Technol, 71(2011), 549–68.

[45] Dransfield, KA., Jain, LK. and Mai, YW.: On the effects of stitching in CFRPs – I. Mode I delamination toughness. Compos Sci Technol, 58(1998), 815–827

[46] Kim K-S, Yi Y-M, Cho G-R, et al. Failure prediction and strength improvement of

unidirectional composite single lap bonded joints. Compos Struct 2008; 82: 513–520

[47] Daniel H, Mathias H, Johannes N, Christian K, Ömer A T, Swen Z, Klaus D. Novel method for determination of critical fiber length in short fiber carbon/carbon composites by double lap joint. Composites: Part B 54 (2013) 365–370

[48] Chohra M, Advani SG, Gokce A, Yarlagadda S. Modeling of filtration through multiple layers of dual scale fibrous porous media. Polymer Composites. 2006;27(5):570-581

[49] Gokce A, Chohra M, Advani SG, Walsh SM. Permeability estimation algorithm to simultaneously characterize the distribution media and the fabric preform in vacuum assisted resin transfer molding process. Composites Science and Technology. 2005;65(14):2129-2139

[50] Crocombe AD, Adams RD. Influence of the spew fillet and other parameters on the stress distribution in the single-lap joint. J Adhesion 1981;13:141‑55

[51] Tsai MY, Morton J, Matthews FL. Experimental and numerical studies of a laminated composite single-lap adhesive joint. J Compos Mater 1995;29(9):1254‑75

[52] Tsai MY, Morton J. The effect of a spew fillet on adhesive stress distributions in laminated composite single-lap joints. Compos Struct 1995;32:123‑31

[53] Mouritz AP, Chang P, Cox BN. Fatigue properties of z-pinned aircraft composite materials. ICAS Int Cong Aeronaut Sci 2006.

[54] E. Greenhalgh, Failure Analysis and Fractography of Polymer Composites, Woodhead Publishing, 2009, ISBN 978-1-84569-217-9

[55] Abusrea, M., R., and Arakawa, K., Evaluation of the strength of CFRP adhesive joints manufactured using VARTM. 10th International Symposium on Advanced Science and Technology in Experimental Mechanics, November 1-4, 2015, Matsue, Japan

[56] Yoon, SY., Arakawa K., Han, SW., Chen, D., and Choi, NS.,. Effect of Compaction

Treatment on Laminated CFRP Composites Fabricated by Vacuum-Assisted Resin-Transfer Molding. 2015; DOI:10.1002/pc.23578

[57] Gu, J.-U., Yoon, H.-S., & Choi, N.-S. (2012). Acoustic emission characterization of a notched aluminum plate repaired with a fiber composite patch. Composites Part A: Applied Science and Manufacturing, 43(12), 2211–2220. doi:10.1016/j.compositesa.2012.07.018

[58] Plain, K. P., & Tong, L. (2011). An experimental study on mode I and II fracture toughness of laminates stitched with a one-sided stitching technique. Composites Part A: Applied Science and Manufacturing, 42(2), 203–210. doi:10.1016/j.compositesa.2010.11.006

[59] Velmurugan, R., Gupta, N. K., Solaimurugan, S., & Elayaperumal, A. (2004). The effect of stitching on FRP cylindrical shells under axial compression. International Journal of Impact Engineering, 30(8), 923–938. doi:10.1016/j.ijimpeng.2004.04.007

[60] Chung, W. C., Jang, B. Z., Chang, T. C., Hwang, L. R., & Wilcox, R. C. (1989). Fracture behavior in stitched multidirectional composites. Materials Science and Engineering: A, 112, 157–173. doi:10.1016/0921-5093(89)90355-9

[61] S. Adanur, Y.P. Tsao. Stitch bonded textile structural composites Proc. 26th Int. SAMPE Tech. Conf. (1994), pp. 25–34

[62] Nogueira A, Drechsler K, Hombergsmeier E, Pacchione M. Investigation of the properties and failure mechanisms of a damage tolerant 3D-reinforcement joint for lightweight structures. SETEC-6th: Advanced Composites, The integrated System 2011.

[63] Akderya, T., Kemiklioğlu, U., & Sayman, O. (2016). Effects of thermal ageing and impact loading on tensile properties of adhesively bonded fibre/epoxy composite joints. Composites Part B: Engineering, 95, 117–122. https://doi.org/10.1016/j.compositesb.2016.03.073

[64] Araújo, H. A. M., Machado, J. J. M., Marques, E. A. S., & da Silva, L. F. M. (2017). Dynamic behaviour of composite adhesive joints for the automotive industry. Composite Structures, 171, 549–561. http://doi.org/10.1016/j.compstruct.2017.03.071

[65] Xiang, J., Zhao, S., Li, D., & Wu, Y. (2017). An improved spring method for calculating the load distribution in multi-bolt composite joints. Composites Part B: Engineering, 117, 1–8. https://doi.org/10.1016/j.compositesb.2017.02.024

[66] Zhu, S., Shao, G., Wang, Y., Zhu, X., & Zhao, Q. (2016). Mechanical behavior of the CFRP lattice core sandwich bolted splice joints. Composites Part B: Engineering, 93, 265–272. http://doi.org/10.1016/j.compositesb.2016.03.036

[67] Li, J., Yan, Y., Zhang, T., & Liang, Z. (2015). Experimental study of adhesively bonded CFRP joints subjected to tensile loads. International Journal of Adhesion and Adhesives, 57, 95–104. https://doi.org/10.1016/j.ijadhadh.2014.11.001

[68] Khashaba, U. A., Aljinaidi, A. A., & Hamed, M. A. (2017). Fatigue and reliability analysis of nano-modified scarf adhesive joints in carbon fiber composites. Composites Part B: Engineering, 120, 103–117. https://doi.org/10.1016/j.compositesb.2017.04.001

[69] Gunnion, A. J., & Herszberg, I. (2006). Parametric study of scarf joints in composite structures. Composite Structures, 75(1), 364–376. https://doi.org/10.1016/j.compstruct.2006.04.053

[70] Neto, J.A.B.P., Campilho, R.D.S.G., da Silva, L.F.M. , Parametric study of adhesive joints with composites. Int J Adhes Adhes, 37 (2012), pp. 96–101

[71] Harding, J., Welsh, L.M., . A tensile testing technique for fibre-reinforced composites at impact rates of strain. J Mater Sci, 18 (6) (1983), pp. 1810–1826

[72] Taniguchi, N., Nishiwaki, T., Kawada, H., . Tensile strength of unidirectional CFRP laminate under high strain rate. Adv Compos Mater, 16 (2) (2007), pp. 167–180

[73] Körber, H., . Mechanical response of advanced composites under high strain rates. Faculty of Engineering of the University of Porto (2012)

[74] Abusrea, M. R., Han, SW., Arakawa, K. and Choi, NS. (2017). Bending strength of novel CFRP composite adhesive joints fabricated from two dry carbon halves using vacuum assisted resin transfer molding. Composites Part B: Engineering, (In press)

[75] Mokhtari, M., Madani, K., Belhouari, M., Touzain, S., Feaugas, X., & Ratwani, M. (2013). Effects of composite adherend properties on stresses in double lap bonded joints. Materials & Design (Vol. 44). Retrieved from http://www.sciencedirect.com/science/article/pii/S0261306912005262

[76] Mitsubishi Rayon CO., LTD., Profile Department, www.mrc.co.jp

[77] Ghasemnejad, H., Argentiero, Y., Tez, T. A., & Barrington, P. E. (2013). Impact damage response of natural stitched single lap-joint in composite structures. Materials & Design, 51, 552–560. http://doi.org/10.1016/j.matdes.2013.04.059

[78] Hufenbach, W., Ibraim, F. M., Langkamp, A., Böhm, R., & Hornig, A. (2008). Charpy impact tests on composite structures – An experimental and numerical investigation. Composites Science and Technology, 68(12), 2391–2400. http://doi.org/10.1016/j.compscitech.2007.10.008

[79] Khalili, S. M. R., Ghadjar, R., Sadeghinia, M., & Mittal, R. K. (2009). An experimental study on the Charpy impact response of cracked aluminum plates repaired with GFRP or CFRP composite patches. Composite Structures, 89(2), 270–274. http://doi.org/10.1016/j.compstruct.2008.07.032

[80] Cheuk, P. T., & Tong, L. (2002). Failure of adhesive bonded composite lap shear joints with embedded precrack. Composites Science and Technology, 62(7–8), 1079–1095. http://doi.org/10.1016/S0266-3538(02)00054-4

[81] Borsellino, C., Calabrese, L., Di Bella, G., & Valenza, A. (2007). Comparisons of processing and strength properties of two adhesive systems for composite joints. International Journal of Adhesion and Adhesives, 27(6), 446–457. http://doi.org/10.1016/j.ijadhadh.2006.01.012

[82] Tan, K. T., Watanabe, N., & Iwahori, Y. (2010). Effect of stitch density and stitch thread thickness on low-velocity impact damage of stitched composites. Composites Part A: Applied Science and Manufacturing, 41(12), 1857–1868. http://doi.org/10.1016/j.compositesa.2010.09.007

[83] Tan, K., Watanabe, N., & Iwahori, Y. (2011). Stitch fiber comparison for improvement of interlaminar fracture toughness in stitched composites. Journal of Reinforced Plastics and Composites, 30(2), 99–109. http://doi.org/10.1177/0731684410383065

[84] Tan, K. T., Watanabe, N., Sano, M., Iwahori, Y., & Hoshi, H. (2010). Interlaminar Fracture Toughness of Vectran-stitched Composites - Experimental and Computational Analysis. Journal of Composite Materials, 44(26), 3203–3229. http://doi.org/10.1177/0021998310369581

[85] Zhao, T., Palardy, G., Villegas, I. F., Rans, C., Martinez, M., & Benedictus, R. (2017). Mechanical behaviour of thermoplastic composites spot-welded and mechanically fastened joints: A preliminary comparison. Composites Part B: Engineering, 112, 224–234. http://doi.org/10.1016/j.compositesb.2016.12.028

APPENDIX